This is to certify that the
dissertation entitled

INVESTIGATION OF ALUMINUM CORROSION IN LITHIUM-ION BATTERY ELECTROLYTES - INFLUENCE OF WATER CONTAMINATION

presented by

Mateusz Łukasz Hupert

has been accepted towards fulfillment
of the requirements for the

Ph.D. degree in Chemistry

Greg M. Swain
Major Professor's Signature

12-2-2002
Date

INVESTIGATION OF ALUMINUM CORROSION IN LITHIUM-ION BATTERY ELECTROLYTES - INFLUENCE OF WATER CONTAMINATION

By

Mateusz Łukasz Hupert

A DISSERTATION

Submitted to
Michigan State University
in partial fulfillment of the requirements
for the degree of

DOCTOR OF PHILOSOPHY

Department of Chemistry

2002

ABSTRACT

INVESTIGATION OF ALUMINUM CORROSION IN LITHIUM-ION BATTERY ELECTROLYTES - INFLUENCE OF WATER CONTAMINATION

By

Mateusz Łukasz Hupert

The susceptibility of high purity (99.999%) aluminum foils to oxidation (formation of a passivation layer) and/or corrosion (pitting and metal loss) during room temperature polarization in $LiPF_6$/ethylene carbonate-dimethyl carbonate (EC-DMC), $LiPF_6$/propylene carbonate (PC), $LiClO_4$/EC-DMC, and $LiClO_4$/PC was investigated. The effect of water on the corrosion process was studied through controlled additions (50-2000 ppm) of the water impurity to the electrolyte/solvent mixture. The testing of two different metal surfaces was performed, (i) aluminum with the native oxide film removed by mechanical polishing under an inert, argon atmosphere, and (ii) aluminum covered with the oxide layer formed by electropolishing in aqueous HBF_4 solution. The susceptibility of aluminum toward corrosion in each of the electrolyte/solvent mixtures was assessed with electrochemical techniques, including cyclic voltammetry (CV), chronoamperometry (CA), and open circuit potential measurements (OCP). Microscopic techniques such as optical microscopy (OM), atomic force microscopy (AFM), and scanning electron microscopy (SEM) were used to study morphological changes of the aluminum surface brought about by the imposed electrochemical conditions. X-ray

photoelectron spectroscopy (XPS), energy dispersive x-ray analysis (EDS), and Raman spectroscopy were used to probe the chemical composition of the surface before and after polarization in non-aqueous electrolyte/solvent mixture. Electrochemical quartz crystal microbalance (EQCM), electrochemical atomic force microscopy (EC-AFM), and electrochemical optical microscopy (EC-OM) were employed to study corrosion/passivation processes *in situ*, during anodic polarization.

Obtained results indicate that none of the investigated electrolyte/solvent systems is corrosive toward aluminum in the absence of added water (below 50 ppm), at least up to 5 V vs. Li/Li^+. A solid passivation layer forms on the surface at such conditions. The passivation layer is composed primarily of aluminum oxide and either aluminum oxyfluoride in $LiPF_6$ solutions or aluminum perchlorate in $LiClO_4$ solutions. An oxide film present on the electropolished aluminum surface improves the corrosion resistance of the metal.

In the presence of added water, anodic polarization of aluminum in $LiClO_4$/EC-DMC and $LiClO_4$/PC leads to pitting and progressive corrosion. A thick layer of corrosion products (mostly $Al(ClO_4)_3$ and $Al(OH)_3$) forms on the mechanically polished aluminum surface. An oxide film, present on the electropolished surfaces, does not prevent the underlying metal from being corroded in $LiClO_4$ solutions with added water impurity. At water levels below 500 ppm the corrosion products deposit in and fill the pits formed under these conditions. At higher water levels (1000 – 2000 ppm) empty pits form, due to evolution of gaseous oxidation products. Addition of water impurity to $LiPF_6$/EC-DMC and $LiPF_6$/PC, does not cause pitting and corrosion of aluminum. The surface remains effectively passivated by an aluminum oxide/oxyfluoride/hydroxy-fluoride layer.

ACKNOWLEDGMENTS

Last five years were incredible learning experience for me. It would not be possible without help, encouragement or simply good word from many people I have met during that time, and whom I would like to acknowledge.

I would like to thank my advisor, Dr. Greg Swain, for the guidance and support during my studies. Thank you, Sir, for giving me all this freedom and letting me learn on my own mistakes. This is, possibly, the best knowledge one can get.

I would also like to thank the present members of my committee: Dr. Bruening, Dr. Ayres, and Dr. Smith. Thank you for all the comments and suggestions concerning my research. I have special thanks to Dr. Brown, Dr. Bialkowski, Dr. Parker, and Dr. Dennison who served as my graduate committee during the three years at Utah State University. Thank you for all the help and scientific discussions, so important at the beginning of the graduate studies. I would also like to acknowledge Prof. Strojek, Dr. Zak, and Dr. Koppang for showing me a different way one can look at electrochemistry.

I would like to thank my wife, Gosik, for her love and support. Thank you for going with me through all the ups and downs during our first five years, from a teaching assistant workshop at USU, through winters of Michigan, to our first taste of Louisiana.

Special thanks belong to the former and the present members of the Swain's research group: Mike, Chen, Jishou, Jian, Shannon, Prerna, Grace, Gloria, Jason B., Jason S., Jin Woo, Show, Josef, Zuzka, and Doug. Thanks guys. I really appreciate your friendship

and, of course, a chance to taste good food from all over the world. JB, thanks for showing me that there is a hope for soccer fans in this country.

I would also like to thank Wiesia and Bogdan Juszczakiewicz for their friendship and providing this great home-like feeling so many thousands miles away from Poland.

Finally and most importantly, I would like to thank my family. Your love, faith and never-ending encouragement meant a lot to me during these years. Mom and Dad thank you for your wisdom. Thank you for sending me to college with a major goal in mind: to broaden my horizons. I am sure, I did. Thank you.

Mateusz

TABLE OF CONTENTS

LIST OF TABLES

LIST OF FIGURES

CHAPTER 1

1. Introduction

Corrosion/passivation of aluminum and its alloys in aqueous solutions has been one of the most widely studied problems in electrochemistry for several decades. This is not surprising considering the degree to which aqueous environments surround us and the importance of aluminum as a construction material in practically all areas of industry, transportation and every day life.[1] Unlike in aqueous environments, corrosion/passivation of aluminum in non-aqueous media has received much less attention in the literature. This situation began to change in recent years and can be credited, in part, to the use of aluminum as a current collector material for modern lithium-ion rechargeable batteries.[2-13] Other applications of aluminum and its alloys in non-aqueous media include aluminum batteries,[14-16] high performance electrolytic capacitors,[17-19] and tanks for alcohol-rich fuels.[20,21]

Since this work is focused on understanding processes that govern corrosion and passivation of aluminum in the electrolytes commonly employed in lithium-ion batteries, the aim of the following paragraph is to familiarize the reader with the concept of the lithium-ion battery and its importance in a modern, portability-oriented market. This is followed by discussion of the function of current collectors in a battery system, along with a description of the desired properties of current collector materials, in general, and

in lithium-ion batteries, in particular. In the next two paragraphs, a review of the literature regarding corrosion/passivation of aluminum in lithium-ion battery electrolytes and review of general mechanisms by which the metal can passivate in solution, are given. Finally, the outline of this dissertation is presented.

1.1. Lithium-ion battery

1.1.1. Overview

In the last few years, lithium rechargeable batteries have become a very popular and convenient energy source for portable electronics. Their success and ubiquitous nature is due to their low weight, small size, and high energy storage capacity. The properties of the Li-ion cells have improved over time, largely due to the introduction of materials that can serve as lithium intercalation hosts: carbon-type (amorphous coke or crystalline graphite) anodes, and lithiated metal oxide ($LiNiO_2$, $LiCoO_2$, $LiMn_2O_4$) cathodes. During operation, lithium ions migrate from the cathode to the anode. Such design eliminates the presence of metallic lithium and enhances cell stability, safety of operation, and the number of charge-discharge cycles that can be achieved. A schematic diagram of a lithium-ion battery during charging and the overall charge-discharge reaction are presented in Figure 1.1.

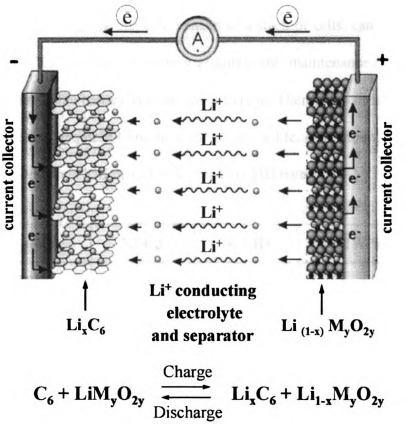

Figure 1.1. Schematic diagram of a lithium-ion rechargeable battery and illustration of the electrochemical processes occurring during charging. M stands for Ni, Co or Mn. Figure adapted from Megahed and Scrosati.[22]

Typical characteristics of the lithium-ion battery and other rechargeable batteries are presented in Table 1.1. It is clear that lithium-ion batteries provide some excellent features in comparison to other rechargeable battery systems. For example, the gravimetric energy density obtained from the lithium-ion cell is approximately twice that of the standard NiCd and ~ 1.5 times that of Ni-MH batteries. This means that products powered by lithium-ion batteries can be made lighter without sacrificing run time. The lithium-ion cell also provides very high cell voltage (3.6 V), which simplifies the

manufacturing process, since one cell, instead of a stack of cells, can be used to achieve desired voltage. The lithium-ion battery requires low maintenance, an advantage that most other rechargeable battery systems cannot claim. There is no memory effect, and no scheduled cycling is required to prolong the battery's life. In addition, the self-discharge capacity loss is less than half that of Ni-Cd and Ni-MH batteries.

	Ni-Cd	**Ni-MH**	**Lead Acid**	**Li-ion**
Gravimetric Energy Density, [Wh/kg]	45-80	60-120	30-50	110-160
Volumetric Energy Density, [Wh/dm^3]	110-180	180-300	80-110	220-360
Cell Voltage, [V]	1.2	1.2	2.0	3.6
Cycle Life	500-1500[a]	500-1000[a]	200-300[a]	500-1000
Self Discharge / Month[b]	15-20%	20-30%	<5%	5-10%
Overcharge Tolerance	moderate	low	high	very low
Peak Load Current[c]	20 C	5 C	5 C	2 C
Fast Charge Time, [h]	0.25-1	2-4	8-16	2-4

Table 1.1. Characteristics of commonly used rechargeable batteries. a – depends on regular maintenance; b – at room temperature; c – C-rate is a current that is numerically equal to the Ah rating of the cell. Data adapted from Buchmann.[23]

All these highly advantageous features have made lithium-ion batteries the fastest growing sector of the battery industry and led to their dominance in the portable electronics market (e.g., cell phones, notebooks, and camcorders). The use of Li-ion technology in other areas, such as power tools, electric vehicles, and medical and space

applications, has been limited, so far. This is due to the fact that despite its overall advantages, Li-ion technology has its drawbacks. First of all, Li-ion cells cannot be charged and discharged as quickly as Ni-Cd or Ni-MH batteries, which precludes their use in high-power applications, such as power tools and electric vehicles. Also, aging is a serious concern with most Li-ion batteries. Some capacity deterioration is commonly observed after one year, whether the battery is in use or not. After two to three years, the battery frequently fails. This considerably limits its use in medical and space applications.[4,23]

Therefore improvements are needed if lithium-ion batteries are to be successfully used in these advanced applications. A good understanding of the processes occurring in the battery, as well as the factors that influence its operation, is necessary if improvements are to be made. One of the most widely studied problems in the lithium-ion battery field over the last decade has been the capacity fade phenomenon.[24 and references therein]

1.1.2. Capacity fade phenomenon

Capacity fade is a general term used to describe all side reactions and processes that occur in a battery during operation and lead to a loss of capacity or premature failure of the battery system. These processes can occur during normal operation or result from abuse of the battery system by subjecting it to overcharge or overdischarge, a condition that is especially common in stacks of cells, where potentials of the individual cells cannot be controlled. Undesirable reactions that occur can involve both active materials (anode, cathode, and electrolyte) and cell hardware (current collectors, separators, and cell housing).

It is not surprising that there has been a significant interest in understanding capacity fade mechanisms. An extensive review of this subject was presented recently by Arora, White, and Doyle.[24] The authors described several undesirable processes that can lead to capacity fade. These include lithium deposition, electrolyte and solvent decomposition, phase changes in the insertion electrode materials, active material dissolution, current collector corrosion, and passive film formation over the electrode and current collector surfaces. Over time, these processes commonly lead to the loss of active material and an increase in the internal impedance of the cell. Figure 1.2 summarizes the various capacity fade processes. For clearer illustration of the conditions at which specific process usually occur, half-cell discharge curves are also presented in this figure.

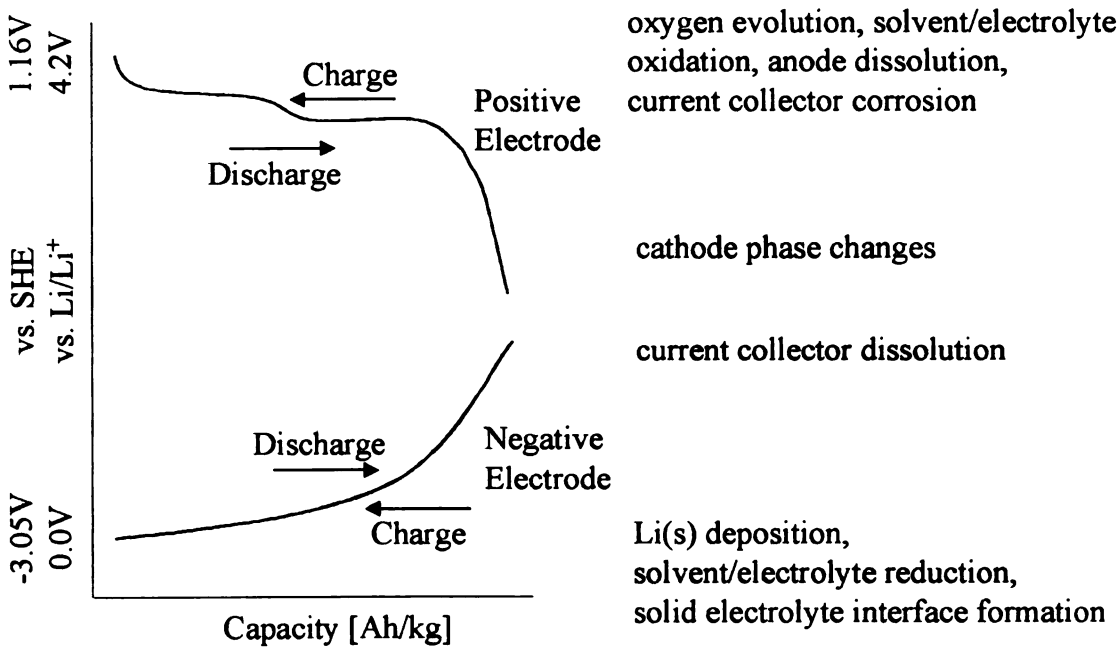

Figure 1.2. Half-cell discharge curves for a lithium-ion battery showing various capacity fade processes. Adapted from Arora *et al.*[24]

There is already much understanding of the capacity fade phenomena involving the cell active materials.[24 and references therein] This is not surprising since these are the components that determine the overall cell characteristics such as storage capacity, maximum voltage, and charge and discharge rates. However, much less is known about the capacity fade phenomena involving cell hardware, in general, and current collectors, in particular. More detailed understanding of these processes is needed. This is especially true for long-term applications of the lithium-ion batteries (space, medical, and military) as well as for introducing new, active materials that can operate at higher voltages. *This dissertation is exclusively focused on the mechanisms that lead to oxidation (formation of a passivation layer) and/or corrosion (pitting and metal loss) of aluminum current collectors in non-aqueous solvents/electrolytes.*

1.1.3. Current collectors

Current collectors are important hardware components, which serve two functions (see Figure 1.1). They act as a substrate for the active material and transfer charge to and from the material. Thus, current collectors must provide good adhesion for active material and offer low electrical resistance for charge transfer. Also, from the electrochemical point of view, the current collector must withstand the same potential extremes the active material does during charging and discharging, without any deterioration or corrosion over the cell life. Lastly, since the mass and volume of current collectors are included in the specific energy density, it is important that they are made in a thin-film form and have sufficient strength to withstand stresses generated during the cell fabrication.[24,25]

Selecting the right current collector material is a very important part of the battery design process. Failure to do so properly may lead to one of several undesirable reactions. These include electrolyte decomposition, passive film formation, and localized or general corrosion. In long-term applications, these unfavorable processes can affect the cell characteristics through an increase in the internal impedance during cycling, loss of adhesion between the active material and the current collector, changes in electrolyte composition and/or formation of corrosion products that can attack or passivate the active electrode materials. These phenomena are very harmful to the performance of the battery and often lead to premature failure of the whole battery system.[4,24,25]

Fulfilling the requirements for the current collector presents a special challenge in the case of lithium-ion batteries. This stems from two major facts: (*i*) the extreme reactivity of active materials used in lithium-ion batteries (e.g., lithium salts, lithiated metal oxides, lithium intercalated carbon) and (*ii*) extremes of the electrochemical potentials applied: 0 to 4.2 V vs. Li/Li^+, or - 3 to 1.2 V vs. NHE.

The negative electrode current collector must resist lithium insertion to form alloys, because alloy formation would deplete lithium from the electrode and also degrade the mechanical properties of the current collector. Copper is commonly used since it offers good resistance toward alloy formation with lithium at negative potentials. It is also relatively cheap, less harmful than other collector materials like nickel, highly conductive, and easily rolled into thin foils.[25,26]

On the other hand, the positive electrode current collector must be resistant to oxidation in the presence of the electrolyte anion. This is a difficult condition to satisfy, since the potential of the positive electrode is usually above the dissolution potential of

all the metals. Also, since electrolyte anions are designed for high solubility and dissociation of their lithium salts, they also form highly soluble salts with other metals (e.g., aluminum). The same is true for the solvent – a high donor number stabilizes not only lithium complexes, but metal salt complexes in general. Therefore, a passivating film is essential for metallic positive electrode current collectors. Aluminum is the most common choice due to its low cost, low density, ductility, and good resistance to oxidation due to the natural, protective oxide layer.[25]

1.2. Corrosion of aluminum in non-aqueous solvent/electrolyte mixtures commonly employed in lithium-ion batteries – literature review

Several investigations of the corrosion/oxidation of aluminum in Li-ion battery electrolytes have been performed in recent years. Both liquids and solid polymers have been tested as the supporting electrolyte. A considerable amount of research has been focused on understanding corrosion/passivation of aluminum in new lithium salts that could overcome the hydrolytic and thermal instability of $LiPF_6$, currently the most commonly used electrolyte.[5-8] These include lithium trifluoromethanesulfonate ($LiCF_3SO_3$), lithium tris(trifluoromethylsulfonyl)methide ($LiC(CF_3SO_2)_3$), and three members of the lithium imide family: lithium bis(trifluoromethylsulfonyl)imide ($LiN(CF_3SO_2)_2$), lithium (trifluoromethylsulfonylnonafluorobutylsulfonyl)imide ($LiN(CF_3SO_2)(C_4F_9SO_2)$), and lithium bis(pentafluoroethylsulfonyl)imide ($LiN(C_2F_5SO_2)_2$). Some researchers have investigated methods to suppress the corrosion/oxidation of aluminum in these and other electrolytes. For example, various

aluminum alloys, fluorocarbon-based polymeric coatings and electrolyte additives (e.g., HF) have been tested for this purpose. The following literature review highlights the crucial findings in the area of aluminum current collectors corrosion.

Kanamura *et al.* investigated the electrochemical reactions taking place on aluminum electrodes during anodic polarization in propylene carbonate (PC) containing 1M $LiClO_4$, $LiBF_4$ or $LiPF_6$.[2] Small oxidation currents (< 0.1 mA/cm^2) were observed during the potential sweep (50 mV/s) up to 5.5 V vs. Li/Li^+ in all three electrolytes. At higher potentials, the anodic current increased significantly in $LiClO_4$ (up to 1 mA/cm^2 at 6.5 V), whereas in $LiBF_4$ and $LiPF_6$, the currents remained below 0.2 mA/cm^2 and 0.1 mA/cm^2, respectively, up to 7 V vs. Li/Li^+. The results indicated that aluminum is most stable in $LiPF_6$. XPS analysis of the aluminum surface after potentiostatic polarization at 5.5 V in $LiPF_6$/PC revealed the presence of an AlF_3/Al_2O_3 layer. XPS of the aluminum surface polarized in $LiClO_4$/PC indicated the presence of an Al_2O_3 layer rich in ClO_4^- and Cl^-. The authors also investigated the resistance of PC toward oxidation using *in situ* FTIR spectroscopy. Spectra of the electrolyte solution, taken in the vicinity of the electrode, revealed the onset potentials for PC oxidation to be 5.2, 4.6, and 4.4 V for $LiPF_6$, $LiBF_4$, and $LiClO_4$, respectively. The oxidation was not significant, therefore the authors concluded that the anodic charge originated primarily from the oxidation of electrolyte and the aluminum surface. This was different from what they observed for a nickel electrode, at which the oxidation current corresponded well with extent of PC decomposition.[27]

Long-term studies of Al current collector corrosion were performed by Braithwaite and coworkers.[4] Aluminum current collectors were aged in $LiPF_6$/propylene carbonate-

diethyl carboate (PC-DEC) and $LiPF_6$/propylene carbonate-dimethyl carbonate (PC-DMC) by continuously applying a simulated electrical cycle analogous to that employed in low-earth-orbit (LEO) aerospace applications. Using impedance spectroscopy, the authors discovered that aluminum became more passive during cycling. XPS and Auger electron spectroscopy measurements indicated that Li was the predominant surface species. Also, twice as much surface F was observed than would be associated with the deposition of $LiPF_6$, suggestive of electrolyte decomposition. SEM studies of the surface structure revealed significant localized pitting. However, the pits were filled with corrosion products forming three-dimensional structures (nodules and mounds). The authors attributed the pitting to possible contamination of electrolyte/ solvent mixture with chloride, which is well known to induce pitting in aqueous environments.[1,28]

Krause *et al.* investigated the stability of aluminum in newly synthesized $LiN(C_2F_5SO_2)_2$ and $LiN(CF_3SO_2)(C_4F_9SO_2)$ electrolytes, and compared the behavior to that in $LiPF_6$, $LiCF_3SO_3$, and $LiN(CF_3SO_2)_2$.[5] Potentiostatic polarization of aluminum at 4.2 V vs. Li/Li^+ led to development of significant oxidation currents, in excess of 10 mA/cm^2, in $LiCF_3SO_3$/PC and $LiN(CF_3SO_2)_2$/PC, whereas in other three electrolytes (PC solvent), small, less than 10 $\mu A/cm^2$, oxidation currents were observed. Potentiodynamic cycling of aluminum electrodes showed evidence for pitting corrosion with protection or repassivation potentials increasing in the order of $LiCF_3SO_3$ (2.78 V) < $LiN(CF_3SO_2)_2$ (3.55 V) < $LiN(C_2F_5SO_2)_2$ (4.50 V) < $LiN(CF_3SO_2)(C_4F_9SO_2)$ (4.62 V). The authors related the increased stability of aluminum in heavier analogues of $LiN(CF_3SO_2)_2$ to the larger molecular size of the anion.

Improved passivation of aluminum in $LiN(CF_3SO_2)(C_4F_9SO_2)$/PC, as compared to $LiCF_3SO_3$/PC and $LiN(CF_3SO_2)_2$/PC, was also observed by Kanamura *et al.*[6] The results of potentiodynamic cycling, XPS analysis, and *in situ* FTIR showed that aluminum corrodes significantly at potentials more positive than 3.8 V vs. Li/Li^+ in either $LiCF_3SO_3$/PC and $LiN(CF_3SO_2)_2$/PC. Both solvent and electrolyte decomposition were also observed at such conditions. In $LiN(CF_3SO_2)(C_4F_9SO_2)$/PC, aluminum was stable up to 4.6 V. The authors attributed the improved passivation properties of the $LiN(CF_3SO_2)(C_4F_9SO_2)$ salt to better distribution of negative charge on the anion, which can stabilize the aluminum surface more efficiently.

Yang *et al.* used the electrochemical quartz crystal microbalance (EQCM) to study aluminum corrosion in electrolytes encountered in present and possible future lithium-ion batteries, including $LiPF_6$, $LiBF_4$, $LiClO_4$, $LiCF_3SO_3$, $LiC(CF_3SO_2)_3$, and $LiN(CF_3SO_2)_2$.[7] They found that the aluminum, with its protective oxide film intact, is relatively corrosion-resistant in these electrolytes. Mechanical damage of the oxide film leads to significant corrosion in PC containing $LiCF_3SO_3$, $LiC(CF_3SO_2)_3$, and $LiN(CF_3SO_2)_2$. The authors observed a decrease of the electrode mass during anodic polarization up to 5 V vs. Li/Li^+ in each of these electrolytes. More detailed EQCM studies of aluminum corrosion in $LiN(CF_3SO_2)_2$/PC revealed that the corrosion process involves the formation of an adsorbed aluminum compound or film that subsequently desorbs. The authors also found that potentiodynamic polarization of aluminum in $LiPF_6$/PC and $LiBF_4$/PC leads to formation of a protective film after the first potentiodynamic scan. An increase in the electrode mass was observed in such cases. In $LiClO_4$/PC, formation of the oxidation product layer was also observed during the first

potentiodynamic scan. This layer did not, however, prevent surface oxidation during subsequent scan.

Walker, Cox and Salomon studied the stability of $LiC(CF_3SO_2)_3$/EC-DMC-MF (EC-DMC-methyl formate) on aluminum, platinum and glassy carbon electrodes.[8] Results of potentiodynamic polarization up to 4.3 V vs. Li/Li^+ indicated that the electrolyte is most stable at aluminum as the lowest oxidation currents were observed. The authors attributed this stability to the formation of a passivation layer on the aluminum surface.

Behl and Plichta used controlled potential coulometry to investigate aluminum degradation in electrolytes composed of an EC/PC/DMC (20:20:60 vol.%) mixture and $LiN(CF_3SO_2)_2$ and $LiC(CF_3SO_2)_3$.[9] They observed that aluminum foils were quite stable in the $LiC(CF_3SO_2)_3$ solution at potentials up to 4.5 V vs. Li/Li^+, but underwent severe corrosion in $LiN(CF_3SO_2)_2$ below 3.5 V vs. Li/Li^+.

An interesting approach toward understanding corrosion/passivation of aluminum in the $(CF_3SO_2)_2N^-$ (Im^-) and $(C_2F_5SO_2)_2N^-$ ($Beti^-$) was taken by Goldman and McEwen.[10] The authors compared the electrochemical properties of these two anions in solvent-free ionic liquids created with the 1-ethyl-3-methyl imidazolium (EMI) cation: EMIIm and EMIBeti. They found that aluminum passivates easily in both neat ionic liquids. Similar oxidation currents were recorded in both EMIIm and EMIBeti. The addition of 10% of propylene carbonate (PC) to either of the ionic liquids had a dramatic effect on aluminum sability. A significant increase in the oxidation current was observed, with the EMIIm being more corrosive than EMIBeti. These results implicate PC as active participant in the corrosion process, at least in these electrolytes. The authors could not, however, determine whether or not the increased corrosion observed in the presence of

PC is due to the solubility of the passivating layer in this solvent, or if the PC is directly involved in the corrosion process.

Corrosion of aluminum current collectors in polymer electrolytes was also studied.[11-13] Munshi and coworkers reported serious corrosion of aluminum current collectors in Li/$(PEO)_8$-$LiCF_3SO_3/V_6O_{13}$) during battery overcharging.[11] The results of Choe et al. showed that aluminum substrates are stable up to 4.2 V vs. Li/Li^+ in polyacrylonitrile-based (PAN) electrolytes containing $LiAsF_6$ and $LiPF_6$, and only up to 3.7 and 3.5 V with $LiN(CF_3SO_2)_2$ and $LiCF_3SO_3$, respectively.[12] Chen et al. investigated the corrosion susceptibility of aluminum current collectors in Li/(PEO)-$LiN(CF_3SO_2)_2/V_2O_{13}$ or TiS_2 cells, during anodic polarization.[13] The authors observed that aluminum is resistant to uniform corrosion. It, however, undergoes localized pitting during overcharge conditions (4 V vs. Li/Li^+), as was shown through SEM studies. The authors also found that aluminum evaluated in a standard electrochemical cell is less prone to the corrosion than when used in a real battery, polarized at the same conditions. They have attributed this to inhomogeneous current flow through the current collector in the battery (e.g., due to the non-uniform electrical resistance of the cathode material), which leads to local breakdown of the passive film on aluminum at sites of locally high current density. This was a very important finding, indicating that if susceptibility of aluminum toward corrosion is evaluated in an electrochemical cell, it should be investigated at potentials higher than overcharge conditions in order for the results to be meaningful.

Some researchers also investigated various methods to suppress the corrosion of aluminum. One of the proposed approaches involves the use of multi-component electrolytes. For example, Behl and Plichta reported that the addition of $LiBF_4$ to 1M $LiN(CF_3SO_2)_2$/EC-PC-DMC significantly reduces the corrosion current observed during potentiostatic polarization of aluminum.[9] They found that complete passivation of aluminum occurs when the concentration of $LiBF_4$ is higher than 0.5M. A steady state oxidation current of less than 10 $\mu A/cm^2$ was observed in 1M $LiN(CF_3SO_2)_2$/EC-PC-DMC with 0.5M $LiBF_4$, at 4.5 V vs. Li/Li^+. This current was two orders of magnitude lower than the one measured in solution without $LiBF_4$.

A similar beneficial effect of added $LiBF_4$ and $LiPF_6$ on the stability of aluminum in $LiN(CF_3SO_2)_2$/PC was observed by Yang et al.[7] The authors learned that aluminum passivates in the 0.5M $LiBF_4$ (or 0.5M $LiPF_6$) + 0.5M $LiN(CF_3SO_2)_2$ in PC, and that the passivation layer is formed from $LiBF_4$ (or $LiPF_6$) as the W/z (molecular weight to charge ratio) obtained from the EQCM measurements were the same as for pure 1M $LiBF_4$/PC or 1M $LiPF_6$/PC.

Other authors investigated the role of additives and anti-corrosion coatings to improve the stability of aluminum. Kanamura *et al.* studied the effect of low levels of HF (0.01 mol/dm^{-3}) on the behavior of aluminum in $LiCF_3SO_3$/PC and $LiN(CF_3SO_2)_2$/PC.[6] The authors observed improved passivation in the presence of HF in both electrolytes. XPS data showed the presence of a fluorine-rich passivation layer on the surface, suggestive of the conversion of native Al_2O_3 to AlF_3 and AlOF. The composition of this layer was independent of the electrolyte type, which implies that it was formed solely from the HF additive. In another study, Braithwaite et al. investigated the effect of low

levels of water impurity (20 ppm) on the long-term stability of aluminum in 1M $LiPF_6$/PC-DEC.[4] Based on impedance data, the authors observed improved passivation in the presence of water. In their studies, they also evaluated the influence of two types of carbon-fluorocarbon-based conductive coatings on the corrosion resistance of aluminum in 1M $LiPF_6$/PC-DEC. They found improved corrosion resistance, which they attributed to sealing of the aluminum surface by coating.

Another approach to reduce the corrosion rate of aluminum was investigated by Chen and coworkers.[13] These researchers proposed the use of a tungsten-aluminum alloy as the current collector material. They found that aluminum surfaces impregnated with ~20 atom % tungsten, by ion implantation, exhibited enhanced resistance to pitting corrosion in poly(ethylene oxide)/$LiN(CF_3SO_2)_2$.

1.3. Passivation of metals in solution – review of possible mechanisms

The mechanisms by which a metal can passivate in solution were reviewed by Kelly and Moran, and can be classified into four types: (1) air formed film, (2) salt film, (3) chemisorption of the solvent, and (4) oxide/oxyhydroxide formation.[29] For a metal to passivate by mechanism 1, the air-formed film must be stable in the solution under the experimental conditions, and thereby form a barrier to corrosive attack of the metal. The type 2 passivation mechanism requires active dissolution of a metal surface at a high enough rate that supersaturation in the solution boundary layer near the metal surface occurs, with respect to the salt composed of the metal cations and electrolyte anions. This salt then precipitates onto the surface to form an adherent, protective layer. The

protective ability of the salt film depends strongly upon its solubility and rate of dissolution. Lower solubility and dissolution rates require lower metal oxidation charge to flow to replace the metal lost by dissolution, thus providing better passivation. When a metal passivates by mechanism 3, solvent molecules must attach to the metal surface irreversibly by either chemical or electrochemical adsorption. Presumably, this adsorbed film protects the metal by raising the activation energy for metal dissolution. The chemical adsorption process typically results in only monolayer coverage and is limited to potentials below the solvent oxidation. Finally, for a metal to passivate by mechanism 4, a source of oxygen atoms must be present in solution, either in the form of atoms, molecules, or some anions containing oxygen. Either through direct chemical reaction, or via an electrochemical reaction, oxygen or oxygen containing anions bind to metal cations at the surface, forming an adherent, three-dimensional oxide/oxyhydroxide film. This last mechanism is the one by which most metals are thought to passivate in aqueous solutions, with water providing the oxygen atoms. However, in anhydrous organic solutions this mechanism is unlikely due to the fact that even if oxygen is present as a structural component of organic solvent, it is strongly bound to the carbon atom(s) and therefore cannot readily participate in the formation of an oxide film. All four mechanisms are presented schematically in the Figure 1.3.

(1) air-formed film

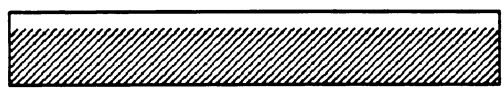

(2) salt film formation

$M \rightarrow M^{n+} + ne^-$

$mM^{n+} + nA^{m-} \rightarrow M_m(A)_n\downarrow$

(3) solvent adsorption

$(solv) \rightarrow (solv)_{ads}$

$(solv) \rightarrow (solv)_{ads} + e^-$

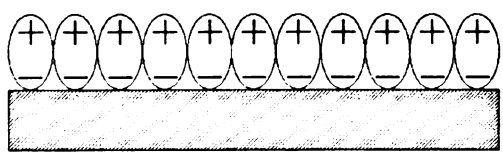

(4) oxide/oxyhydroxide formation

$M \rightarrow M^{2n+} + 2ne^-$

$M^{2n+} + nH_2O \rightarrow MO_n\downarrow + 2nH^+$

$M^{2n+} + 2nH_2O \rightarrow M(OH)_{2n}\downarrow + 2nH^+$

Figure 1.3. Schematic diagrams of possible passivation mechanisms for metal (M) in a solution.[29]

Work by Scanlon, Kruger and Moran on the passivation of iron in 0.5M $LiAsF_6$/dimethoxyethane, indicated a fifth possible passivation mechanism - electropolymerization of the solvent.[30] The authors showed that significant suppression of corrosion can occur if a layer of polymerized solvent forms on the metal surface. However, as pointed by the authors, this mechanism is limited to a select few solvent/electrolyte/metal systems and, thus, should not be treated as general passivation mechanism in non-aqueous environments.

A very good example of how different mechanisms may provide passivity to the metal surface is the work by Kelly *et al.* on the passive behavior of iron in 0.5M $LiClO_4$/PC.[31] The authors showed that under different circumstances, competition between different mechanisms of passivation or a domination of one of the mechanisms, may occur. They observed that in anhydrous (< 1 ppm) PC solutions, below the oxidation potential of PC, bare Fe passivated via oxidative chemisorption of solvent molecules. However, at potentials above 3.6 V vs. Li/Li^+, PC was oxidized to CO_2, and therefore adsorbed solvent film did not provide protection to the metal surface anymore. At this point bare Fe remained passivated through the formation of salt film composed of $Fe(ClO_4)_2$. The presence of this film was confirmed by both x-ray microanalysis and XPS. They also observed that the air-formed film on the metal surface provided a protection over the wide range of potentials. High stability of the air formed film was attributed to the lack of aggressive species in anhydrous solution. The authors postulated that adsorbed solvent film formed on the top of the air-formed film during anodic polarization, although they could not directly prove their postulate.

1.4. Outline of the dissertation

This dissertation is devoted to understanding the mechanisms that lead to oxidation (formation of a passivation layer) and/or corrosion (pitting and metal loss) of aluminum in non-aqueous electrolytes commonly used in lithium-ion batteries. Important parameters studied include the role of the electrolyte type (e.g., $LiClO_4$ vs. $LiPF_6$), the organic solvent type (e.g., propylene carbonate (PC) vs. a mixture of dimethyl carbonate and ethylene carbonate (DMC-EC)), the effect of water contamination (50-2000 ppm), and the physicochemical properties of the aluminum surface (e.g., bare vs. oxide coated). An overview of each chapter is given below along with a synopsis of the findings.

A description of the experimental setup and protocols used during the measurements is presented in Chapter 2. Chapter 3 describes potentiodynamic and potentiostatic examination of the susceptibility of aluminum to corrosion/passivation in dry (<50 ppm H_2O) $LiClO_4$/EC-DMC, $LiClO_4$/PC, $LiPF_6$/EC-DMC, and $LiPF_6$/PC. It was determined that aluminum passivates well in all four electrolyte/solvent mixtures. XPS analysis of the surfaces revealed that passivation occurs through different mechanisms depending on the electrolyte. The results presented in that chapter serve as a comparison for the data presented in Chapter 4, which reflect a study of the effect of water contamination of the solvent on the corrosion/passivation process.

In Chapter 4, the effect of water contamination on the corrosion/passivation of the aluminum in $LiPF_6$/EC-DMC, $LiPF_6$/PC, $LiClO_4$/EC-DMC, and $LiClO_4$/PC is presented. Controlled water additions of 50 – 2000 ppm were investigated. It was determined that water does not have a significant influence on corrosion in $LiPF_6$, as the aluminum

surface remains passivated, even in the presence of relatively high (500 ppm) water levels. On the other hand, the presence of water is detrimental to the passivation of aluminum in $LiClO_4$. Electrochemical and microscopic (optical microscopy and scanning electron microscopy) measurements showed evidence of significant surface pitting. Raman spectroscopy and energy dispersive x-ray analysis (EDS) indicated that $Al(ClO_4)_3$ is the major corrosion product.

Chapter 5 presents results of a detailed examination of the passivation and/or corrosion of aluminum using *in situ* and *ex situ* atomic force microscopy (AFM). The formation of a solid passivation layer was observed in all dry solvent/electrolyte mixtures. Roughening of the electrode surface was observed in $LiPF_6$, when water was present. It was also found that pitting in $LiClO_4$ solutions containing water leads to formation of either mounds (pits filled with corrosion products) or empty pits, depending on the amount of water present. Mounds were observed when the water level was below 500 ppm, whereas empty pits were found at higher water levels.

Chapter 6 examines the corrosion of aluminum in $LiPF_6$/EC-DMC and $LiClO_4$/EC-DMC with *in situ* electrochemical quartz crystal gravimetry (EQCM). Correlations between electrochemical charge and corresponding electrode mass change were used to determine the products of the corrosion/passivation processes. Finally, a summary of all the data is given in the Chapter 7.

CHAPTER 2

2. Experimental Section

2.1. Preparation of aluminum electrodes

Aluminum discs (9.5 or 14 mm in diameter) were cut from high purity foil (1 mm thick, 99.999%, Goodfellow Cambridge Ltd.) with a bench press and ferrule. The discs were cleaned by rinsing with hexane, acetone, methanol, and deionized water. One side of each disc was then either mechanically polished in hexane, or mechanically polished and electropolished in order to obtain a low-oxide or oxide-coated surface, respectively.

2.1.1. Mechanical polishing

The discs were mechanically polished in hexane using successively finer silicon carbide (SiC) polishing paper (320, 600, 1200, 2000 grit). Each polishing step was followed by a 10 min sonication in hexane. The discs were then transported to an Ar-purged glove box for a final polish with a 2000 grit SiC paper. After the final polish, the discs were soaked in hexane inside a sealed container, taken out of the glove box for a 15 min sonication, and placed back inside a glove box for electrochemical evaluation.

2.1.2. Electropolishing

Prior to electropolishing, the discs were mechanically polished, as described above, to remove the native oxide film and decrease the surface roughness. Electropolishing was

performed in a 3% aqueous solution of HBF_4, at a constant current - a procedure adapted from an Alzak commercial electropolishing process.[32] No solution stirring was involved. The disc was mounted in a home-built Teflon® cell by means of a Viton® o-ring and spring loaded clamp. The disc served as the anode and was placed in parallel to a cathode made from high purity aluminum foil. The distance between the electrodes was 25 mm. Constant current polarization was conducted in two steps, first at 36 mA/cm^2 for 30 min and then at 9 mA/cm^2 for 10 min. The constant current was applied using a HP 6209B DC power supply (Hewlett-Packard, Rockville, MD), and the potential difference between the electrodes was monitored with a Servogor 124 strip chart recorder (NGI Norma Goerz Instruments GmbH, Austria). After electropolishing, the discs were rinsed with deionized water, soaked in KOH (7.5% w/w; 20 s) and H_2SO_4 (30% w/w; 30 s), thoroughly rinsed with deionized water and dry ethanol, soaked in dry ethanol for 30 min, rinsed with hexane, and stored in hexane until use.

2.2. Surface characterization techniques

Changes in the aluminum surface morphology brought about by the imposed electrochemical conditions were studied *ex-situ* with optical microscopy (OM), atomic force microscopy (AFM), and scanning electron microscopy (SEM). Changes in the morphology were also studied *in situ* with electrochemical optical microscopy (ECOM) and electrochemical atomic force microscopy (ECAFM). The chemical composition of the surface, before and after polarization, was investigated with energy dispersive x-ray microanalysis (EDS), x-ray photoelectron spectroscopy (XPS) and Raman spectroscopy.

2.2.1. Atomic force microscopy (AFM)

The atomic force microscopy (AFM) was performed with a Nanoscope IIIa instrument (Digital Instruments, Veeco Metrology Group; Santa Barbara, CA) in the contact mode. Si_3N_4 tips mounted on gold cantilevers (200 μm legs, 0.12 N/m spring constant) were used to acquire topographical images in air. Two types of data were collected for each image: height and deflection. Height data are recorded at constant cantilever deflection and correspond to the change in piezo height. They were used for determination of height of the structures present on aluminum surface. Deflection data, on the other hand, are collected at constant piezo position and come from the differential signal of the top and bottom photodiode segments. They provide a sensitive edge-detection technique.

ECAFM was performed with a Nanoscope II microscope (Digital Instruments, Veeco Metrology Group; Santa Barbara, CA). Images were collected in the contact mode with Si_3N_4 tips mounted on gold cantilevers (100 μm legs, 0.58 N/m spring constant). A commercial electrochemical fluid cell (Digital Instruments) was employed, which consisted of a glass body, a silicone o-ring, an aluminum disc working electrode, a Li/Li^+ reference electrode, and platinum wire counter electrode. The geometric area of the exposed disc was 0.4 cm^2. The microscope head was placed inside a glove box specially designed for the ECAFM studies, which was constantly purged with N_2 allowing removal of water down to the 500 ppm level (procedure for determination of water content inside a glove box is described in paragraph 2.6.2.). A Li/Li^+ reference electrode, protected from direct contact with N_2, was constructed. It consisted of the polyethylene body, a glass wool plug, a piece of lithium metal, a nickel wire as a contact to lithium,

and a "hot glue" seal. The electrode was assembled inside an Ar-filled glove box and stored in vial with the specific electrolyte solution. The typical equilibrium potential of this reference electrode was within 5 mV of freshly scratched lithium rod in the same electrolyte solution.

Figure 2.1 shows pictures of (A) the entire ECAFM experimental setup, (B) liquid cell, and (C) a schematic diagram of how the Li/Li^+ reference electrode was prepared.

2.2.2. Optical microscopy (OM)

Optical micrographs of the aluminum discs were obtained using an Olympus BH-2 microscope supplied with a DP11 digital camera (1712 x 1368 pixels). 10x and 80x objectives were used giving total magnifications of 300x and 2400x, respectively. Images of at least three different, most representative spots on aluminum surface were collected.

For the ECOM work, the microscope was placed inside an Ar-filled glove box (Coy, Grass Lake, MI; < 100 ppm H_2O). The measurements were performed in a specially designed, home-built cell, which consisted of a Teflon® base and body, a glass optical window and a 4-screw metal clamp (Figure 2.2). The aluminum disc was mounted on the bottom of the cell using a Chemraz® o-ring. The geometric area of the exposed surface was ~ 0.4 cm^2, and the cell volume was approximately 0.1 cm^3. A platinum wire served as the counter electrode and freshly scratched lithium rod was used as the reference electrode.

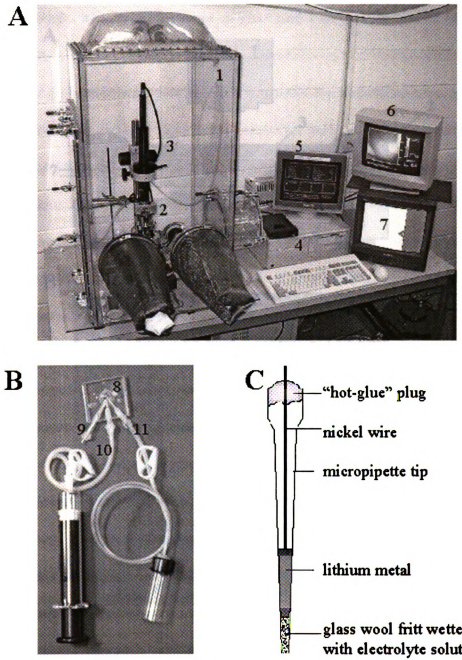

Figure 2.1. (A) Experimental setup for the ECAFM measurements including, 1 – glove box; 2 – ECAFM microscope head; 3 – optical microscope; 4 – computer with monitors 5 & 6; 7 – optical microscope monitor. (B) 8 – ECAFM fluid cell; 9 – Li/Li^+ reference electrode; 10 – solution inlet with syringe; 11 – solution outlet with built-in Pt-wire auxiliary electrode and collection vessel. (C) Schematic diagram of how the Li/Li^+ reference electrode was prepared.

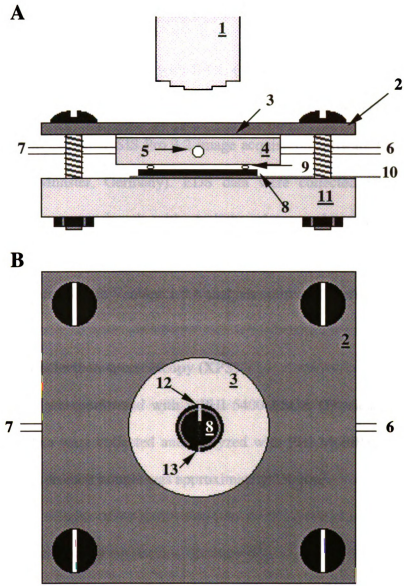

Figure 2.2. Diagram of the electrochemical cell used for the *in-situ* optical microscopy. (A) side view and (B) top view. 1 – microscope objective lens; 2 – metal clamp with screws; 3 – optical window; 4 – Teflon® body; 5 – lithium reference electrode port; 6 – solution inlet; 7 – solution outlet; 8 – aluminum disc electrode; 9 – Chemraz® o-ring; 10 – copper current collector; 11 – Teflon® base; 12 – lithium reference electrode; and 13 – platinum wire counter electrode.

2.2.3. Scanning electron microscopy (SEM) and energy dispersive x-ray micro-analysis (EDS)

SEM and EDS were performed with JEOL-6400V electron microscope. SEM images were collected at a 2048 x 1536 pixel resolution with an ADDA II digital image acquisition system and AnalySIS Pro 3.2 image acquisition software (both Soft Imaging System GmbH, Munster, Germany). EDS data were collected with a Vantage DI microanalysis system equipped with a light element detector (ThermoNORAN, Middletown, WI). A 30° take off angle and 20 kV accelerating voltage were used. Data analysis was performed with Vantage 1.5.1 analysis software (ThermoNORAN).

2.2.4. X-ray photoelectron spectroscopy (XPS)

XPS analysis was performed with a PHI 5400 ESCA (Physical Electronics, Eden Prairie, MN). Data were collected and analyzed with PHI MultiPak V 6.0A software. The area analyzed on each sample was approximately 250 μm^2.

2.2.5. Raman spectroscopy

Raman spectra were obtained in a back-scattered collection mode with a Raman 2000 spectrometer equipped with a 2080 Raman Microprobe attachment and a 2090 Direct Video Module (all from Chromex, Inc., Albuquerque, NM). The intermediate resolution 1200 grove/mm grating was used. The excitation light was from a frequency doubled Nd-YAG laser (30 mW, 532 nm), focused to a spot size of approximately 5 μm. This yielded an estimated power density of 150 kW/cm^2. Spatial distribution of the Raman features was accomplished using an in-line imaging mode. In this mode, the laser

light was focused into a line ~60 μm in length and ~2 μm in width. The estimated power density in line-imaging mode was 25 kW/cm^2. Spectra were collected every 1μm along the line.

2.3. Electrochemical measurements

The cyclic voltammetric (potentiodynamic) and potential step (potentiostatic) measurements were performed using a CS-2000 computerized potentiostat (Cypress Systems, Inc., Lawrence, KS). Open circuit potentials were recorded with either the CS-2000 potentiostat or with a Servogor 124 strip chart recorder (NGI Norma Goerz Instruments GmbH, Austria) that was fitted with an operational amplifier (CA3140A, Intersil) in a voltage follower configuration, in order to increase the input resistance to 1.5 TΩ.

All electrochemical measurements were made in a single compartment, glass cell. Freshly scratched lithium rods (98+%, Aldrich) were pressed against nickel wires and served as the auxiliary and reference electrodes. The aluminum disc working electrode was mated to the bottom of the cell with a Chemraz® 514 o-ring (Ace Glass, Inc.) and a metal clamp. The geometric area of the exposed electrode was 0.2 cm^2, and all currents reported are normalized to this area. The cell was assembled and operated in an Ar-purged glove box (Coy, Grass Lake, MI) with a moisture level below 100 ppm.

2.4. Electrochemical quartz crystal microbalance (EQCM)

Electrochemical quartz crystal microbalance (EQCM) studies were performed with EQCN-701 quartz crystal microbalance and a PS-205B potentiostat (both Elchema, Potsdam, NY). The system was interfaced to a PC using an AT-MIO-16X, 16-bit data acquisition card (National Instruments, Austin, TX) and Voltscan software (Elchema). All measurements were conducted in a single compartment, home built, Teflon® cell. 10 MHz, commercially-available quartz crystals, with aluminum evaporated on the surface (Elchema), were used as the working electrode. A theoretical mass sensitivity of 4.4 ng/Hzcm^2 was possible with these crystals. The quartz crystal resonator was mated to the bottom of the cell with two silicone o-rings (Digital Instruments, Santa Barbara, CA) and a spring-loaded clamp. The piezoelectrically-active area of the crystal was determined by size of the metal electrodes deposited on the surface and was equal to ~ 0.2 cm^2. The electrochemically-active area was determined by the silicone o-ring and matched piezoelectrically-active area. All currents reported were normalized to the 0.2 cm^2 area. Freshly scratched lithium rods were pressed against nickel wires and served as the auxiliary and reference electrodes. The cell was assembled and operated in an Ar-purged glove box (Coy, MI) with a moisture level below 100 ppm. A scheme of the experimental setup is presented in Figure 2.3.

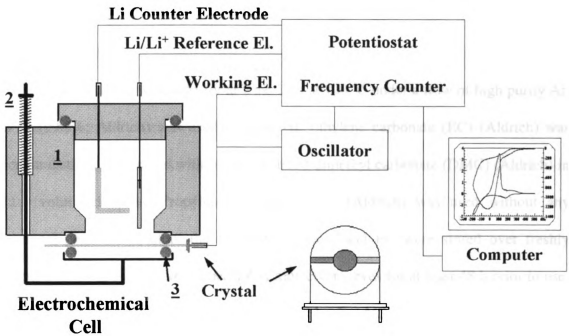

Figure 2.3. The EQCM experimental setup including, 1 – Teflon cell; 2 – spring-loaded clamp; and 3 – silicone o-ring.

The instrument was validated using the reversible electrodeposition of Cu on Au. This was done by potentiodynamic cycling of the gold QCM electrode (Elchema) at 50 mV/s in 5 mM $Cu(NO_3)_2$ + 0.1 M HNO_3 from 500 mV to –200 mV vs. Ag/AgCl. The charge recorded during the deposition was equal to the stripping charge with a value of 650 μC. Using a value of n = 2, the deposition charge corresponds to deposition of 214 ng of Cu. This value is in good agreement with the 218 ng value calculated from the measured frequency change, using the Sauerbrey equation (see Chapter 6, Eq. 6.1).

2.5. Chemicals

$LiClO_4$ (Aldrich) was dried for at least 12 h at 120°C under a flow of high purity Ar. $LiPF_6$ (99.9%; Aldrich) was used as received. Ethylene carbonate (EC) (Aldrich) was vacuum distilled and mixed with freshly distilled dimethyl carbonate (DMC) (Aldrich) in a 1:1 volumetric ratio. Propylene carbonate (PC) (Aldrich) was used without any additional purification. Both the EC:DMC mixture and PC were stored over freshly activated (500°C, 5 h, Ar atmosphere) 4 Å molecular sieves for at least 48 h prior to use. The water content in the solvents was measured by GC-MS (Hewlett-Packard G1800B, with EI detector). Standard additions of water to the solvent were made and the intensity of m/z = 18 signal was monitored. The water content was estimated to be < 50 ppm in both solvents.

1 M solutions of electrolytes in organic solvents were prepared in a N_2-purged glove box (Coy, Grass Lake, MI). The glove box atmosphere was constantly circulated through a drying column filled with Drierite (W. A. Hammond Drierite Company, Xenia, OH). The humidity inside the glove box was maintained below 500 ppm. After preparation, the solutions were purged with Ar for 30 min and tightly sealed in containers. The containers were then transferred to the Ar-filled glove box and placed inside a dessicator until use in the electrochemical measurements.

2.6. Remaining information

2.6.1. Data analysis and plotting

Mathematical operations on numerical data and plotting of numerical data were performed using PSI-Plot 4.57 data analysis software (Poly Software International, Salt Lake City, UT).

2.6.2. Determination of water content inside glove boxes

The relative humidity (RH; [%]) inside the glove boxes was measured using a CMM80 digital thermohygrometer (Mannix, Lynbrook, NY). Assuming an atmospheric pressure of 1 atm, the estimated water content (C_w; [ppm]) was calculated according to the following equation:

$$C_w = RH \cdot p_w \cdot 10^4$$

where p_w is a water vapor pressure (0.023 atm, at 20°C).[33]

CHAPTER 3

3. Electrochemical Investigation of the Corrosion/Passivation of High-Purity Aluminum in $LiClO_4$/EC-DMC, $LiClO_4$/PC, $LiPF_6$/EC-DMC, and $LiPF_6$/PC

3.1. Introduction

In the last few years, lithium rechargeable batteries have become a popular and convenient energy source for portable electronic devices. Their success and ubiquitous nature is due to their low weight, small size, and high-energy storage capacity. Due to these highly attractive attributes, there is considerable interest in using the lithium-ion technology for new applications such as electric vehicles, medical devices, and space technology. These new applications require batteries that are reliable over prolonged periods of time. Therefore, the long-term stability of all battery components becomes an issue. Corrosion of current collectors is of particular importance, considering their role in the rechargeable battery systems. The current collector serves two major functions. It acts as a substrate for the active electrode material, and transfers charge to and from the material. The current collector must offer low resistance to charge transfer, provide good adhesion for active material, and be sufficiently durable to withstand the stresses produced during the battery fabrication. It also, from an electrochemical point of view,

must withstand the same potential extremes the active material does during charging and discharging, without any deterioration or corrosion over the cell life.

Aluminum and copper are the most commonly used current collector materials for the positive and negative electrodes, respectively, in lithium-ion batteries. Aluminum is used mainly because of its low cost, low density, ductility, and good resistance to oxidation due to its natural, protective oxide layer. Copper, on the other hand, besides being inexpensive and ductile, offers good resistance toward the formation of alloys with lithium at negative potentials. Unfortunately, both copper and aluminum are prone to corrosion and/or oxidation in the electrolyte/solvent mixtures typically used in lithium-ion batteries.[24,25 and references therein]

Several investigations of the corrosion/oxidation of aluminum in non-aqueous electrolytes have been performed. Both liquids[2-10] and solid polymers[11-13] have been tested as the supporting electrolyte. Much attention has also been paid to several new electrolyte salts that might overcome the hydrolytic and thermal instability of $LiPF_6$, which is currently the most commonly used electrolyte. These new salts include $LiCF_3SO_3$, $LiN(CF_3SO_2)_2$ and $LiC(CF_3SO_2)_3$.[5-7,9,10] In general, considering the state of the aluminum electrode surface after anodic polarization, results from these studies can be classified in two ways: (i) pitting corrosion or (ii) surface passivation.

This chapter examines the corrosion/oxidation of high purity aluminum (99.999%) in $LiPF_6$/EC-DMC, $LiPF_6$/PC, $LiClO_4$/EC-DMC, and $LiClO_4$/PC. Testing was performed using two different metal surfaces, (i) aluminum with the native oxide film removed by mechanical polishing under an inert, argon atmosphere, and (ii) aluminum, first

mechanically polished, and then electropolished in an aqueous solution of HBF_4. The second surface preparation was chosen to mimic the oxide film that likely forms during fabrication of commercial batteries. Aluminum current collectors in the batteries are commonly pretreated by acid-base etching to improve the adhesion of the active cathode material with the surface.[24] Electropolishing was also chosen because it produces a very smooth and reflective surface, which was necessary for the AFM measurements discussed in Chapter 5. Electrochemical techniques, including cyclic voltammetry (CV), chronoamperometry (CA), and open circuit potential measurements (OCP) were used to asses the susceptibility of aluminum toward corrosion/passivation in each of the electrolyte/solvent mixtures. X-ray photoelectron spectroscopy (XPS) was used to study the elemental composition of any passivating film formed during electrochemical polarization.

3.2. Results and discussion

3.2.1. Pretreatment and characterization of Al electrodes

The Al disc electrodes were either mechanically polished in hexane under a blanket of Ar or electropolished prior to evaluation, as described in Chapter 2. Figure 3.1 A-D presents contact mode AFM images of the (A) as received, (B) mechanically polished, and (C, D) electropolished aluminum surfaces. It is evident that both polishing methods smooth the as received surface. For example, the surface roughness decreased from greater than 150 nm over a 100 μm^2 area for the as received aluminum, to less than 40

nm for the mechanically polished surface, and to less than 3 nm for the electropolished surface.

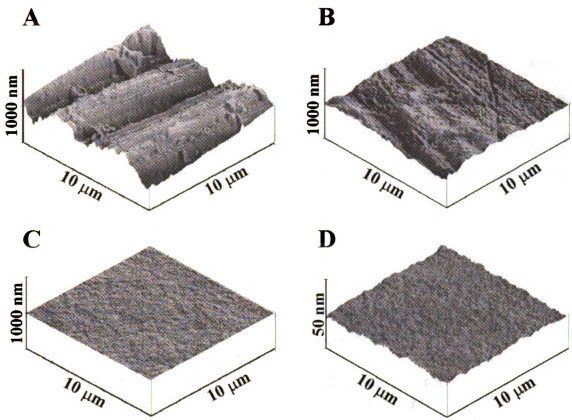

Figure 3.1. AFM images of aluminum surfaces (A) as received, (B) after mechanical polishing, (C) after electropolishing, and (D) after electropolishing with enhanced z-axis as compared to (C).

XPS analysis of the mechanically polished surface revealed the presence of Al (2p, 74.5 eV) and O (1s, 532 eV) peaks with an atomic ratio of O/Al = 1.6, consistent with Al_2O_3 (O/Al = 1.5). A lower binding energy Al (2p, 71 eV) peak, consistent with Al

metal, was also observed. Thus, the Al_2O_3 film thickness must be less than 10 nm, as this is a typical escape depth for the photoelectrons in the instrument used. XPS analysis of the electropolished surface also revealed the presence of an Al_2O_3 layer (O/Al = 1.6). The film thickness was estimated to be 5-10 nm, based on a depth profiling results presented in Figure 3.2. Traces of B (1s, 188 eV) and F (1s, 686 eV) were also detected on the surface of the oxide film, but not in the film itself, indicating that the electropolishing did not incorporate the tetrafluoroborate anion. Carbon impurities were also detected on both polished surfaces. This is most likely a result of the exposure to hexane.

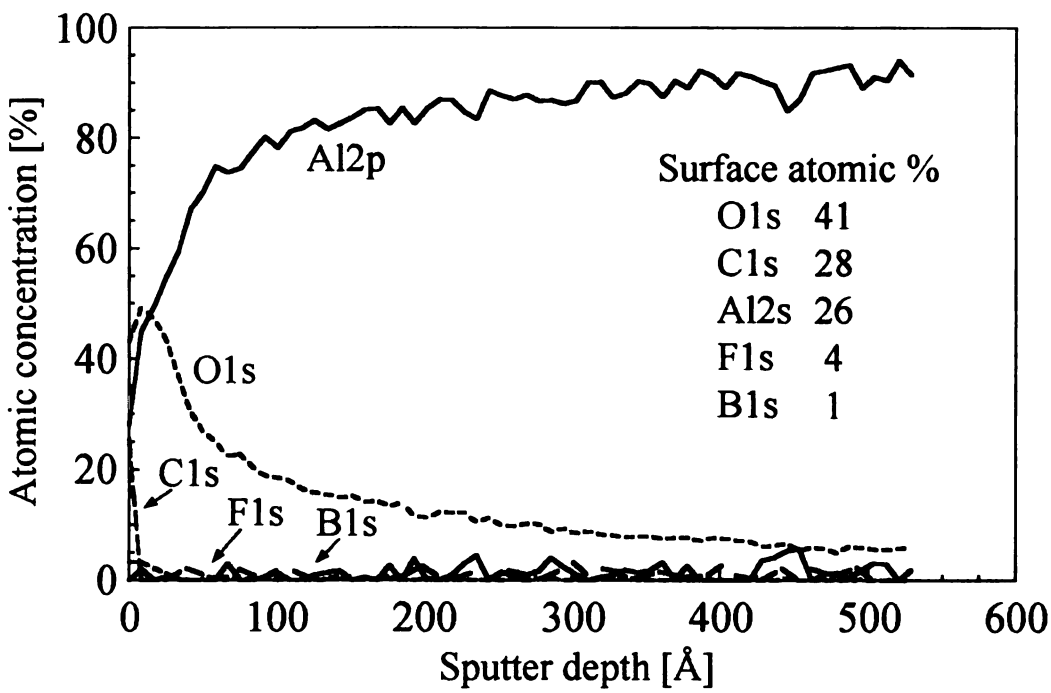

Figure 3.2. XPS depth profiles for an electropolished aluminum surface.

3.2.2. Open circuit potential (OCP) measurements

OCP measurements were conducted to assess the susceptibility of aluminum toward corrosion and/or oxidation. It is generally accepted that OCP measurements for active metals covered with a passivating oxide layer can be quite variable from sample-to-sample, even if all experimental parameters are kept constant.[34] Thus, it was not our objective to evaluate the absolute magnitude of the OCP, but rather to study the general trends of magnitude and dynamics associated with reaching a pseudo steady-state value. Atanasoski reported OCP values for oxide-covered aluminum in the $KAlCl_4$/PC in the range of 2.4-2.8 V vs. K/K^+ (2.5-2.9 V vs. Li/Li^+).[35] When the underlying aluminum surface was exposed, *in situ*, by rotation against a stainless steel blade, the OCP decreased to 1.6-1.7 V vs. K/K^+ (1.7-1.8 V vs. Li/Li^+). After removal of the scrapping blade, the OCP slowly increased, approaching 2.3-2.4 V vs. K/K^+ (2.4-2.5 V vs. Li/Li^+) during a 10 h solution exposure. Clearly, the surface passivated over time and the author concluded that a passivation reaction occurs between bare aluminum and PC because the OCP values were independent of the electrolyte composition and concentration.

Typical results in $LiPF_6$/EC-DMC, $LiPF_6$/PC, $LiClO_4$/EC-DMC, and $LiClO_4$/PC, for mechanically polished and electropolished aluminum, are presented in Table 3.1 Values in parenthesis represent the rate of OCP change recorded over a 1 h period at the beginning and end of the 10 h measurement. OCP values for the mechanically polished electrodes are initially more active (negative) than they are for the electropolished surfaces, in both solvent systems, particularly for $LiClO_4$. The OCP also increases rapidly at the beginning of the exposure, as the rate of change is the highest. The more active potential and the rapid positive increase are consistent with a low oxide,

incompletely passivated surface. Over time, the OCP shifts to more positive (noble) values before approaching a pseudo steady-state value. This trend is consistent with the formation of a passivating layer on the surface. These trends are similar to those reported by Atanasoski, suggesting that the mechanical polishing procedure produces a low oxide (i.e., defective), active aluminum surface.[35]

	Mechanically Polished		Electropolished	
	OCP [mV vs. Li/Li^+] (rate of change [mV/h])		OCP [mV vs. Li/Li^+] (rate of change [mV/h])	
Electrolyte	Initial	10 hours	Initial	10 hours
	EC-DMC			
$LiClO_4$	1800 (150)	2120 (7)	2250 (20)	2380 (1)
$LiPF_6$	2050 (130)	2380 (11)	2230 (20)	2340 (7)
	PC			
$LiClO_4$	1850 (180)	2220 (8)	2450 (4)	2510 (3)
$LiPF_6$	2170 (100)	2400 (10)	2380 (5)	2400 (1)

Table 3.1. Typical results of OCP measurements.

Further analysis of the data presented in Table 3.1. indicates that the OCP values in $LiPF_6$ are ~200 mV higher than in $LiClO_4$ for the mechanically polished aluminum in both solvents. Also, the OCPs in $LiPF_6$ are practically independent of the solvent, whereas the values in $LiClO_4$ solutions show some solvent dependence. For example, the values in PC are 100 – 150 mV more positive than in EC-DMC. These observations probably reflect a slightly different passivation mechanism in each electrolyte. Another observation is that the presence of the oxide layer on the electropolished surface causes

the initial OCP values to be 200-400 mV higher. This is likely because the passivating layer is less defective. In summary, the mechanically polished aluminum surface shows a greater tendency toward corrosion/oxidation than does the electropolished surface. Also, both surfaces show a greater tendency toward corrosion/oxidation in $LiClO_4$ than in $LiPF_6$.

3.2.3. Cyclic voltammetry in $LiPF_6$/PC and $LiPF_6$/EC-DMC

Cyclic voltammetric i-E curves for mechanically polished aluminum (5 mV/s) in 1M $LiPF_6$/PC and 1M $LiPF_6$/EC-DMC, after a 10 h soak at OCP conditions, are presented in Figure 3.3A. A similar response is seen for both solvents. The oxidation current begins to increase at ~ 2800 mV. During the first positive scan, there is significant anodic current between 3000 and 5000 mV, with three oxidation peaks around 3300, 3850, and 4300 mV vs. Li/Li^+. The anodic charge passed during the first scan was 21 mC/cm^2 and 20 mC/cm^2, respectively, in EC-DMC and PC. There is very little charge passed during subsequent scans indicating that anodic reactions occurring during the first scan are electrochemically irreversible, and the reaction products passivate the surface. No significant current flows after the first scan, in either solvent, at potentials up to 5000 mV vs. Li/Li^+.

Figure 3.3B presents cyclic voltammetric i-E curves for electropolished aluminum (5 mV/s) in 1M $LiPF_6$/PC and 1M $LiPF_6$/EC-DMC. A response, similar in shape to that for the mechanically polished surface is observed. The oxidation current begins to increase near 3000 mV in both solvents. However, the oxidation charge during the first scan, between 3000 and 5000 mV, is much lower (about 5 times) than the charge

observed during the first scan for the mechanically polished surface. The anodic charge is 3.4 mC/cm^2 and 3.9 mC/cm^2, respectively, for EC-DMC and PC. This is due to the fact that the electropolished surface is covered by a less defective oxide film, which provides protection to the surface. Interestingly, only the first anodic peak at 3300 mV vs. Li/Li^+ is present. This suggests that the two other peaks observed for the mechanically polished surface are associated with oxidation of the electrolyte/solvent species at the unprotected metal sites.

Figure 3.4 presents cyclic voltammetric i-E curves for mechanically polished aluminum (two different electrodes) in 1M $LiPF_6$/EC-DMC immediately after being placed in the cell, and after 10 h at OCP. A significant positive shift in the onset potential for the oxidation current is evident for the conditioned electrode, being about 600 mV more positive than for the unconditioned one. The oxidation charge for the conditioned electrode is 22 mC/cm^2 and for the unconditioned electrode is 26 mC/cm^2; ~ 20% more. This observation is consistent with the positive shift of the OCP during the extended soaking, and indicates that passivation progressively occurs. The aluminum surface is effectively passivated to potentials as positive as 5000 mV due to reactions with the electrolyte/solvent system that occur during open circuit exposure, and during anodic polarization between 3000 and 5000 mV vs. Li/Li^+.

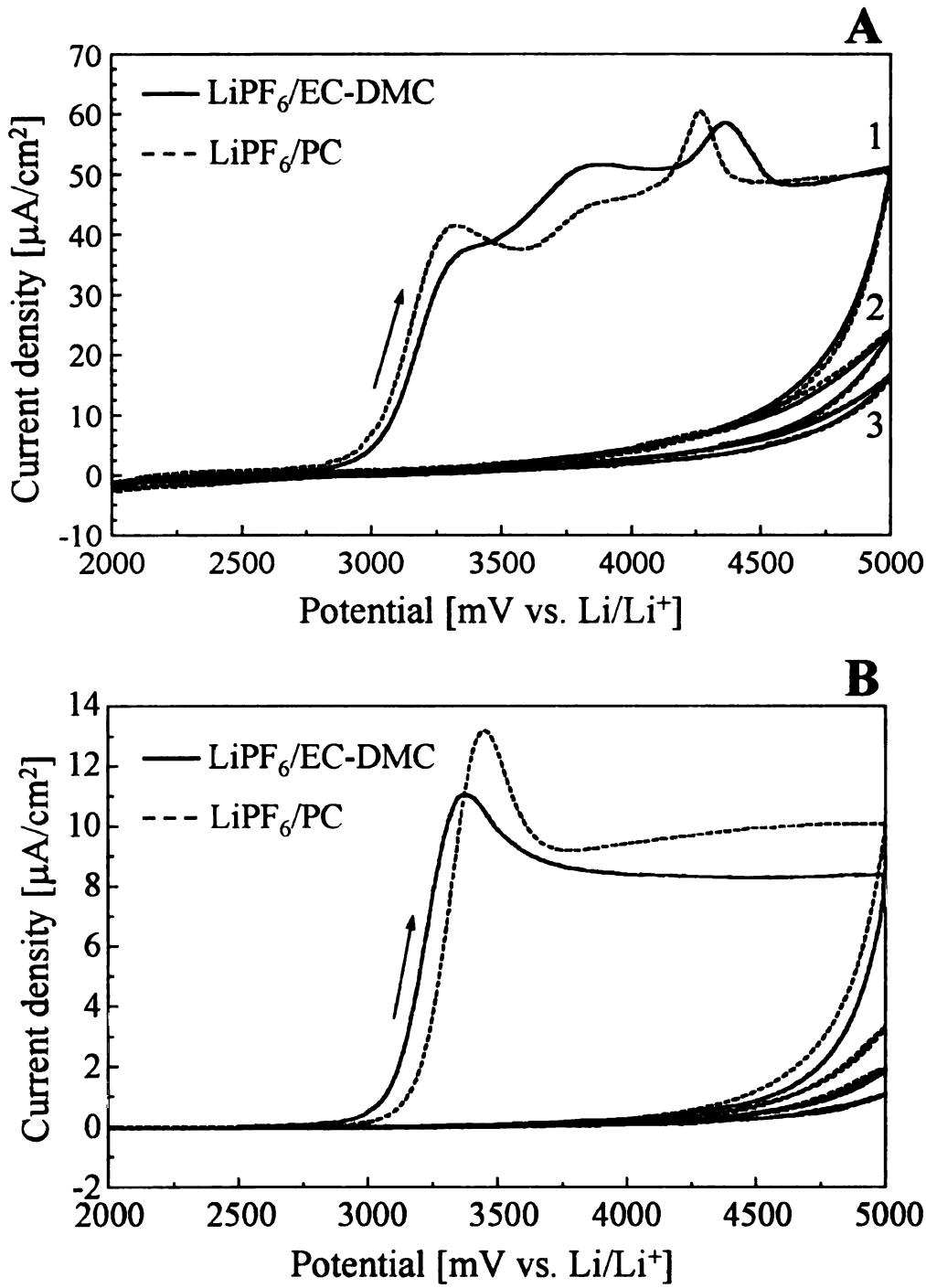

Figure 3.3. Cyclic voltammetric i-E curves recorded at room temperature in 1M $LiPF_6$/PC and 1M $LiPF_6$/EC-DMC for (A) mechanically polished, and (B) electropolished aluminum electrodes. Scan rate = 5 mV/s. Prior to the CV measurements the electrodes were kept at OCP for 10 h. Numbers correspond to scan number.

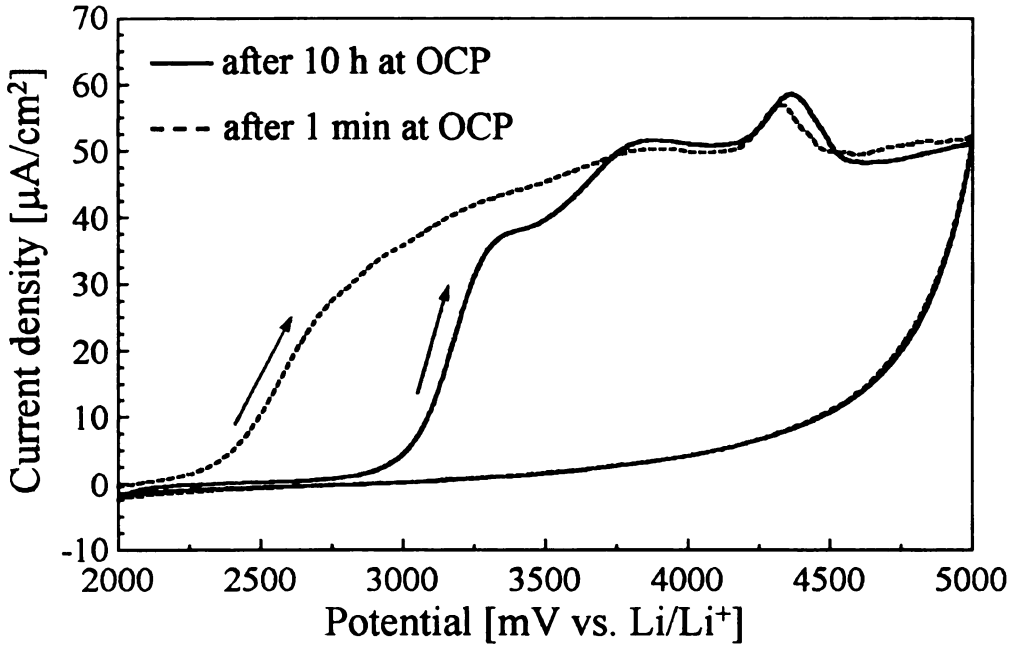

Figure 3.4. Cyclic voltammetric i-E curves recorded at room temperature in 1M $LiPF_6$/EC-DMC for two different, mechanically polished aluminum electrode. Scan rate = 5 mV/s.

These results are in agreement with those of other researchers who have studied aluminum polarization in $LiPF_6$.[2,4,5,7] Although, it is difficult to directly compare results from laboratory-to-laboratory due to differences in experimental conditions, all of these studies have shown that aluminum passivates during the initial stages of anodic polarization. Probably, the most comparable data with our work can be found in the studies of Kanamura *et al.*[2] and Yang *et al.*[7]. Kanamura *et al.* investigated the electrochemical reactions taking place on aluminum electrodes during anodic polarization in $LiPF_6$/PC.[2] Small oxidation currents (< 0.1 mA/cm^2) were observed during the potential sweep at 50 mV/s up to 7 V vs. Li/Li^+. XPS studies of aluminum after anodic polarization revealed the presence of a passivation layer composed of AlF_3 and Al_2O_3. Yang and coworkers used cyclic voltammetry and electrochemical quartz crystal

gravimetry (EQCM) to study the passivation of aluminum in $LiPF_6$/PC.[7] On a sputtered aluminum surface, that was mechanically polished prior to the measurement, they observed current densities in the range of 60 $\mu A/cm^2$ during the first potentiodynamic scan at 50 mV/s. Very little charge was observed during the second scan indicating that passivation of the surface occured. EQCM data showed an increase of the electrode mass, consistent with the buildup of a passivation layer. The authors were unable, however, to assign the apparent mass-to-charge ratio (W/z) of 26, obtained from EQCM measurement, to any single oxidation product (for example, the W/z for Al_2O_3 is 8, for AlF_3 is 19, and for $Al(PF_4)_3$ is 145).

3.2.4. Cyclic voltammetry in $LiClO_4$/PC and $LiClO_4$/EC-DMC

Cyclic voltammetric i-E curves for mechanically polished aluminum (5 mV/s) in 1M $LiClO_4$/PC and 1M $LiClO_4$/EC-DMC, after 10 h at OCP, are presented in Figure 3.5A. As was the case for $LiPF_6$, similarly shaped polarization curves are observed in both solvents. An anodic charge of 13 mC/cm^2 and 11 mC/cm^2 is observed during the first scan between ~ 2500 and 5000 mV vs. Li/Li^+ in EC-DMC and PC, respectively. There is little charge passed during subsequent scans, indicating the anodic reactions are electrochemically irreversible and the reaction products passivate the surface. In contrast to the $LiPF_6$-based electrolyte/solvent mixtures, the current begins to flow at a more negative potential of 2500 – 2700 mV and rises slowly until reaching a maximum at ~ 4500 mV vs. Li/Li^+.

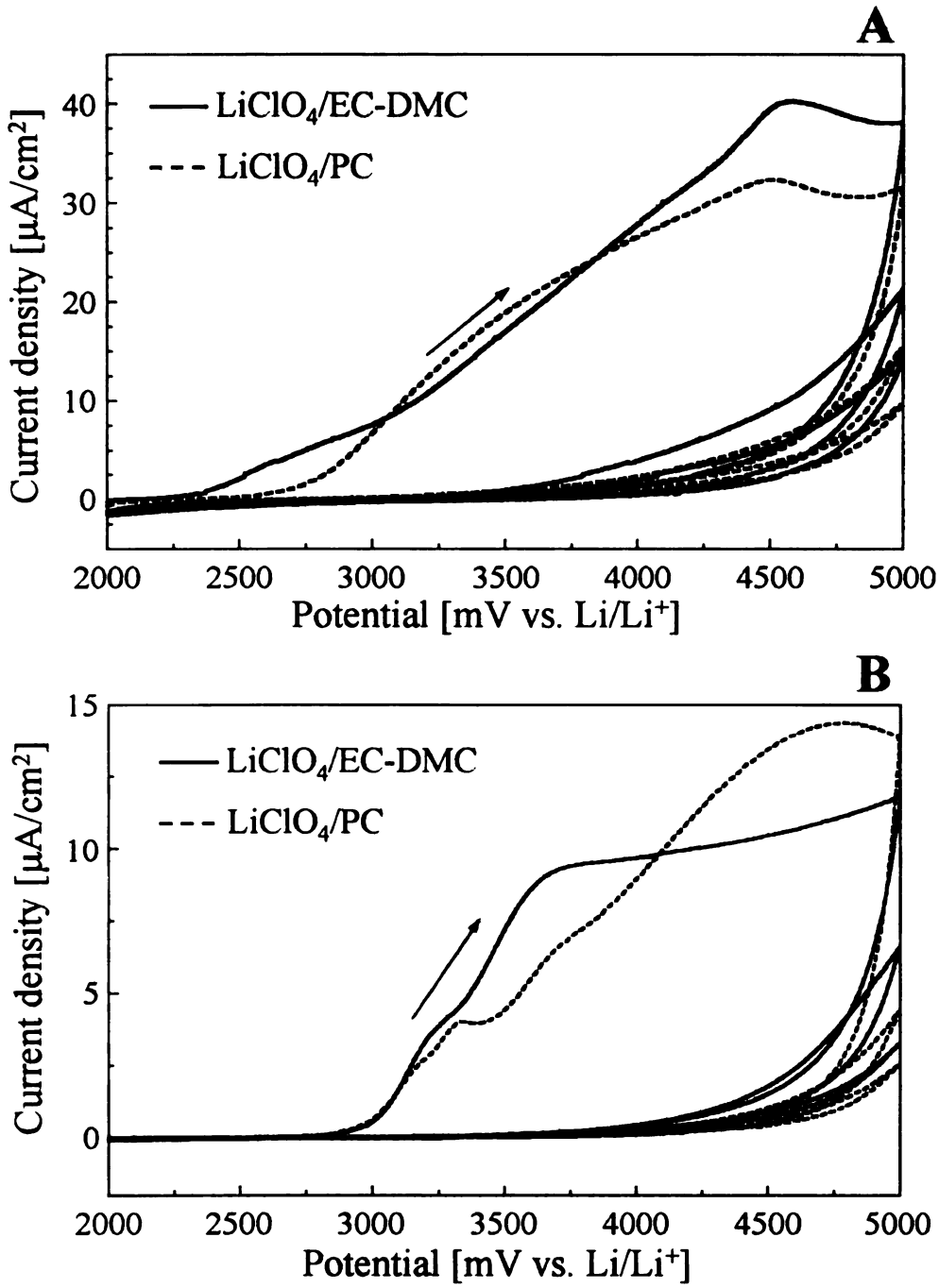

Figure 3.5. Cyclic voltammetric i-E curves recorded at room temperature in 1M $LiClO_4$/PC and 1M $LiClO_4$/EC-DMC for (A) mechanically polished, and (B) electropolished aluminum electrodes. Scan rate = 5 mV/s. The electrodes were stored at OCP for 10 h before the CV measurements.

Figure 3.5B presents the cyclic voltammetric i-E curves for electropolished aluminum (5 mV/s) in 1M $LiClO_4$/PC and 1M $LiClO_4$/EC-DMC. Again, similar behavior is observed in both solvents. The onset potential for the oxidation current is shifted positive, as compared to the mechanically polished surface, to 3000 mV. The electrode is also passivated by the oxidation reaction products after the first scan. The oxidation charge for the first scan (3.8 mC/cm^2 in both solvents) is much lower (about 4 times) than the charge observed for the mechanically polished electrode. This is due to protective properties of a thicker and less defective surface oxide layer after electropolishing.

Mechanically polished aluminum, stored at OCP in either $LiClO_4$/PC or $LiClO_4$/EC-DMC for 10 h, showed only a slightly smaller (~ 5 %) oxidation charge during the first scan when compared to electrodes that were tested right after placement in the electrochemical cell. These results agree well with the OCP measurements, which indicated much weaker passivation in $LiClO_4$-based electrolyte/solvent mixtures (~200 mV lower OCP) compared to the $LiPF_6$ solutions.

Other researches have studied the polarization of aluminum in $LiClO_4$/PC. Our results are comparable to those of Kanamura *et al.* who showed the oxidation charge is associated primarily with the formation of a mixed aluminum oxide layer on the surface.[2,3] The authors observed oxidation currents < 100 $\mu A/cm^2$ during the potential sweep, at 50 mV/s up to 5.5 V vs. Li/Li^+ in 1M $LiClO_4$/PC. Our results, however, are in contrast with those of Yang *et al.* who showed significant oxidation currents, reaching 0.8 mA/cm^2 at 5 V vs. Li/Li^+ during the first potentiodynamic cycle, at 50 mV/s, in 1M $LiClO_4$/PC.[7] The EQCM data for this scan showed a large mass increase of the electrode,

which indicated the formation of a thick layer of oxidation products. This layer was not well passivating as an oxidation current of 0.5 mA/cm^2 was recorded during a subsequent scan, along with a further increase of the mass of the electrode. It is interesting, however, that the shapes of the i-E curves recorded by Yang *et al.* show characteristics of pitting corrosion, and are very similar to our results obtained in $LiClO_4$-based mixtures containing added water impurity. This is discussed further in Chapter 4 of this dissertation.

3.2.5. Chronoamperometry

The passivation of aluminum in $LiClO_4$/PC, $LiClO_4$/EC-DMC, $LiPF_6$/PC, and $LiPF_6$/EC-DMC was also studied with chronoamperometric measurements. Figure 3.6 presents chronoamperometric i-t curve for a mechanically polished electrode in 1M $LiPF_6$/PC, during an anodic step from 2500 to 5000 mV. The current rises quickly and then decreases as the double layer charging followed by the oxidation process are completed. The current decays to a low and steady value of ca. 0.8 $\mu A/cm^2$. The charge passed was 7.3 mC/cm^2. Very low steady state current and charge indicate quick passivation of the surface.

Similarly shaped chronoamperometric i-t curves were observed in all electrolyte/solvent systems. A summary of the chronoamperometric data for both mechanically polished and electropolished electrodes is presented in Table 3.2. The oxidation charge and the onset potential for the oxidation current, recorded during the first potentiodynamic scan, are also summarized in the table. These results show that the oxidation charge is independent of the type of solvent for both mechanically polished and electropolished surfaces. A larger oxidation charge was observed in $LiPF_6$ than in

$LiClO_4$ solutions for the mechanically polished electrodes. This indicates that the passivation process occurs through different mechanism in either electrolyte. On the other hand, the oxidation charge for the electropolished surface was much smaller and practically the same in all four electrolytes/solvent systems. This is due to protective properties of less defective surface oxide layer produced by electropolishing.

The mass of aluminum oxidized during potentiostatic polarization is also reported in Table 3.2. The m_{ox} values were calculated using Faraday law with assumption that the whole anodic charge corresponded to the formation of Al^{3+}. It is clear that the loss of aluminum is negligible even in the case of mechanically polished electrodes for which $m_{ox} < 2.2\ \mu g/cm^2$ was observed. Such weight corresponds to uniform loss of ~ 10 nm of aluminum.

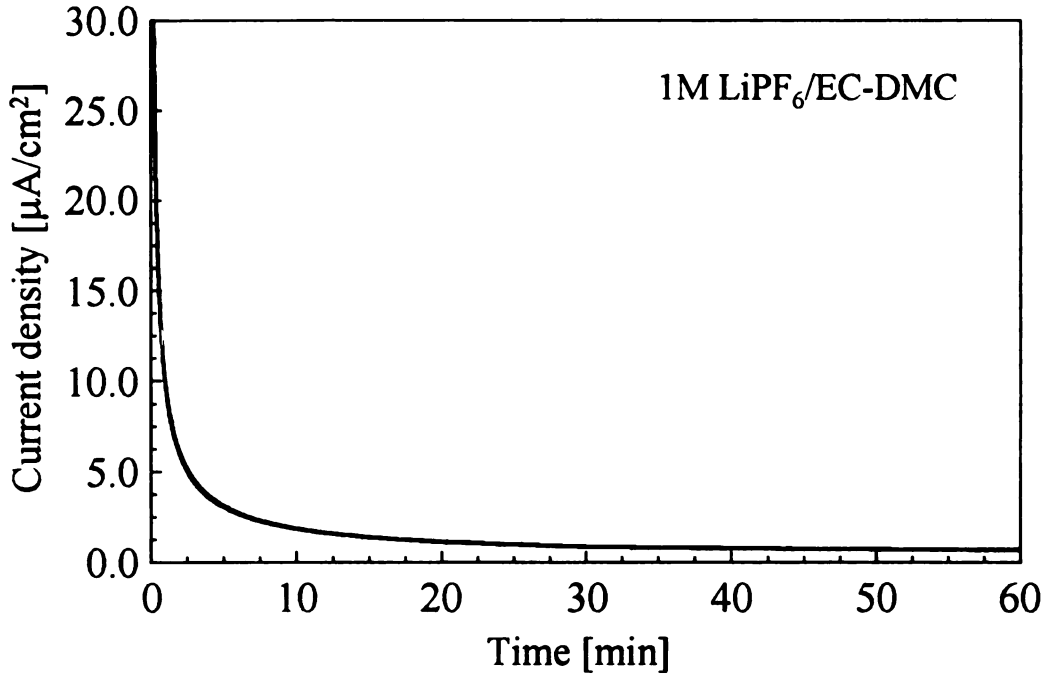

Figure 3.6. Chronoamperometric i-t curve recorded at room temperature for an electropolished aluminum electrode in 1M $LiPF_6$/PC. Potential step from 2500 to 5000 mV.

	E_{onset} [a)] [mV vs. Li/Li^+]	Q_{ox} (CV) [a)] [mC/cm^2]	Q_{ox} (CA) [b)] [mC/cm^2]	I_{ox} (CA) [b)] [$\mu A/cm^2$]	m_{ox} (CA) [$\mu g/cm^2$]
mechanically polished					
EC-DMC					
$LiClO_4$	2750	13	18	2.5	1.7
$LiPF_6$	3050	21	24	4.0	2.2
PC					
$LiClO_4$	2800	11	20	3.0	1.9
$LiPF_6$	3030	20	23	4.0	2.1
electropolished					
EC-DMC					
$LiClO_4$	3010	3.8	7.8	0.80	0.73
$LiPF_6$	3100	3.4	6.5	0.65	0.60
PC					
$LiClO_4$	2970	3.8	7.0	0.75	0.65
$LiPF_6$	3180	3.9	7.3	0.75	0.68

Table 3.2. Summary of the cyclic voltammetric and chronoamperometric polarization data for both mechanically polished and electropolished aluminum. The cyclic voltammetric data (a) are for the first scan and the chronoamperometric data (b) are for a 1h potential step to 5000 mV vs. Li/Li^+.

It is important to indicate at this point that mechanical polishing or electropolishing did not generate fully reproducible surfaces. The variations in the currents for experiments performed at virtually identical conditions were in the order of 10-30%. However, the shapes of potentiodynamic and potentiostatic curves were reproducible and indicative of the passivation of the surface.

3.2.6. XPS analysis of aluminum surface

XPS was used to probe the chemical nature of the passivating layer formed on aluminum in $LiClO_4$ and $LiPF_6$. Table 3.3 presents results for mechanically polished aluminum (*i*) prior to any electrochemical evaluation, (*ii*) after a 10 h soak at OCP in 1M $LiPF_6$/EC-DMC or 1M $LiClO_4$/EC-DMC, and (*iii*) after 1 h at 5 V vs. Li/Li^+ in these two electrolytes. The treated electrodes were washed with DMC and dried in a flow of Ar before the XPS measurements. All samples were stored in hexane during transport to the XPS chamber.

Two peaks for Al (2p, 71 and 75 eV) were observed for all mechanically polished samples. The major peak at 75 eV was assigned to Al_2O_3 and/or AlF_3, depending on the electrolyte, and the minor peak at 71 eV was assigned to Al metal. The intensity ratio of these two peaks is presented in parentheses. The fact that an Al metal peak (71 eV) is observed suggests that the passivating film is thinner than 10 nm. The carbon impurity detected (1s, 285 eV) is consistent with C-C or C-H bonding. It probably resulted from storing electrodes in hexane during transport and/or contamination of the XPS chamber (pump oil).

As expected, only Al and O were detected on mechanically polished aluminum. The relative atomic abundance (18 and 29 atomic %) of these two elements indicates that the surface was covered by a thin-film of Al_2O_3. Similar results were obtained for mechanically polished aluminum soaked in $LiClO_4$/EC-DMC indicating that the surface does not react with the electrolyte at open circuit. O and Al were also the major elements detected on the surface after anodic polarization in $LiClO_4$/EC-DMC. However, the atomic ratio at which these two elements are present (O/Al = 2.9) does not correspond directly to the formation of Al_2O_3 (O/Al = 1.5). A possible explanation for the increased

O is the presence of Cl (2p, 209 eV), consistent with a ClO_4 surface moiety. This suggests that $Al(ClO_4)_3$ is a component in the passivating layer. Since Al/O/Cl atomic ratio in $Al(ClO_4)_3$ is equal 1/12/3, the relative atomic abundance of Cl (2p, 209 eV) equal to 4 % indicates that 16 % atomic O and 1.3 % atomic Al detected on the surface is bound as $Al(ClO_4)_3$. Thus, 30 % atomic O and ~ 15 % atomic Al is present in some other form. Atomic ratio of O/Al in the remaining species is equal to 2 and is still higher than the value expected for pure Al_2O_3. This may indicate that the mixture $Al_2O_3/Al(OH)_3$ is present on the surface rather than pure Al_2O_3. The Cl (2p, 209 eV) signal was also accompanied by much weaker (~15 % of the peak at 209 eV) peak for a Cl (2p, 200 eV) that is characteristic of Cl^-. Presence of Cl^- indicates partial electrooxidation of ClO_4^-.

	Relative atomic abundance [%]						
Treatment	Al[a] (Al^0/Al^{3+})	Li	C	O	Cl	F	P
mechanically polished	18 (0.10)	nd	53	29	nd	nd	nd
soaked in $LiClO_4$/EC-DMC	22 (0.10)	nd	40	38	nd	nd	nd
1 hr at 5 V in $LiClO_4$/EC-DMC	16 (0.01)	nd	34	46	4	nd	nd
soaked in $LiPF_6$/EC-DMC	13 (0.17)	15	30	15	nd	26	1
1 hr at 5 V in $LiPF_6$/EC-DMC	14 (0.06)	7	27	14	nd	36	2

Table 3.3. Summary of the XPS data for mechanically polished aluminum surfaces before and after 1 h potentiostatic polarization at 5 V vs. Li/Li^+. The following peaks were used for determination of relative atomic abundance: Al^{3+} (2p, 75 eV), Al^0 (2p, 71 eV), Li (1s, 56 eV), C (1s, 285 eV), O (1s, 532 eV), Cl (2p, 209 eV), F (1s, 686 eV), and P (2p, 135 eV). a) – total aluminum detected.

Previously, Eggert and Heitbaum investigated the electrooxidation of $LiClO_4$ in PC at Pt electrodes by differential electrochemical mass spectrometry (DEMS).[36] Later, using the same technique, Cattaneo and Ruch investigated the oxidation of $LiClO_4$ at MnO_2 electrodes.[37] Both groups found that the oxidation of perchlorate starts at ~ 4.5 V vs. Li/Li^+, and leads to formation of ClO_2 and HCl. The following mechanism was assumed for this process:

$$ClO_4^- \rightarrow {}^{\bullet}ClO_4 + e^- \rightarrow ClO_2 + 2\,O_{ad} + e^- \quad [3.1]$$

$$ClO_2 + H^+ + e^- \rightarrow HCl + O_2(g) \quad [3.2]$$

$$2\,O_{ad} \rightarrow O_2(g) \quad [3.3]$$

$O_2(g)$ and O_{ad} are formed as reaction products and both can react with aluminum to form Al_2O_3. The formation of Al_2O_3 significantly improves the passivation of Al in $LiClO_4$ electrolyte/solvent systems.

Previously, Kanamura *et al.* investigated the oxidation of aluminum in $LiClO_4$/PC.[2,3] Based on the XPS analysis of aluminum polarized at 5.5 V vs. Li/Li^+ for 1 h, they concluded that the surface is covered with highly porous Al_2O_3. They also detected the presence of ClO_4^- and Cl^- in the surface oxide film, which they assigned to electrochemical oxidation of ClO_4^-.

Significant amounts of Li and F, in addition to Al and O, were detected on the surface after both soaking at the OCP, and polarizing the aluminum in $LiPF_6$/EC-DMC. A very small amount of P was also detected indicating that the majority of F did not

come from the electrolyte anion (PF_6^-) but rather from its decomposition products. It is well known that $LiPF_6$ undergoes slow hydrolysis in the presence of trace water, according to the following reactions:[24 and references therein]

$$LiPF_6 \rightleftarrows PF_5 + LiF\downarrow \qquad [3.4]$$

$$PF_5 + H_2O \rightarrow 2HF + POF_3 \qquad [3.5]$$

Hydrolysis products may then react with the aluminum oxide on the surface to form a mixed aluminum fluoride and oxyfluoride passivation layer. Fluoride may also precipitate as LiF or migrate into the oxide film and react electrochemically with the aluminum metal surface. Possible reactions are as follows:

$$Al_2O_3 + 6HF \rightarrow 2AlF_3\downarrow + 3H_2O \qquad [3.6]$$

$$Al_2O_3 + 2HF \rightarrow 2AlOF\downarrow + H_2O \qquad [3.7]$$

$$Li^+ + F^- \rightarrow LiF\downarrow \qquad [3.8]$$

$$Al + 3F^- \rightarrow AlF_3\downarrow + 3e^- \qquad [3.9]$$

If one assumes that, on the anodically polarized surface, all the P was present as PF_6^- and all the Li as LiF, then the Al/O/F atomic ratio is equal 1/1/1.2. This indicates formation of the mixed aluminum oxide/oxyfluoride/fluoride layer on the surface. On the other hand, significant amounts of Li that were detected on the surface of mechanically polished aluminum after soaking in the $LiPF_6$/EC-DMC, and the relative abundances of

other elements indicate that fluorine was predominantly present as LiF and the proportion of F in oxyfluoride layer was much lower than on the surface that was anodically polarized.

These observations seem to resolve a discrepancy between results reported by Krause *et al.*[5] and Kanamura *et al.*[2] Kanamura and coworkers, using XPS, identified Al_2O_3 and AlF_3 as the main components of a passivation layer formed after polarization at 5.5 V vs. Li/Li^+ in $LiPF_6$/PC. Contrastingly, Krause *et al.* found primarily Al_2O_3 and LiF on a surface polarized at 4.2 V vs. Li/Li^+ in the same solution. A significant difference in the polarization potential used by both groups may explain the difference in the chemical composition of the passivation layer. At lower potentials, precipitation of LiF dominates, whereas at higher potentials electrochemical oxidation of aluminum and formation of AlF_3 occurs.

The formation of a surface layer in both $LiPF_6$/PC and $LiClO_4$/PC has been also confirmed by electrochemical quartz crystal microbalance (EQCM).[7] It was observed that an increase in the mass of the aluminum electrode occured during potentiodynamic cycling in both electrolytes. The authors were unable, however, to assign the values of apparent mass to charge ratio (26 for $LiPF_6$ and 220 for $LiClO_4$), to any single product formed on the surface.

3.2.6. Stability of passivation layer

The stability of the passivation layer formed in $LiClO_4$/EC-DMC and $LiPF_6$/EC-DMC was investigated. Three potentiodynamic scans were performed for mechanically polished aluminum in both electrolytes. After the third scan, the electrodes remained at

open circuit for 1 h, after which time a fourth potentiodynamic scan was recorded. The oxidation charge during the fourth scan in $LiClO_4$/EC-DMC increased approximately 2 times over that for the third scan, from 2.9 to 5.5 mC/cm^2. On the other hand, the fourth scan recorded in the $LiPF_6$/EC-DMC was not significantly different from the third scan. A similar observation was made when the passivated electrodes were left at OCP for 5 min during which time the solution was agitated by the flow of Ar. These results indicate a greater stability for the passivation layer formed in $LiPF_6$/EC-DMC than for the one formed in $LiClO_4$/EC-DMC. These results also support the passivation mechanism proposed above. The $Al(ClO_4)_3$ formed, is soluble in EC-DMC, and is stable only when supersaturation conditions are met. Both mixing and open circuit soaking cause some dissolution of the layer, leading to the increased anodic charge during the subsequent polarization scan. On the other hand, the fluoride/oxyfluoride film formed during polarization in $LiPF_6$/EC-DMC is insoluble in the organic solvent. It is thus stable toward both the hydrodynamic conditions of mixing and slow dissolution at open circuit. This is important information indicating that, although aluminum is stable in $LiClO_4$ electrolytes at highly anodic potentials, multiple charge-discharge cycles may lead to corrosion of the surface.

3.2.7. Passivation of aluminum in $LiClO_4$/EC-DMC, $LiClO_4$/PC, $LiPF_6$/EC-DMC, and $LiPF_6$/PC – mechanism

In the present research, OCP measurements, as well as voltammetric and chronoamperometric data, show that aluminum passivates in all four electrolyte/solvent systems. However, the mechanisms by which passivation occurs seem to be different in

either electrolyte. First of all, OCPs measured for mechanically polished (low oxide) aluminum surface in $LiPF_6$, are significantly more noble (~ 200 mV) than these observed in $LiClO_4$. The OCPs are also solvent independent in $LiPF_6$ solutions whereas some solvent dependence is observed for $LiClO_4$ with PC passivating better than EC-DMC mixture. Also, XPS data indicate a significant amount of fluorine and lithium present on the surface of aluminum after 10 h soaking in $LiPF_6$/EC-DMC, whereas no lithium or chlorine were detected on the aluminum soaked in $LiClO_4$/EC-DMC. These results imply that at OCP conditions, aluminum passivates by solvent adsorption in $LiClO_4$ (see mechanism (3) p. 18), and by salt film formation (see mechanism (2) p. 18) in $LiPF_6$ solutions. Of course, it is also possible that both mechanisms (3) and (2) are operative in $LiPF_6$.

Passivation of aluminum in $LiClO_4$/EC-DMC and $LiClO_4$/PC by the solvent adsorption mechanism is also supported by research of other authors. Previously, Atanasoski showed that the OCP values of aluminum in PC were independent of the type of electrolyte (KCl vs. $KAlCl_4$) and electrolyte concentration.[35] Thus, the author concluded that a passivation reaction occurs between the aluminum surface and PC molecules. Passivation by solvent adsorption of iron and stainless steel in $LiClO_4$/PC was also proposed.[31,38,39] It was shown that such a mechanism is operative for potentials up to the oxidation potential of PC and suggested that an adsorbed solvent layer raises the activation energy for metal dissolution, thus providing protection to metal surface.

A different passivation mechanism seems to be operating in $LiPF_6$ solution at OCP conditions. XPS data indicate the formation of a salt film as the passivation layer. XPS data suggest, however, that the salt film is not a simple precipitate of $Al(PF_6)_3$. The

amount of phosphorus relatively to amount of fluorine detected on the surface, is too small to support this mechanism. The salt film is rather a result of the reaction of aluminum and/or aluminum oxide with the products of electrolyte hydrolysis, as described earlier in this chapter.

Results of potentiodynamic cycling and potentiostatic polarization in dry electrolyte/solvent mixtures indicate that the aluminum surface remains passivated in all examined solutions, at least for the potentials up to 5 V vs. Li/Li^+. Passivation by solvent adsorption at such highly anodic potentials is not very likely due to possible solvent oxidation. Although it has been shown by Kanamura *et al.*[2,3] that bulk oxidation of PC does not occur on aluminum at potentials up to 5.0 V vs. Li/Li^+ in $LiClO_4$ and 5.4 V vs. Li/Li^+ in $LiPF_6$ due to presence of the oxide layer, significant oxidation of PC on platinum was shown to take place at potentials as low as 3.6 V vs. Li/Li^+.[40] It is thus not likely for the solvent molecules adsorbed on the surface to protect metal at highly anodic potentials. Kelly *et al.* showed previously that at potentials higher than the oxidation potential of PC, iron passivates in $LiClO_4$/PC through formation of salt film ($Fe(ClO_4)_2$).[31] A similar mechanism in which $Al(ClO_4)_3$ is formed, can be envisioned for passivation of aluminum in $LiClO_4$ solutions. This mechanism is supported by the XPS results. XPS data show the presence of aluminum oxide and perchlorate on the surface of aluminum after anodic polarization. This mechanism is also supported by AFM and EQCM data presented in the Chapters 5 and 6, respectively.

Anodic polarization in $LiPF_6$/PC and $LiPF_6$/EC-DMC also leads to passivation of the surface through formation of the salt film. XPS data indicate formation of mixed aluminum fluoride/oxyfluoride layers rather than $Al(PF_6)_3$. The very low solubility of

aluminum fluoride/oxyfluoride deposits provides highly stable corrosion protection for aluminum in PC and EC-DMC. These results are in agreement with the results of other authors.[2,5]

3.3. Conclusions

The stability of aluminum during anodic polarization in $LiClO_4$/PC, $LiClO_4$/EC-DMC, $LiPF_6$/PC, and $LiPF_6$/EC-DMC was studied. It was found that aluminum passivates in all four electrolyte/solvent mixtures. The susceptibility to corrosion/oxidation was greater for the mechanically polished than for the electropolished surface due to thinner and more defective Al_2O_3 film on the former. Different mechanisms of passivation are found in the two electrolytes. At OCP conditions, aluminum is passivated by both an Al_2O_3 layer and adsorbed solvent molecules in $LiClO_4$ solutions. In $LiPF_6$, the passivation layer consists of Al_2O_3 plus some salt precipitation (e.g., LiF). After anodic polarization, XPS measurements indicate the formation of highly stable, fluoride rich passivation layer in $LiPF_6$, composed of a mixture of Al_2O_3, AlOF, AlF_3, and LiF. On the other hand, the passivation layer formed in $LiClO_4$ is composed mostly of Al_2O_3 and $Al(ClO_4)_3$. This layer is the less stable of the two, seemingly due to slow dissolution of $Al(ClO_4)_3$. The potentiostatic and potentiodynamic polarization do not indicate any significant effect of the solvent composition (PC vs. EC-DMC) on the extent of oxidation processes.

CHAPTER 4

4. Investigations of Aluminum Corrosion in $LiPF_6$/EC-DMC, $LiPF_6$/PC, $LiClO_4$/EC-DMC and $LiClO_4$/PC - Influence of Water Contamination

4.1. Introduction

The results presented so far indicate that aluminum is effectively passivated in solution of either $LiClO_4$ or $LiPF_6$ in EC-DMC or PC. Any localized corrosion that occurs during the first few polarization scans to 5000 mV vs. Li/Li^+ is effectively inhibited by deposition of the oxidation products. However, an interesting question to address is, *what is the effect of water contamination on the stability of the aluminum?*

Interestingly, there has not been much attention paid to the role of water impurity on the corrosion susceptibility of aluminum in Li-ion battery electrolytes. It is especially surprising, considering the fact that water is the most common contaminant in the non-aqueous electrolyte/solvent systems.[29] This is because it is extremely difficult to remove water from a polar solvent down to trace levels. It is also important to realize that water may form during battery operation as a product of solvent decomposition, or may enter the battery interior, in the form of atmospheric moisture, due to degraded sealing.[24] Thus,

understanding the effect trace amounts of water have on the corrosion/oxidation of aluminum in non-aqueous electrolytes seems to be an important issue.

The influence of water on the passivation of metals in organic solvents was reviewed by Kelly and Moran.[29] The authors reported that most metals, in neutral anhydrous solvent/electrolyte mixtures, passivate by either solvent adsorption or salt film formation. The presence of low levels of water (100 – 1000 ppm) interferes with both of these processes and leads to increased surface reactivity. Water may affect the adsorbed solvent by adsorbing competitively on the metal surface with its smaller size relative to organic solvent being advantageous. Once adsorbed, it may participate directly in the oxidation of the metal or increase corrosion/oxidation rate by effectively solvating newly created metal cations. Water also interferes with formation of the salt film by increasing its solubility. Only at high water concentrations (70-90 mole %) is passivation restored due to formation of a stable, oxide/hydroxide layer.

Corrosion/passivation of aluminum in lithium-ion battery electrolytes in the presence of water contamination has received limited attention in the literature. Braithwaite *et al.* investigated the effect of low levels of water contamination (20 ppm) on the long-term stability of aluminum in 1M $LiPF_6$/PC-DEC.[4] Based on impedance data, the authors observed improved passivation in the presence of water. They did not, however, investigate the reason for the improvement. Kanamura *et al.* studied the effect of low levels of HF (0.01 mol/dm^{-3}) on the stability of aluminum in $LiCF_3SO_3$/PC and $Li(CF_3SO_2)_2N$/PC.[6] Improved passivation was observed. Since HF was added as an aqueous solution, the effect of water could not be separated in their research.

Presently, the effect of water contamination on the corrosion/oxidation of high purity aluminum (99.999%) in $LiPF_6$/EC-DMC, $LiPF_6$/PC, $LiClO_4$/EC-DMC, and $LiClO_4$/PC was investigated. 50 – 2000 ppm levels of water were studied through controlled additions of water to the solvent/electrolyte mixture. Testing was performed using two different metal surfaces, (*i*) aluminum with the native oxide film removed by mechanical polishing in hexane under an inert, argon atmosphere, and (*ii*) aluminum, first mechanically polished, and then electropolished in an aqueous solution of the HBF_4. Cyclic voltammetry (CV), chronoamperometry (CA), and open circuit potential measurements (OCP), were used, in addition to optical microscopy (OM), atomic force microscopy (AFM), and scanning electron microscopy (SEM), to study morphological changes brought about by the imposed electrochemical conditions. Energy dispersive x-ray analysis (EDS), and Raman spectroscopy were used to probe the chemical composition and structure of the surface before and after polarization.

4.2. Results and discussion

4.2.1. Corrosion of aluminum in $LiClO_4$/EC-DMC/H_2O and $LiClO_4$/PC/H_2O mixtures – mechanically polished surface

Figure 4.1 shows cyclic voltammetric i-E curves (5mV/s) for mechanically polished aluminum in 1 M $LiClO_4$/EC-DMC with 500 ppm of added water. The voltammetric response is much different in the presence of water impurity than in the dry electrolyte (Chapter 3). The first positive scan resembles, to some extent, the one observed for the dry electrolyte (see Figure 3.3A). A gradual increase in the anodic current starts at 2700

mV and continues until ca. 4600 mV at which point the current increases significantly. There is current crossover at the positive limit of 5000 mV such that the current during the reverse scan is larger than during the forward scan. This is characteristic of a corrosion process in which breakdown of a passivation layer occurs on the forward scan. In case of the anodic polarization of aluminum, this behavior usually indicates pitting corrosion.[28] At the potential E_{pit}, or ca. 4600 mV, the passive layer breaks down and current flows due to the oxidation of the exposed aluminum. During the reverse scan, a large anodic current flows for the same range of potentials until repassivation occurs at E_{pass}, at ca. 3600 mV.

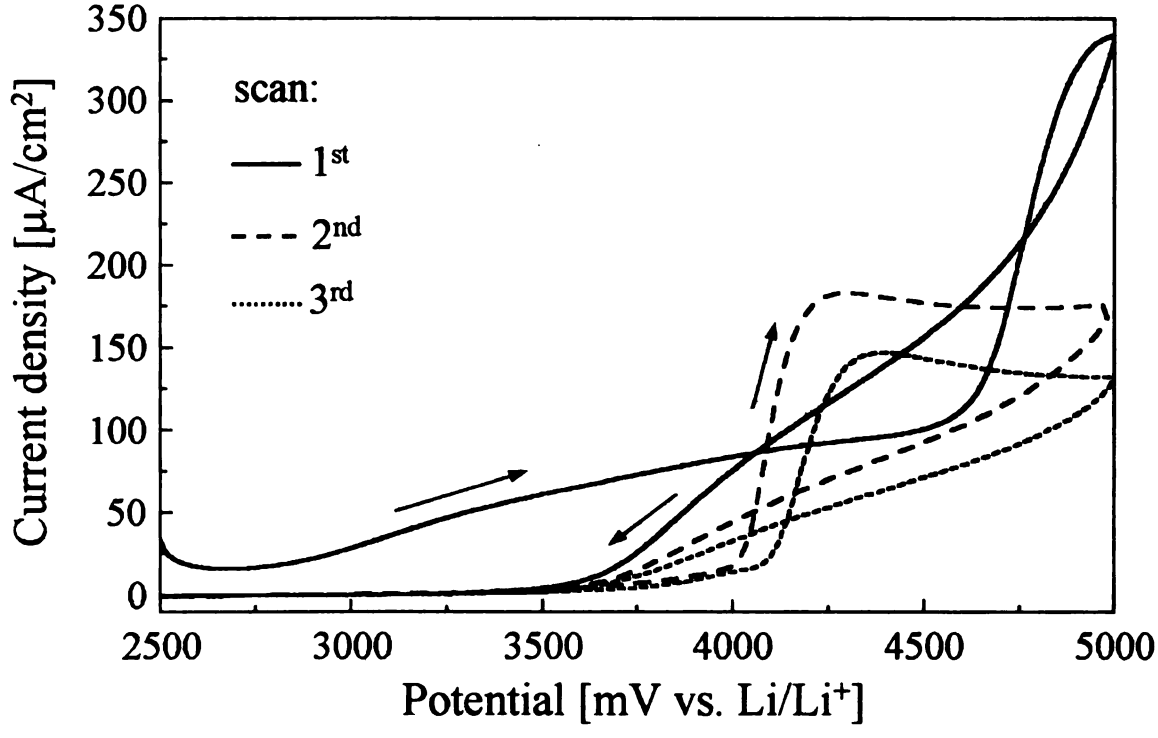

Figure 4.1. Cyclic voltammetric i-E curves recorded for mechanically polished aluminum at room temperature in 1M $LiClO_4$/EC-DMC with 500 ppm of added H_2O. Scan rate = 5 mV/s.

The second and third potentiodynamic scans also show characteristics of pitting corrosion with current crossovers. The current decreases with each scan, however, indicating a reduction in the active area. Also, E_{pit} and E_{pass} change. The onset potential, or E_{pit}, for the anodic current is ca. 4000 mV. There is a peak current, at 4200 mV and 4300 for 2^{nd} and 3^{rd} scans, respectively, during the forward sweep. The current continues the decrease after reversing the scan at 5000 mV with a small current crossover near 4000 mV. The current and charge associated with the crossover decrease with each scan. Repassivation, or E_{pass}, occurs near 3500 mV for all the scans. This behavior suggests that water contamination causes localized pitting of the aluminum, but the oxidation products that form passivate the surface to some extent. However, even after the 3^{rd} cycle, there is still a significantly greater anodic charge passed during the forward scan than is present in the dry electrolyte. Therefore, this level of water impurity appears to cause extensive corrosion and oxidation of the aluminum surface. Similar results were obtained when PC was used as a solvent.

Table 4.1 summarizes the potentiodynamic polarization results for 1M $LiClO_4$/EC-DMC and 1M $LiClO_4$/PC with different levels of added water. OCP for dry and for 2000 ppm solutions are also presented. Each measurement was performed on a freshly, mechanically polished surface (hexane and inert Ar atmosphere). The OCP shifts more negative (active) with added water in both electrolyte/solvent systems, with the larger shift seen in $LiClO_4$/PC. Also, and most importantly, the anodic charge passed during the 1^{st} scan increases proportionally with the added water. This indicates that water is an active participant in the corrosion process. Interestingly, at 50 ppm of added water, the current crossover in the i-E curves was not observed during the first two scans. This implies that water is essential for activation of the surface and only after the activation occurs, does the surface undergo corrosion. At lower water levels activation time is longer, and thus pitting is not observed during the initial scans.

ppm of added H_2O	E_{oc} (10 h) [mV vs. Li/Li^+]	E_{pit} [mV vs. Li/Li^+]			E_{pass} [mV vs. Li/Li^+]			Q_{ox} [mC/cm^2]		
		scan number			scan number			scan number		
		1	2	3	1	2	3	1	2	3
		$LiClO_4$/EC-DMC								
2000	2050	4100	3900	3950	3500	3550	3550	250	160	120
500	-	4550	4000	4100	3550	3600	3600	80	55	40
50	-	***	***	4500	***	***	4100	35	12	8
0	2120	***	***	***	***	***	***	15	4.0	2.0
		$LiClO_4$/PC								
2000	1800	4400	3800	3900	3500	3550	3550	185	140	110
500	-	4600	3900	4000	3650	3650	3650	75	50	35
50	-	***	***	4550	***	***	4050	30	10	7
0	2220	***	***	***	***	***	***	12	2.5	1.5

Table 4.1. Summary of the potentiodynamic cycling data for mechanically polished aluminum in $LiClO_4$/EC-DMC and $LiClO_4$/PC with different levels of added water. Scan rate = 5 mV/s. The potential range scanned was from 2.5 to 5.0 V vs. Li/Li^+. (***) - Pitting was not observed.

Similarly to what was observed in dry electrolytes, mechanical polishing did not generate fully reproducible surface as the variations in the currents for experiments performed at virtually identical conditions, were in the order of 20-40%. However, the shapes of voltammograms and pitting and passivation potentials were reproducible.

The formation of a partial passive layer after the 3rd scan was observed by SEM. Figure 4.2 presents representative SEM images of a mechanically polished aluminum surface prior to (Figure 4.2A) and after 3 potentiodynamic scans from 2000–5000 mV vs. Li/Li$^+$ in 1M $LiClO_4$/EC-DMC with 500 ppm of added H_2O (Figure 4.2B, C, and D). A relatively smooth surface is observed for aluminum before polarization. Multiple grooves, which originated from mechanical polishing, are clearly visible. On the other hand, a thick, highly porous layer of the corrosion product covers the surface after polarization. The deposit is not strongly attached to the aluminum surface as it can be easily removed by washing with DMC. Figure 4.2C shows the structure of the aluminum surface after the surface layer was removed. A new, highly damaged surface is observed. Multiple cracks and pores indicate significant corrosion and dissolution of aluminum. Images of the cracks obtained at higher magnification show clearly that damage reaches deep into aluminum electrode. This is well visible on the image of one of the cracks presented in Figure 4.2D. A similar, weakly passivating layer and highly damaged aluminum surface were also observed after polarization in the $LiClO_4$/PC containing 500 ppm of added H_2O.

SEM images confirm what the voltammetric data indicated, that corrosion of the aluminum surface occurs when water is present in the $LiClO_4$/EC-DMC or $LiClO_4$/PC. The resulting corrosion/oxidation product deposits do not completely passivate the

surface due to a porous and defective morphology.

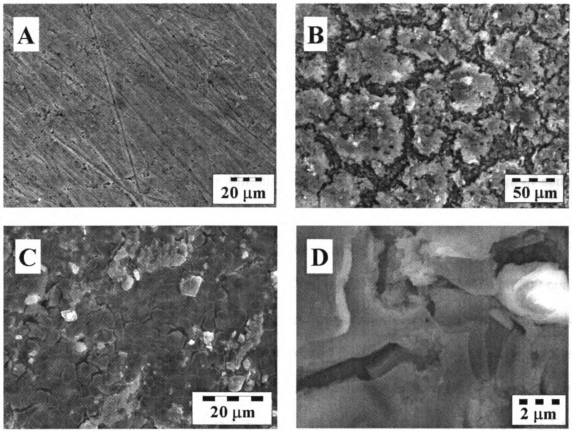

Figure 4.2. SEM images of the mechanically polished aluminum surface. (A) An untreated and (B,C, and D) after 3 potentiodynamic scans from 2000–5000 mV vs. Li/Li^+ in $LiClO_4$/EC-DMC with 500 ppm of added H_2O. (C, D) The images are the same as (B) but the deposited layer has been removed by washing with DMC.

The stability of the passivating layer was also investigated in the following experiments. First the mechanically polished electrode was exposed to five potentiodynamic cycles in 1M $LiClO_4$/EC-DMC + 500 ppm H_2O. The oxidation charge recorded during the fifth cycle was equal to 35 mC/cm^2, and E_{pit} and E_{pass} were 4000 and 3550 mV vs. Li/Li^+, respectively. The electrolyte was then turbulently mixed by argon bubbling, and three consecutive potentiodynamic scans were recorded between

2500-5000 mV. The oxidation charge increased to 72 mC/cm^2 for the sixth (total) scan and then again decreased for the consecutive scans. E_{pit} initially decreased to 3800 mV for the sixth scan and then increased to 3950 mV with further scans. E_{pass} was practically the same for all scans. The increased oxidation charge and decreased pitting potential after disruption of the passivating layer, indicates that indeed, the passivation layer formed on the aluminum surface in the presence of water does not provide a good protection to the surface, and only diminishes corrosion rates through blockage of some of the active area. After disruption of this layer, the corrosion proceeds at increased rates until a build-up of a new corrosion product layer occurs.

Second, 50 potentiodynamic scans at 5 mV/s, in 1M $LiClO_4$/EC-DMC with 500 ppm of added H_2O, were performed on the mechanically polished electrode to achieve a stable oxidation charge of 16 mC/cm^2, E_{pit} = 3850 V, and E_{pass} = 3550 mV. The electrode was then soaked in the solution for 1h at OCP. This was followed by a single potentiodynamic scan. The oxidation charge for this scan increased to 29 mC/cm^2. Interestingly, E_{pit} also increased by 200 mV, whereas E_{pass} remained the same. The increased E_{pit} indicates some passivation of the electrode occurs at OCP. This may be explained by reaction of aluminum metal with water. It is well known that bare aluminum reacts spontaneously with water to form an aluminum oxide/hydroxide layer, which gives aluminum its passivity in aqueous solutions.[1] Such a reaction, although hindered, can also take place in non-aqueous solutions with added water. It leads to coverage of the active aluminum sites by an oxide/hydroxide layer. At OCP, water diffuses to the metal surface, reacts with metal, and forms a stable film that increases the initial corrosion resistance of metal. However, during anodic polarization, aluminum dissolves rapidly. Due to the limited amount of water present, a well passivating oxide/hydroxide layer cannot form.

4.2.2. Corrosion of aluminum in $LiClO_4$/EC-DMC/H_2O and $LiClO_4$/PC/H_2O mixtures – electropolished surface

It is well known that a layer of aluminum oxide passivates the surface and increases the corrosion resistance of the underlying metal. To determine if the Al_2O_3 layer can prevent corrosion in $LiClO_4$/EC-DMC/H_2O and $LiClO_4$/PC/H_2O mixtures, anodic polarization of electropolished aluminum was performed. Figure 4.3 shows potentiodynamic scans recorded at 5 mV/s, in 1 M $LiClO_4$/PC + 200 ppm H_2O. The aluminum oxide layer seems to passivate the surface during the first three scans, as the current density is similar to that observed in the electrolyte mixture without added water. However, closer analysis of the results of the third scan reveals characteristic crossover of the i-E curve, suggestive of pitting corrosion. Further cycling clearly reveals the incidence of corrosion (Figure 4.3B). In addition to current crossover, the anodic charge continuously increases during cycling. This is an indication of an increasing electrochemically active area due to corrosion.

The surface of the electropolished aluminum electrode after anodic polarization was investigated by optical microscopy. Figure 4.4 presents representative photomicrographs of the surface after the 3^{rd} and 50^{th} (conditions the same as in the Figures 4.3 A and B) potentiodynamic scans in 1 M $LiClO_4$/PC + 200 ppm of H_2O. During the initial stages of corrosion, multiple circular pits (1 – 6 μm diameter) are randomly formed on the surface. The pits grow in diameter and new pits develop over time, with neighboring pits coalescing as the corrosion proceeds. Eventually, the oxide film is completely destroyed, with only isolated regions of the film (smooth areas) intact after the 50^{th} scan. This observation explains the progressively increasing current density observed during the

early stages of the potentiodynamic scans, as presented in Figure 4.3B. Similar results were also obtained when EC-DMC was used as the solvent.

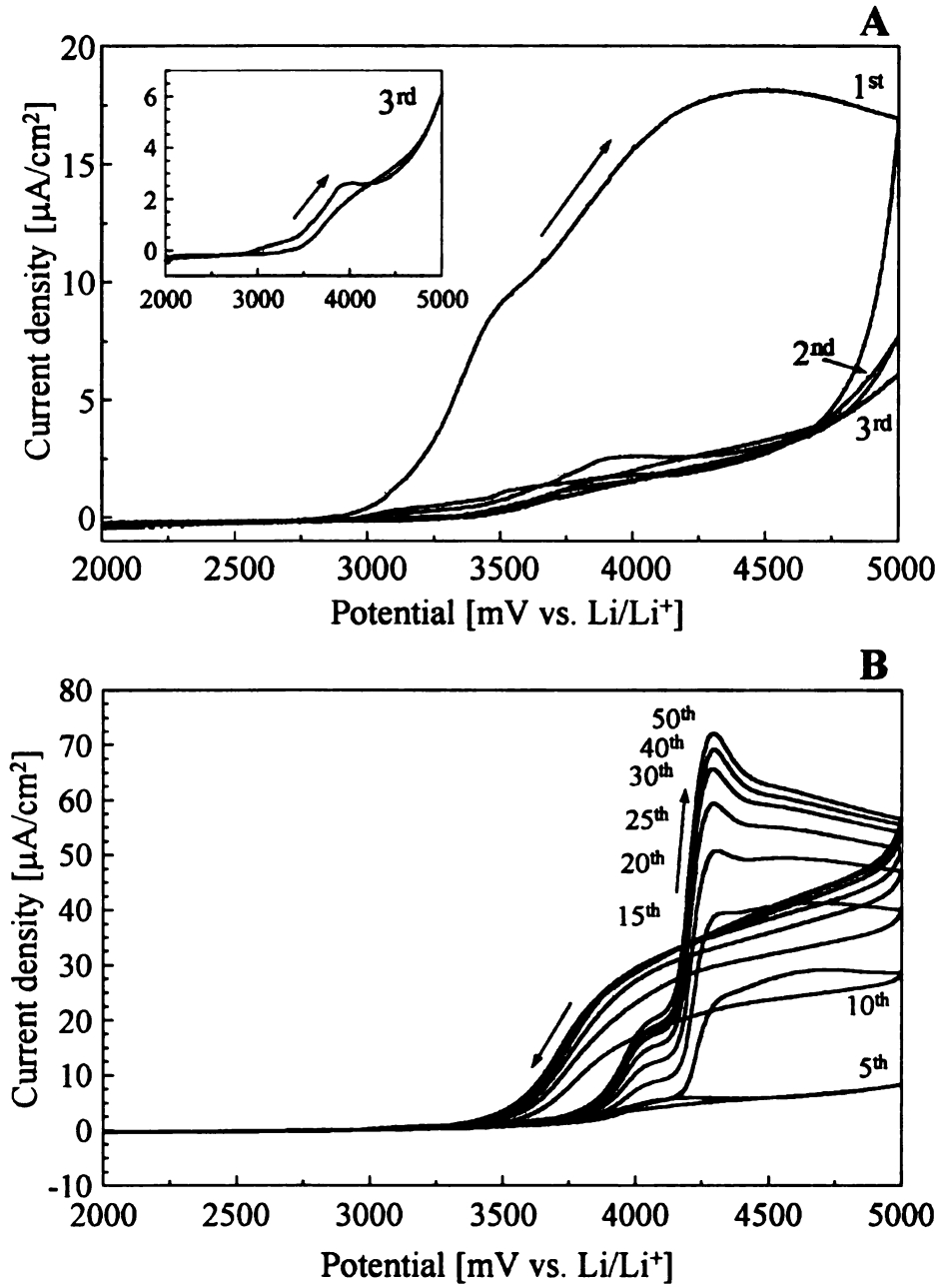

Figure 4.3. Cyclic voltammetric i-E curves recorded at room temperature for an electropolished aluminum electrode in 1M $LiClO_4$/PC + 200 ppm of H_2O during (A) the first three scans and (B) scans 5 through 50. Scan rate = 5 mV/s

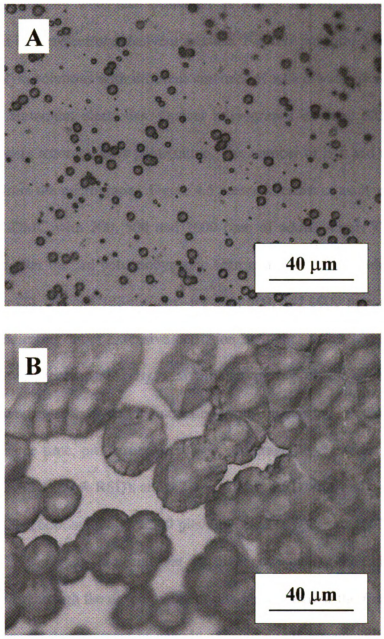

Figure 4.4. Photomicrographs of the electropolished aluminum surface after 3 (A) and 50 (B) potentiodynamic scans in 1M $LiClO_4$/PC + 200 ppm of H_2O (conditions as in Figure 4.3).

Pit size and density were also evaluated as a function of the amount of water impurity present in the electrolyte/solvent mixture. For this purpose, 3 potentiodynamic scans in electrolyte solutions with different amounts of added water were performed on electropolished aluminum electrodes. Optical micrographs of three different areas on each electrode were recorded after polarization. The number of pits and their sizes were then estimated from the micrographs. Figure 4.5 presents results of such measurements in 1M $LiClO_4$/EC-DMC with 200, 500 and 1000 ppm of added water. The total anodic charge recorded after the 3rd potentiodynamic scan increased in the order of increasing amount of water (21, 59, and 123 mC/cm^2 for 200, 500, and 1000 ppm of added water, respectively), indicating more extensive corrosion at higher water levels. The flow of anodic charge was accompanied by a significant pitting of the aluminum surface. Interestingly, average pit diameter increased with increasing water concentration, whereas at the same time, pit density decreased. Average pit diameters were 3.0 ± 1.3 (43 % RSD), 5.3 ± 2.1 (39 % RSD), and 9.2 ± 3.1 (34 % RSD) μm, and pit densities were 8500 ± 800, 4400 ± 600, and 2600 ± 500 $pits/mm^2$ at 200, 500, and 1000 ppm of water, respectively. These results indicate that at higher water concentrations, corrosion proceeds primarily through the development of pits formed during the first scan, whereas at lower water levels, development of already existing pits is accompanied by formation of the new ones. It is possible that at lower water levels pits partially repassivate through deposition of corrosion products and thus corrosion through pit development is inhibited.

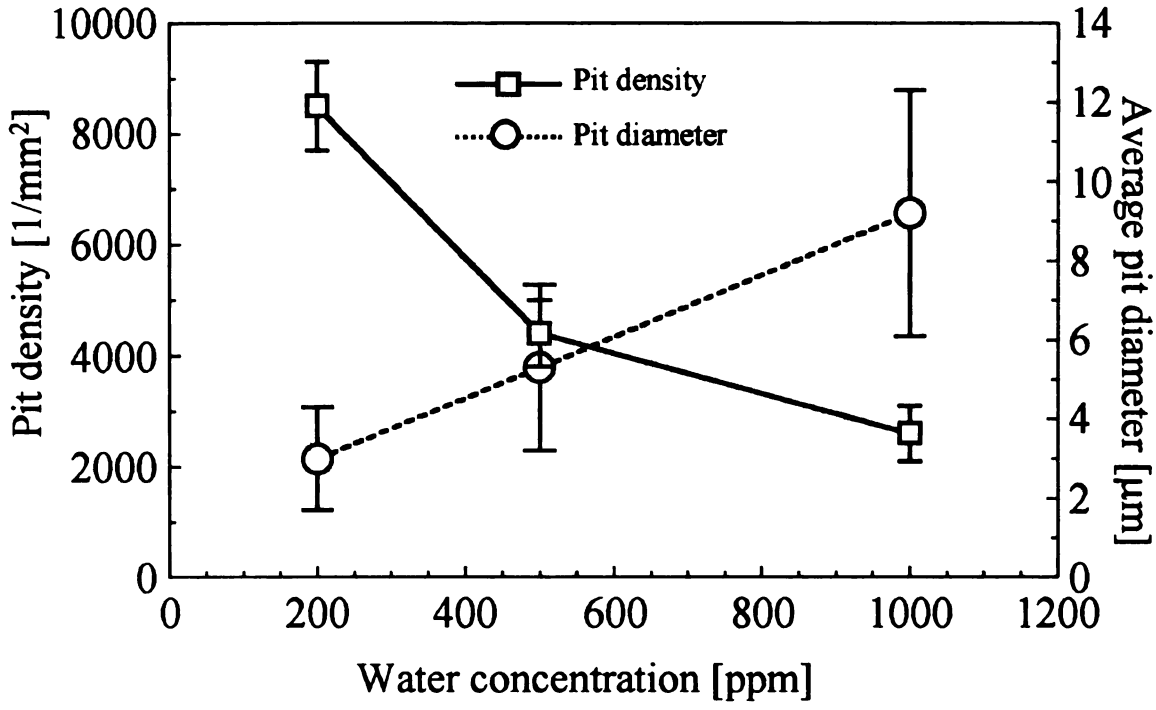

Figure 4.5. Pit density and average pit diameter as a function of concentration of water impurity in 1M $LiClO_4$/EC-DMC. Data recorded after 3 potentiodynamic scans from 2000 to 5000 mV vs. Li/Li^+, at 5 mV/s.

Higher magnification (x 2400) microscopic evaluation of the pits formed on the aluminum surface after potentiodynamic cycling in $LiClO_4$ in either PC/H_2O or EC-DMC/H_2O showed another interesting trend. In general, pits formed at lower water levels (< 500 ppm), were filled with corrosion products, indicating the deposition of the products inside the pit. On the other hand, some of the pits formed at higher water levels (1000ppm) seemed to be free of any corrosion products. Deposition of corrosion products at lower water levels was also observed by the EDS-SEM and Raman spectroscopy data, which are presented in the following section of this chapter, as well as by AFM imaging, which is discussed in Chapter 5.

Development of the corrosion pits and their coalescence during the polarization scans was also observed by *in-situ* optical microscopy. A Teflon cell with an optical window was constructed for this purpose, as described in Chapter 2. Measurements were performed in such a way that the aluminum electrode was first subjected to three potentiodynamic cycles from 2500 to 5000 mV vs. Li/Li^+, at 5 mV/s, so the formation of the pits could be easily observed on the surface with a lower magnification lens (x 300). A higher magnification lens (x 2400) was then used to image the pitted area during a subsequent potentiodynamic scan. The potentiodynamic i-E curves showed clear evidence for corrosion with E_{pit} = 4050 and E_{pass} = 3450 mV, and with shapes similar to those presented in Figure 4.3B. A sequence of images, acquired at different potentials during the 4^{th} potentiodynamic scan, is presented in Figure 4.6. The first picture (top, left) presents an image recorded at the beginning of the 4^{th} potentiodynamic scan, at potential of 2500 mV vs. Li/Li^+. Three, similarly shaped circular pits (~ 8 μm in diameter) are clearly visible on the surface. As the potential sweep proceeds, growth of the pits is observed. The last picture (bottom, right) presents an image recorded at the end of the potentiodynamic scan, at 2500 mV. It is evident that pit diameter increased nearly two times, to ~ 15 μm, during the span of potential cycle. A coalescing of the neighboring pits is also visible. The lighter areas around the pits are due to lifting of the oxide layer by the growing corrosion products. This is further discussed in Chapter 5.

It is clear that the evolution of pits occurs only in the range of potentials where the oxidation current flows. For example, the size of the pits remained constant in the potential range 2500 – 4000 mV during the forward scan, and 3300 – 2500 mV during the reverse scan. The pits grew, however, above E_{pit}, where significant oxidation current

flowed and did not cease until E_{pass}. This provides direct evidence that aluminum corrosion and dissolution occur only at the highly oxidizing potentials.

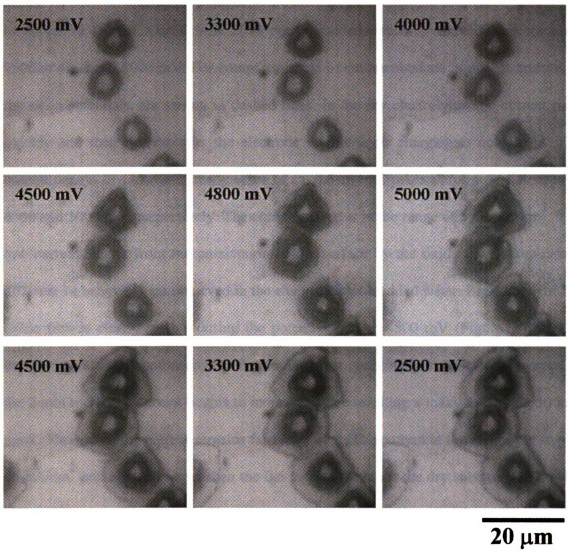

Figure 4.6. Photomicrographs of the electropolished aluminum surface, recorded *in-situ* during the 4th potentiodynamic scan at 5 mV/s in 1M $LiClO_4$/EC-DMC with 1000 ppm of added H_2O. Magnification 2400 x.

4.2.3. Corrosion of aluminum in $LiClO_4$/EC-DMC/H_2O and $LiClO_4$/PC/H_2O mixtures – chronoamperometric studies

Breakdown of the passivating Al_2O_3 film on electropolished surfaces was also observed in chronoamperometric measurements. Figure 4.7 presents chronoamperometric i-t curves in 1M $LiClO_4$/PC with 2000 ppm of added water, for the anodic steps from 2500 to 4500 and 5000 mV. For comparison, the i-t curves obtained in dry electrolyte, at the same potentials, are shown as dashed lines. In the dry electrolytes, the current rises quickly and then decreases as the electrode double layer charging is completed. The current decays to a low and steady value of ca. 0.6 and 0.8 $\mu A/cm^2$ for potential steps to 4500 and 5000 mV, respectively. The charge passed is in the range of 5 - 7 mC/cm^2. The low currents result from the passivation of the surface by the oxide layer. Completely different i-t behaviors are observed in the electrolyte with added water. Breakdown of the oxide film is clearly visible during the potential step to 4500 mV (Figure 4.7A). The current quickly rises and decays as the double layer charging is completed. However, at the 2 min mark, the current begins to increase before reaching a maximum at the 30 min mark. Thereafter, the current remains fairly constant. The current at the end of the step is 55 $\mu A/cm^2$ and is much larger than the 0.6 $\mu A/cm^2$ seen for the dry solvent. The anodic charge passed is 170 mC/cm^2. The i-t curves for the 5000 mV potential step have similar shapes (Figure 4.7B). The inset shows the i-t curves for the first 3 min. Once again, a second current increase is observed. At the higher applied potential, the induction period is greatly reduced, from 2 min to 0.2 min, and the maximum current is reached after about 0.5 min. The current decreases at much higher rate after the second current maximum, than was seen for the 4500 mV step. The current at the end of the step is ca.

50 $\mu A/cm^2$, about the same as for the 4500 mV step. The total charge is, however, much larger, 360 mC/cm^2. Clearly, the extent of the oxidation is greater at the higher potential, but the rate of oxidation at the 60 min mark is the same for both potentials. The curves indicate that exposure to potentials of 4500 mV or greater, causes localized breakdown of the passivating oxide film. Pit growth occurs at a diffusion-limited rate, as evidenced by the near steady state or decreasing current density after the second current maximum.

Photomicrographs of the electropolished aluminum surface after 1 h potential steps to 4500 and 5000 mV in 1M $LiClO_4$/PC with 2000 ppm of added water are presented in Figure 4.8 A and B. Complete destruction of the smooth oxide film is observed after exposure to 5000 mV, whereas some areas of intact oxide layer are visible on the surface after exposure to 4500 mV. Interestingly, compared to the micrograph of the surface after 50 potentiodynamic scans (Figure 4.4), a much higher pit density is observed, with an overall lower pit diameter. This indicates that during potentiodynamic cycling, corrosion proceeds primarily through development of already existing pits. There is enough time for the electrolyte/solvent mixture to diffuse to the pitted area when electrode potential is below E_{pit}. Since the corroded area is more prone to further corrosion than a neighboring oxide-coated surface, corrosion proceeds by further development of the existing pits. Under potentiostatic conditions, the greater charge causes the oxide film to break down at multiple locations. A higher pit density and smaller pit diameter are thus observed.

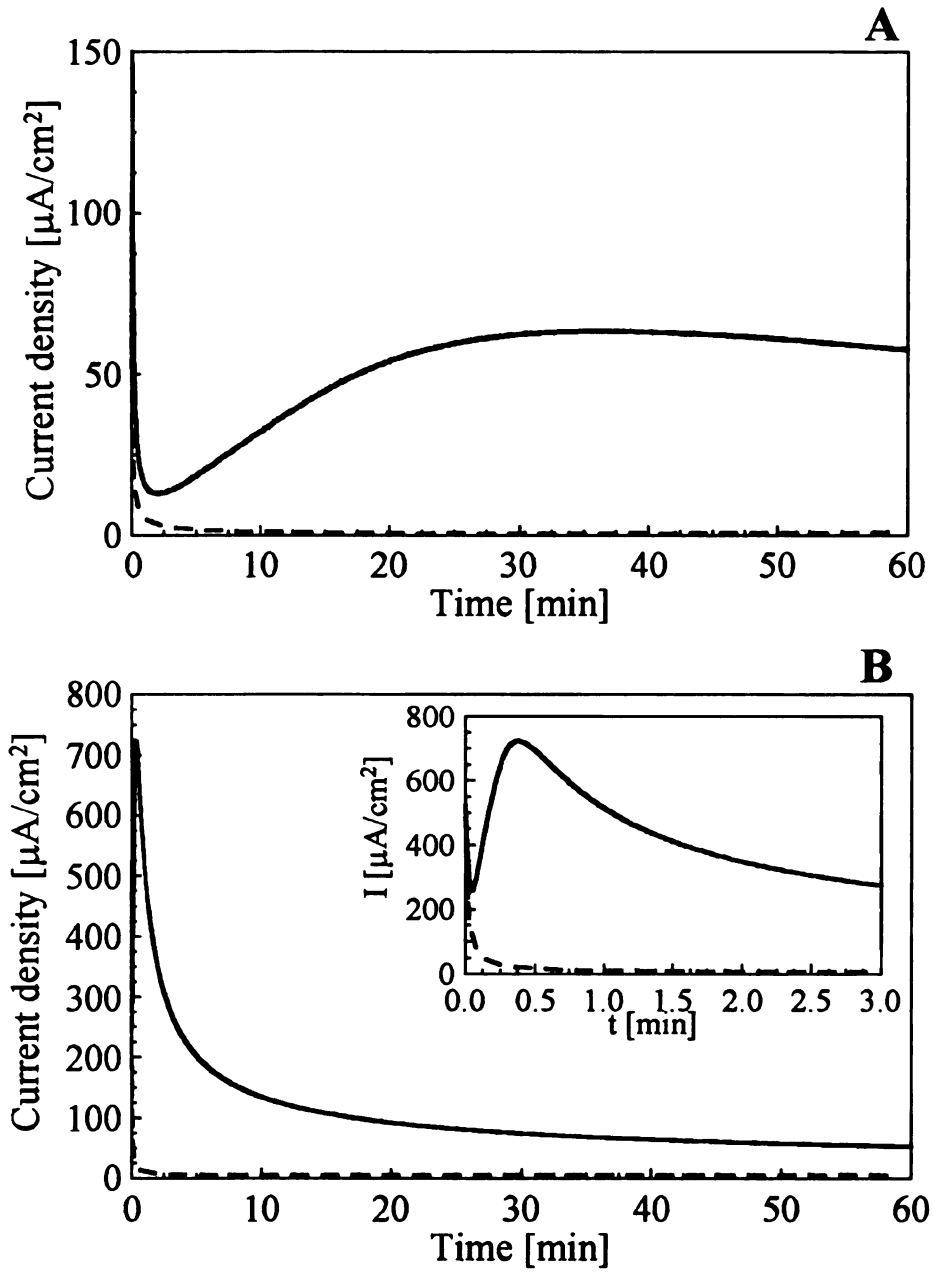

Figure 4.7. Chronoamperometric i-t curves recorded at room temperature for an electropolished aluminum electrode in 1M $LiClO_4$/PC. (A) Curves for a potential step from 2500 to 4500 mV. (B) Curves for a potential step from 2500 to 5000 mV. Solid line – electrolyte solution with 2000 ppm of water added. Dashed line – electrolyte with no added water.

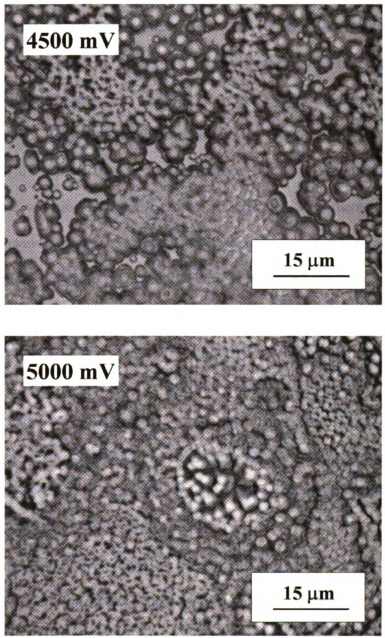

Figure 4.8. Photomicrographs of the electropolished aluminum surface after a 1 h potential step to (A) 4500 and (B) 5000 mV in 1M $LiClO_4$/PC with 2000 ppm of added water.

Mechanically polished aluminum electrodes were also evaluated by chronoamperometry. Table 4.2 summarizes the chronoamperometric results in 1M $LiClO_4$/EC-DMC and 1M $LiClO_4$/PC with different levels of added water. Each measurement was performed on a freshly, mechanically polished surface (hexane and inert Ar atmosphere). The potential was stepped from 2500 to 5000 mV vs. Li/Li^+ for 1 h. Clearly, both the anodic charge and the current at the end of the step in the two solvents, increase with increasing amount of added water. This increase is not directly proportional, however. There is a much larger increase when the amount of water is quadrupled from 500 to 2000 ppm, than when it is increased ten times, from 50 to 500 ppm. This may indicate that, at higher water content, some other process takes place on the surface. A possible process is increased solubility of the $Al(ClO_4)_3$ layer formed on the surface, as it was proposed by Kelly for iron in $LiClO_4$/PC. This result is in agreement with previous voltammetric results, which indicated increased corrosion at water levels higher than 500 ppm. Also, both the oxidation current and charge at the 1 h mark are higher in EC-DMC than in PC. This may be explained by higher viscosity of PC and thus lower mobility of water in this solvent.

The chronoamperometric results for electropolished aluminum in 1M $LiClO_4$/EC-DMC and 1M $LiClO_4$/PC with 2000 ppm of added water are also presented in Table 4.2, for comparison. Although only the 2000 ppm water level was investigated on electropolished surfaces, it is clear that both the oxidation current and charge at the 1 h mark are much lower on the electropolished surface than on the mechanically polished one, at the same level of added water impurity. This is in agreement with our voltammetric results, which indicated some protective properties of the aluminum oxide layer.

	$LiClO_4$/EC-DMC		$LiClO_4$/PC	
ppm of added H_2O	Q_{ox} [mC/cm^2]	I_{ox} [μA/cm^2]	Q_{ox} [mC/cm^2]	I_{ox} [μA/cm^2]
mechanically polished				
2000	750	105	600	80
500	265	40	200	30
50	245	35	180	25
0	18	2.5	20	3.0
electropolished				
2000	420	55	360	50

Table 4.2 Summary of the chronoamperometric data for mechanically polished and electropolished aluminum. Potential step from 2500 to 5000 mV vs. Li/Li^+, for 1 h. Oxidation charge and current data were collected at 1 h mark.

4.2.4. Chemical composition of the corrosion products in $LiClO_4$/EC-DMC/H_2O and $LiClO_4$/PC/H_2O mixtures – energy dispersive x-ray microanalysis (EDS) and Raman spectroscopy studies

The elemental composition of the precipitated corrosion products was investigated with energy dispersive x-ray microanalysis (EDS). Figures 4.9 and 4.10 present representative x-ray analysis data for the mechanically polished aluminum surface before and after polarization (3 potentiodynamic scans at 5 mV/s; 2000-5000 mV vs. Li/Li^+) in 1M $LiClO_4$/PC with 500 ppm of added H_2O. Black crosses on the SEM images indicate the sampling points. Before polarization, Al, O and traces of C were the only elements detected on the surface. A highly porous layer of corrosion products forms on the surface

during polarization, as evidenced in the SEM image in Figure 4.10. A large signal for Cl is present and the O signal increases over that observed for the surface prior to polarization. These results suggest that the perchlorate anion plays an active role in the corrosion of aluminum.

Somewhat similar results were also obtained for the electropolished surface. Figure 4.11 (top) presents a SEM image of the surface after 3 potentiodynamic scans (5 mV/s; 2000-5000 mV vs. Li/Li^+) in 1M $LiClO_4$/PC with 200 ppm of added H_2O. Corrosion pits (~ 4 μm in diameter) are clearly observed in SEM image. Energy dispersive x-ray analysis spectra acquired inside and outside of the pit are also present in Figure 4.11. Clearly, the pits present are filled with corrosion products. The elemental composition of the corrosion products within the pits is similar to the composition of the corrosion products on the mechanically polished surface, based on the peak intensity ratios in the spectra. On the other hand, neither Cl nor increased amounts of O were detected on the undamaged Al_2O_3 regions (spectrum 2). This indicates that the pitting corrosion process is very localized. However, for higher water concentrations (2000 ppm), clean pits were often observed. EDS indicated much lower amounts of Cl or O for such a case (Figure 4.12). This observation suggests that at higher water concentrations, the corrosion products are highly soluble and afford little protection to the corroding metal. Analogous results were also obtained for $LiClO_4$/EC-DMC/H_2O mixtures.

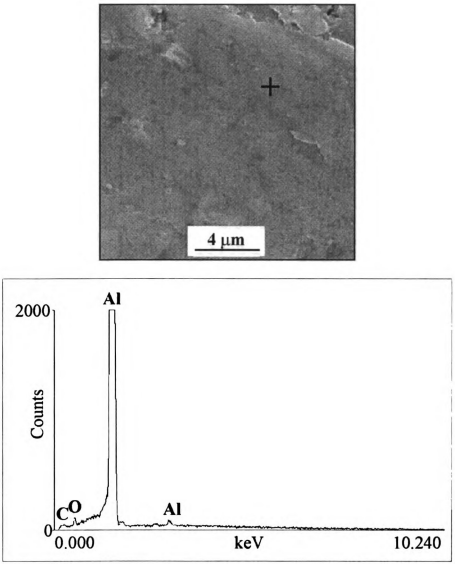

Figure 4.9. An SEM image and an energy dispersive x-ray analysis spectrum for mechanically polished aluminum prior to polarization.

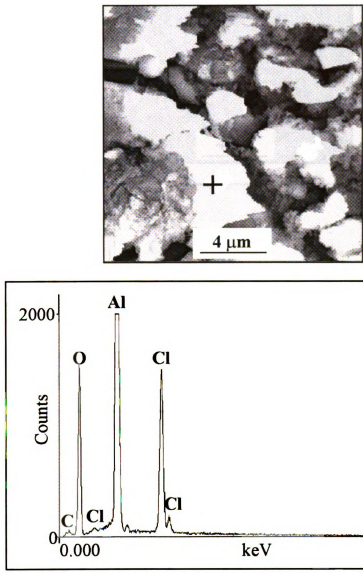

Figure 4.10. An SEM image and an energy dispersive x-ray analysis spectrum for mechanically polished aluminum after potentiodynamic polarization (3 scans at 5 mV/s; 2000-5000 mV vs. Li/Li^+) in 1M $LiClO_4$/PC + 500 ppm H_2O.

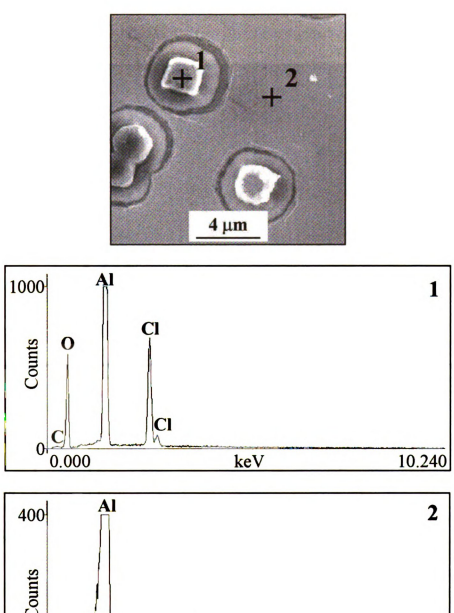

Figure 4.11. An SEM image and energy dispersive x-ray analysis spectra for electropolished aluminum after potentiodynamic polarization (3 scans at 5 mV/s; 2000-5000 mV vs. Li/Li^+) in 1M $LiClO_4$/PC + 200 ppm H_2O. Spectrum 1 corresponds to a region inside the pit while spectrum 2 corresponds to a region outside.

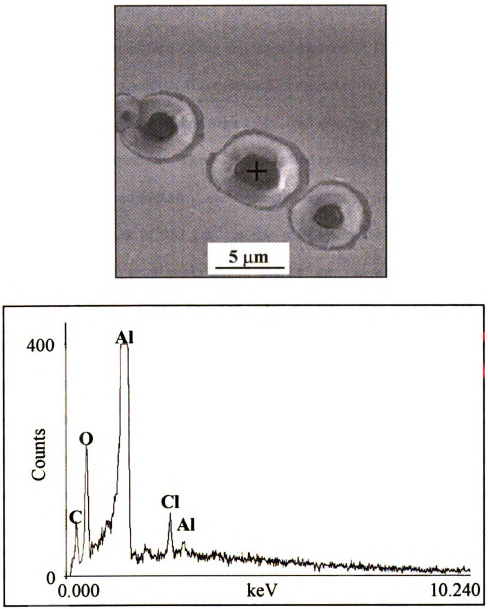

Figure 4.12. An SEM image and an energy dispersive x-ray analysis spectrum for electropolished aluminum after 2 potentiodynamic scans (5 mV/s; 2000-5000 mV vs. Li/Li^+) in 1M $LiClO_4$/PC + 2000 ppm H_2O.

The deposited corrosion products were also investigated by Raman spectroscopy. Figure 4.13 shows a Raman spectrum for corrosion product in a pit formed on an electropolished aluminum surface during anodic polarization in 1M $LiClO_4$/PC with 500 ppm of added H_2O. The spectrum was collected in air, after the electrode was removed from the electrochemical cell, washed with DMC, and dried in flow of Ar. Three sharp peaks are present in the spectrum. They were identified as modes characteristic of ClO_4^-. The peaks at 457 cm^{-1} and 630 cm^{-1} are associated with the $\nu_2(e)$ and $\nu_4(f)$ vibrations, respectively, and the peak at 933 cm^{-1} is due to a symmetric stretch $\nu_1(a_1)$ of the perchlorate anion.[41] Two small peaks at 715 and 845 cm^{-1} as well as a group of three peaks centered at 2940 cm^{-1} were assigned to PC residue.[41] The peaks at 715 and 845 cm^{-1}, are associated with out-of-plane C=O ring bending and ring breathing, respectively. Three peaks around 2940 cm^{-1} are associated with C-H stretches. The broad peak observed at 3500 cm^{-1} is most probably due to the presence of mixed aluminum hydroxides and is associated with (OH)-stretching.[42] For comparison, Raman spectra of the unpolarized electropolished surface, bulk $LiClO_4$ and $Al(ClO_4)_3 \cdot H_2O$ crystals are presented in Figure 4.13. A red shift of the symmetric $\nu_1(a_1)$ stretch (933 vs. 955 cm^{-1}) for the corrosion product is seen, and this indicates free ClO_4^-. A similar shift is also observed for hydrated perchlorate salts.[43] Analogous results were also obtained for $LiClO_4$/EC-DMC/H_2O mixtures.

The presence of surface ClO_4^- was also observed for the mechanically polished electrodes after polarization. This indicates that the mechanism of the corrosion process is the same for both electropolished and mechanically polished electrodes. The difference is the extent of the corrosion and the amount of corrosion product on the surface.

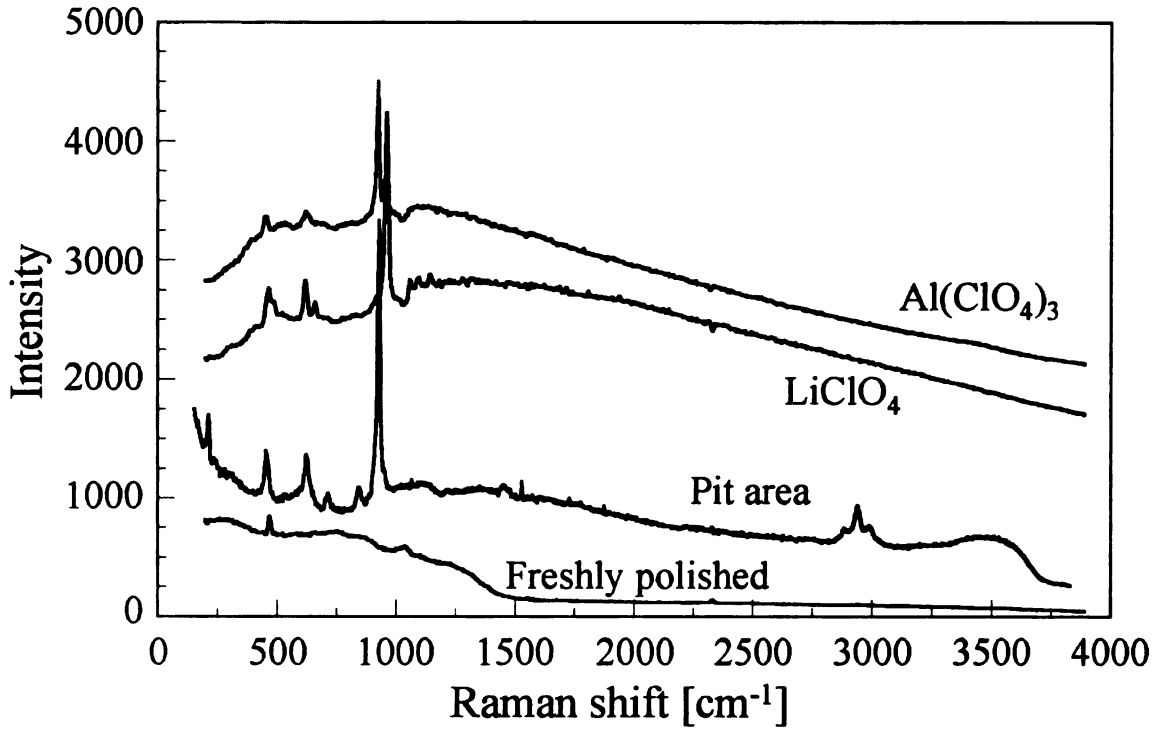

Figure 4.13. Raman spectrum of the corrosion product in the center of a pit on electropolished aluminum. The pit and corrosion product were formed after 2 potentiodynamic scans from 2500 to 5000 mV vs. Li/Li^+ in 1M $LiClO_4$/PC with 500 ppm of added H_2O. Scan rate = 5 mV/s. Spectra for the freshly electropolished surface, and solid samples of $LiClO_4$ and $Al(ClO_4)_3 \cdot H_2O$ are shown, for comparison.

The spatial distribution of Raman features across a pitted area is shown in the line-imaging profile in Figure 4.14. A photomicrograph of the pit formed and the line profile are shown in Figure 4.14A. Figure 4.14B presents the set of 14 Raman spectra collected along the profile. Clearly, ClO_4^- is present only inside the pit. The presence of ClO_4^- in the corrosion product is probably caused by ion migration into corroding area and formation of solid $Al(ClO_4)_3$.

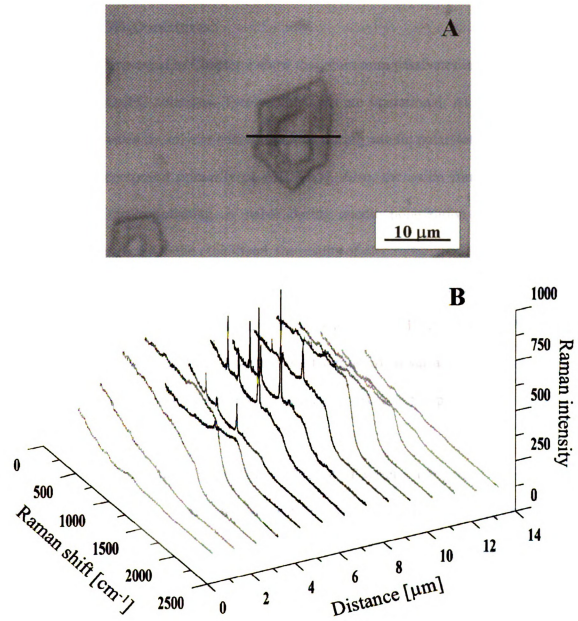

Figure 4.14. (A) Photomicrograph of a corrosion pit on the electropolished aluminum surface after 2 cyclic voltammetry scans between 2500 and 5000 mV vs. Li/Li^+ in 1M $LiClO_4$/EC-DMC + 500 ppm of water. Scan rate = 5 mV/s. The black line indicates Raman spectra line profile. (B) A series of Raman spectra obtained along the line shown in 1 µm increments. Acquisition time = 10 min.

4.2.5. Mechanism of aluminum corrosion in $LiClO_4$/EC-DMC/H_2O and $LiClO_4$/PC/H_2O mixtures

The results presented in Chapter 3 show that aluminum passivates in dry $LiClO_4$/EC-DMC and $LiClO_4$/PC solutions. Two mechanisms are operational. At OCP conditions, aluminum passivates by solvent adsorption, and during anodic polarization by formation of a salt film, composed primarily of $Al(ClO_4)_3$. Also, the oxide film, formed on the surface during electropolishing, is stable during anodic polarization and additionally passivates the surface. On the other hand, the results of electrochemical, microscopic, and spectroscopic investigations presented in this chapter indicate that water interferes strongly with the passivation of aluminum in $LiClO_4$/EC-DMC and $LiClO_4$/PC. Severe corrosion of either mechanically polished or electropolished surfaces is observed when the solvent is contaminated with water, particularly at levels $\geq$ 500 ppm.

Previously, Kelly *et al.* studied the influence of water on the passivity of iron in $LiClO_4$/PC.[31,44] They observed that water interferes with all three passivation mechanisms (solvent adsorption, air-formed oxide film, and salt film formation) commonly observed in non-aqueous electrolyte/solvent mixtures. The authors showed that water levels as low as 100 ppm are detrimental to the stability of iron in $LiClO_4$/PC solutions. On bare iron surfaces, water molecules compete with the solvent molecules for adsorption sites on the surface. The presence of surface water lowers the activation energy for metal dissolution, destroying the passivation provided by a chemisorbed solvent layer. The presence of an air-formed oxide film on the surface did not prevent iron from corroding in electrolyte solutions with added water. This was attributed to the

oxidation of water and acidification of electrolyte solution. Under such conditions, localized breakdown of the air-formed film occurs. Finally, the presence of water led to increased solubility of the $Fe(ClO_4)_2$ layer formed on the surface during polarization, thus destroying the passivity provided by salt film.

A similar mechanism in which water interferes with the passivation of aluminum in $LiClO_4$/EC-DMC and $LiClO_4$/PC is proposed and is consistent with the experimental observations. First of all, water can interfere with the adsorption of the solvent molecules at OCP conditions. This seems to be true as the OCP values were lower (i.e., more active) in both $LiClO_4$/PC and $LiClO_4$/EC-DMC in the presence of water. The effect was especially pronounced in PC, in which the addition of 2000 ppm of water lowered the OCP by ~400 mV. This can be explained by strong competition between water and organic solvent molecules for the adsorption sites on the metal/metal oxide surface. Zelenay and coworkers observed previously that water displaces PC molecules and adsorbs on the platinum electrode surface.[45] The maximum measured surface concentration of water reported by the authors was ~ 1.4×10^{14} molecules/cm^2 (in 0.1M $LiClO_4$/PC with 1500 ppm of added water).

During anodic polarization, water may react with aluminum to form a mixed aluminum oxide and hydroxide layer according to the following reactions:

$$2Al + 3H_2O \rightarrow Al_2O_3 + 6\,H^+ + 6\,e^- \qquad [4.1]$$

$$Al + 3H_2O \rightarrow Al(OH)_3 + 3\,H^+ + 3\,e^- \qquad [4.2]$$

$$Al + 2H_2O \rightarrow AlOOH + 4\,H^+ + 4\,e^- \qquad [4.3]$$

Such a bilayer greatly improves passivity of aluminum in aqueous solutions.[1] However, since only limited amounts of water are present in the non-aqueous electrolyte/solvent mixture, the oxide/hydroxide layer is not continuous, which significantly limits its protective capabilities. In fact, Kelly *et al.* showed that corrosion of iron occurs in $LiClO_4$/PC when water at the levels of 5 mM (75 ppm) to 17 M (26 %) are present in the electrolyte/solvent mixture.[31,44] Only at water levels exceeding 17 M limit, is stable passivation restored due to the formation of a continuous oxide/hydroxide layer.

A non-uniform oxide film was observed in present studies. SEM imaging shows a highly porous passivation layer on the surface of mechanically polished aluminum after anodic polarization in $LiClO_4$/EC-DMC/H_2O and $LiClO_4$/PC/H_2O.

Reactions 4.1-4.3 also indicate a possible explanation for the low resistance of the oxide film present on the electropolished surface toward pitting corrosion in $LiClO_4$/EC-DMC/H_2O and $LiClO_4$/PC/H_2O. These reactions lead to localized acidification of the electrolyte mixture. It is well known that, in aqueous solutions, pitting of aluminum is not likely in neutral solutions. It occurs, however, in acidic environments.[1]

Another reaction is also likely to induce pitting of the electropolished surface. XPS results for the aluminum surface after anodic polarization in $LiClO_4$/EC-DMC, presented in Chapter 3, indicate that at high anodic potentials, oxidative decomposition of ClO_4^- occurs and Cl^- forms. The corrosive properties of Cl^- are well established in aqueous solutions. Cl^- as a small ion with high diffusivity, tends to penetrate the oxide layer at weak points (flaws) enhancing dissolution of the base metal, thus leading to pitting.[1,28] A similar effect of the Cl^- can be expected in PC/H_2O and EC-DMC/H_2O solutions. Interestingly, pitting of the aluminum surface is not observed in dry electrolytes which

may be explained by the low activity of Cl^- caused by strong ion pairing observed in organic carbonates.[46] The synergism between water and Cl^- was also observed before, by Kelly, for corrosion of iron in $LiClO_4$/PC.[44]

Finally, water can increase dissolution of the salt film formed during anodic polarization. As XPS, EDS, and Raman spectroscopy data show, the $Al(ClO_4)_3$ is a product of aluminum dissolution during anodic polarization in either dry or water contaminated solvents. The formation of $Al(ClO_4)_3$ in dry solvents effectively passivates the surface due to supersaturation and precipitation of the salt deposit at the active sites on the metal surface. The presence of water increases the solubility of $Al(ClO_4)_3$, thus, diminishing the passivation. In the present studies, this effect was especially visible at higher water concentrations (> 500 ppm) as empty pits were observed on the surface.

4.2.6. Corrosion of aluminum in $LiPF_6$/EC-DMC/H_2O and $LiPF_6$/PC/H_2O mixtures

The addition of water to $LiPF_6$/EC-DMC or $LiPF_6$/PC did not have as much of an effect on the susceptibility of aluminum to corrosion, as it did in the $LiClO_4$-based electrolyte/solvent systems. Passivation of the aluminum was observed to occur after the first potentiodynamic scan, similar to what was seen for the water free electrolytes. Figure 4.15 presents potentiodynamic i-E curves (5 mV/s) for the first cycle in 1M $LiPF_6$/EC-DMC with 500 ppm of added H_2O. Curve (A) is the response for the mechanically polished electrode, (B) the response for the mechanically polished electrode after 10 h at OCP, and (C) the response for the electropolished electrode. For comparison, the response for the mechanically polished electrode during polarization in solution without intentionally added water is showed in (D). Since consecutive cycles did not

show any signs of further oxidation or corrosion of the aluminum surface, they are not presented here for clarity.

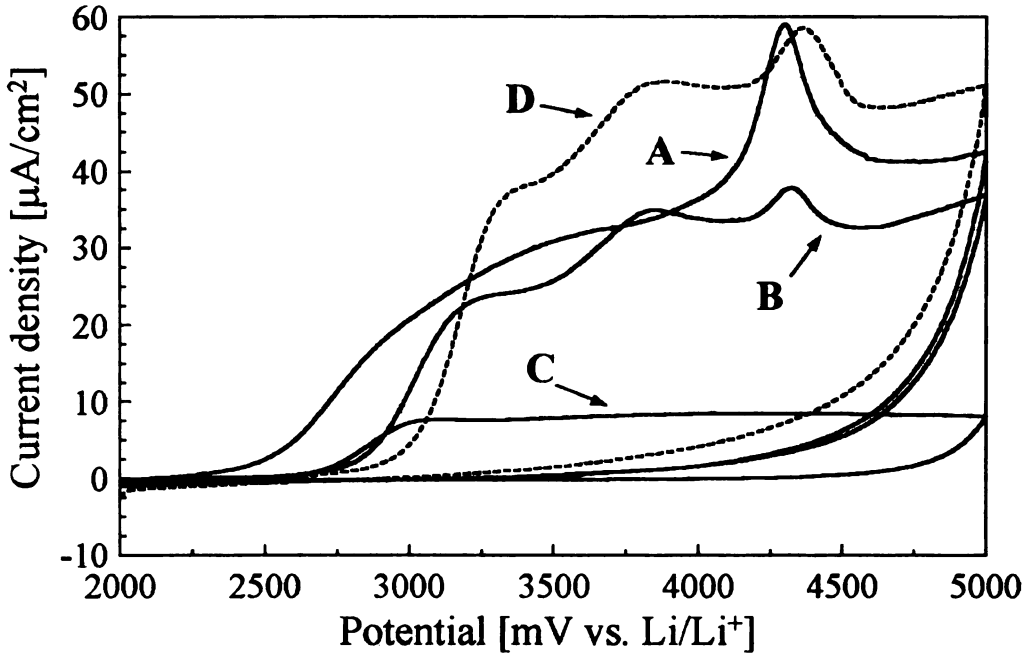

Figure 4.15. Cyclic voltammetry (1st scan) in 1M $LiPF_6$/EC-DMC + 500 ppm H_2O. (A) – mechanically polished aluminum; (B) – mechanically polished aluminum after 10 h at OCP in the same electrolyte mixture; (C) electropolished aluminum; (D) – mechanically polished electrode, no added water. Scan rate = 5 mV/s.

As can be seen, oxidation current and charge recorded during the first cycle in electrolyte solution with added water are smaller than in dry electrolyte. This indicates that the $LiPF_6$/EC-DMC/H_2O solution better passivates the surface. There is also significant difference in the peak height observed for the oxidation peak at 4300 mV vs. Li/Li^+ for the electrode cycled right after placement in the cell and for one that was kept at OCP for 10 h before cycling. This may indicate that the peak at 4300 is due to

oxidation of water or oxidation of aluminum in the presence of water. It is also possible that this peak arises due to interaction of aluminum with products of the hydrolysis of $LiPF_6$. It is well known that $LiPF_6$ is not stable in the presence of water and is hydrolyzed quickly according to reactions:[24]

$$LiPF_6 \rightleftarrows PF_5 + LiF\downarrow \qquad [4.4]$$

$$PF_5 + H_2O \rightarrow 2HF + POF_3 \qquad [4.5]$$

Fast hydrolysis of $LiPF_6$ was also observed during our studies. For example, preparation of the solution with higher than 500 ppm water content caused gas evolution, etching of the glass cell and fast corrosion of lithium electrodes.

XPS analysis of the surface revealed the atomic presence of the following elements: Al (2p, 75 eV) – 17 atomic %, Li (1s, 56 eV) – 10 atomic %, C (1s, 285 eV) – 19 atomic %, F (1s, 686 eV) – 31 atomic %, O (1s, 532 eV) – 22 atomic %, and P (2p, 135 eV) – 1 atomic %. These results are similar to those obtained in electrolytes with no added water indicating the mechanism of passivation is similar, and is based on the improved passivity of the aluminum oxyfluoride film over the aluminum oxide film in the non-aqueous electrolytes.

The important information gained is that aluminum passivates in $LiPF_6$/EC-DMC, even in the presence of water. This also means that the presence of HF, a hydrolysis by-product, does not induce corrosion. Passivation of aluminum in the presence of water and HF was previously observed by Kanamura *et al.*[6] The authors successfully used small additions of aqueous hydrofluoric acid in order to suppress corrosion in otherwise strongly corrosive $LiCF_3SO_3$/PC and $LiN(CF_3SO_2)$/PC mixtures. Results of their XPS

studies indicated that the passive layer was a mixture of AlF_3 and AlOF. The chemical composition of the passivation layer was independent on the electrolyte, indicating that its passivating properties resulted directly from the presence of fluoride in the electrolyte/solvent mixture.

The surface of the electropolished aluminum, after polarization in $LiPF_6$/EC-DMC + 500 ppm H_2O, was visually different from the surface before polarization. The normally very reflective surface appeared "milky" at the area that was exposed to the electrolyte solution. OM and SEM, however, did not reveal any noticeable changes in the surface structure. AFM microscopy, on the other hand, showed a uniform, surface roughening (nm range). AFM results are described in detail in the next chapter.

4.3. Conclusions

The presence of added water inhibits the passivation of aluminum in $LiClO_4$/EC-DMC and $LiClO_4$/PC at highly oxidizing potentials (5 V vs. Li/Li^+). Pitting and progressive corrosion is accompanied by the formation of a highly porous, non-protective layer of the corrosion products on the surface. The native oxide film does not prevent the underlying aluminum metal from being corroded in $LiClO_4$-based solvent/electrolyte mixtures when water impurity is present. Significant pitting of the surface occurs under such conditions. Due to the limited solubility of the corrosion products (mostly $Al(ClO_4)_3$), the pits fill with the corrosion products, forming mounds on the surface.

On the other hand, water does not significantly affect the passivity of aluminum in $LiPF_6$/PC and $LiPF_6$/EC-DMC. This is most probably due to formation of the

oxyfluoride layer that is very effective at protecting aluminum surfaces during anodic polarization.

CHAPTER 5

5. Aluminum Corrosion in $LiPF_6$/EC-DMC and $LiClO_4$/EC-DMC – Investigations Using Atomic Force Microscopy (AFM)

5.1. Introduction

Monitoring changes in the surface structure of an electrode is an essential component of research concerned with understanding electrochemical processes, such as corrosion, passivation, and deposition. Over the years, various microscopic techniques have been used for this purpose. Historically, optical microscopy (OM), scanning electron microscopy (SEM), and transmission electron microscopy (TEM) have been the most often used techniques. The introduction of scanning tunneling microscopy (STM) in 1982,[47] and development, in the subsequent years, of atomic force microscopy (AFM) provided researchers with new, powerful tools for the analysis of surface structure.[48]

AFM is one of the most important and widely used forms of scanning probe microscopy. It provides very high lateral resolution, superior to OM and SEM, and in some cases, can achieve atomic resolution. AFM can also produce topographical images of electrically insulating surfaces, materials that cannot be probed with STM. Another powerful feature of AFM is its ability to image surface structure while immersed in a liquid.[49] This feature has provided a revolutionary approach for the *in situ* characterization of electrode surfaces and electrochemical processes. The combination

of AFM with various galvanostatic and potentiostatic electrochemical techniques, called electrochemical atomic force microscopy (ECAFM), makes possible the study of electrode surface morphology while electrochemical reactions are underway. The technique has been used for studying such phenomena as underpotential deposition (upd),[50,51] potential-driven adsorption and desorption,[52,53] and formation and self-organization of monolayers.[54]

AFM has been also shown to be very effective for studying electrode processes at much larger than atomic or molecular dimensions. Three-dimensional topographical imaging of a surface, at the nanometer to micrometer scale, is particularly useful for *in situ* monitoring of processes such as electrochemical corrosion (general and localized),[55-57] passivation,[58-60] and metal plating and stripping.[61-63] In many cases, ECAFM has enabled the verification of reaction mechanisms that otherwise could only be based on electrochemical measurements and *ex situ* microscopy. For example, ECAFM studies of pitting corrosion of metals in aqueous environments have confirmed the importance of the surface inhomogeneities (grain boundaries, inclusions, and second-phase precipitates) in assisting passivation layer breakdown and initiation of corrosion.[55,56]

Metal corrosion processes in non-aqueous media have not been extensively studied with AFM or ECAFM. There are only a few examples of such studies in the literature. Bellucci et al. investigated the passivation of Ni in 0.1M H_2SO_4/DMF and 0.1M H_2SO_4/acetonitrile solutions.[64] The electrochemical measurements indicated the formation of a thin, poorly passivating layer and the possibility of salt precipitation onto the metallic surface. AFM images showed that in both solvents, the sample surface was very inhomogeneous with flakes and fractures, which confirmed the results of electrochemical measurements. ECAFM has also been extensively used to investigate the

corrosion/passivation of lithium in non-aqueous electrolytes. This is mostly due to developments in lithium and lithium-ion batteries.[65-67]

To the best of my knowledge, there are no reports on the use of AFM to study aluminum corrosion in non-aqueous media. The use of AFM and ECAFM to monitor topographical changes in the aluminum surface during anodic polarization in 1M $LiClO_4$/EC-DMC and 1M $LiPF_6$/EC-DMC, is described herein. The imaging modes were also used to study the corrosion mounds and pits formed during anodic polarization in $LiClO_4$/EC-DMC/H_2O mixtures. All measurements were made using electropolished aluminum electrodes. Electropolishing produces a very smooth surface, which proved to be essential for the observation of small deposits formed on the surface. It also produces a very reflective surface, which was very useful during the studies of corrosion pit formation, as the pits could easily be located with an optical microscope to allow for proper positioning of the AFM tip.

5.2. Results and discussion

5.2.1. *Ex-situ* atomic force microscopy – dry electrolytes

Results presented so far indicate that aluminum passivates in dry electrolyte/solvent mixtures. Both electrochemical measurements and XPS data indicate that a passivation layer forms on the surface, protecting the metal from further corrosion. The formation of the passivation layer could not be confirmed by either OM or SEM. Thus, a goal was to see if it could be observed with AFM, which provides superior resolution, both vertically and horizontally, as compared with OM and SEM

Figure 5.1 presents representative contact mode *ex situ* images of (A) an untreated electropolished surface, and electropolished surfaces after anodic polarization in (B) $LiClO_4$/EC-DMC and (C) $LiPF_6$/EC-DMC. The images were acquired after the electrodes were cycled in the corresponding electrolyte/solvent mixture (3 scans; 5 mV/s; 2500 – 5000 mV vs. Li/Li^+), rinsed with copious amounts of DMC, and dried in a flow of argon inside the dry box. The formation of the 50-200 nm deposits, evenly distributed over the aluminum surface, is observed for both electrolytes. Their average height is only 5 – 10 nm, which explains why they were difficult to observe by OM or SEM. Interestingly, the deposit morphology and surface coverage are similar in both electrolytes indicating that their formation is directly influenced by the structure of the oxide film. The formation of localized deposits implies that the initial oxidation processes take place at pores and defects in the oxide film, as is the case in aqueous environments.[28] The corrosion products are largely insoluble in organic solvent and they deposit in the localized regions where they are formed. The deposition of the corrosion products effectively passivates the surface. It was also observed that these deposits strongly adhere to the surface as they could not be removed by ultrasonication in DMC or by moderate scratching with the AFM tip. This also proves that these deposits were not some kind of precipitate from the electrolyte solution, but rather were products of the reaction between electrolyte and the aluminum surface.

Interestingly, similar surface deposits were also observed on electrodes simply soaked in $LiPF_6$/EC-DMC for a period of 10 h, whereas no deposits were observed on electrodes soaked in $LiClO_4$/EC-DMC. These observations are consistent with the electrochemical and XPS data discussed in the Chapter 3. In other words, the aluminum surface reacts with the $LiPF_6$ hydrolysis products (e.g., HF), even at OCP.

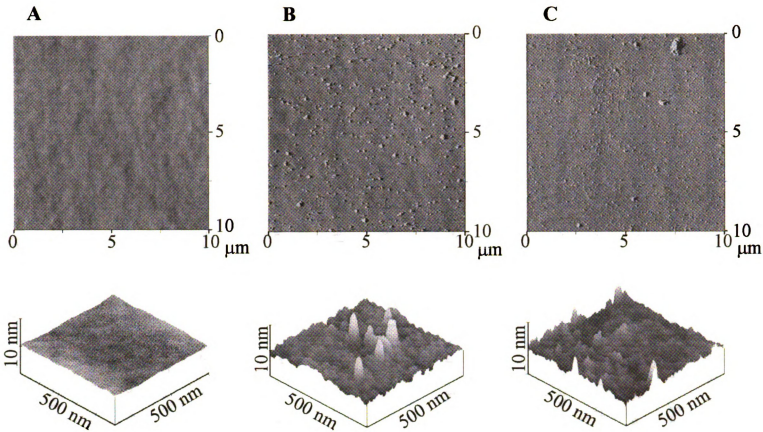

Figure 5.1. *Ex situ* AFM images of an electropolished aluminum surface before (A) and after anodic polarization (3 scans; 5 mV/s; 2500 – 5000 mV vs. Li/Li^+) in (B) 1M $LiClO_4$/EC-DMC and (C) 1M $LiPF_6$/EC-DMC. Top images were obtained in the deflection mode and bottom images in the height mode.

5.2.2. *Ex situ* atomic force microscopy - $LiPF_6$/EC-DMC/H_2O

Data presented in Chapter 4 indicate that the passivation of aluminum in 1M $LiPF_6$/EC-DMC occurs even in the presence of added water. Previously, Braithwaite *et al.* observed, with electrochemical impedance spectroscopy, that aluminum passivation in 1M $LiPF_6$/PC-DEC improves when the water is present as a contaminant.[4] The improved passivation was attributed to stabilization of the passivation layer by water molecules. On the other hand, Kanamura *et al.* observed improved passivation in non-aqueous electrolytes, in the presence of HF.[6] They attributed the improved passivation to reaction of HF with aluminum oxide and the formation of AlF_3 and AlOF according to reactions:

$$Al_2O_3 + 6HF \rightarrow 2AlF_3\downarrow + 3H_2O \qquad [5.1]$$

$$Al_2O_3 + 2HF \rightarrow 2AlOF\downarrow + H_2O \qquad [5.2]$$

They confirmed the existence of such a layer with XPS, and concluded that AlOF and AlF_3 have better passivating properties in non-aqueous electrolytes than does Al_2O_3.

HF was not purposely added to the electrolyte/solvent mixture in present research. Its presence is, however, expected considering the fact that HF is a product of $LiPF_6$ hydrolysis (Chapter 3, reactions [4] and [5]). Taking this into account, a passivation layer of different structure than the one observed in dry electrolytes is expected. Again, as in the case for the dry electrolyte, the formation of the passivation layer could not be confirmed by OM or SEM. It was observed, however, that the appearance of the naturally shiny, and very reflective electropolished surface, changed. The surface became "milky" in the area exposed to the electrolyte solution during polarization. If this change in

appearance was accompanied by different surface structure, it should be possible to observe such changes with AFM.

Figure 5.2 presents the AFM images of the electropolished aluminum surface after 3 cyclic voltammetric scans in 1M $LiPF_6$/EC-DMC with 500 ppm of added H_2O. The potential was scanned between 2000 – 5000 mV vs. Li/Li^+ at 5 mV/s. After the last scan was completed, the electrode was washed with DMC and dried in the flow of argon. The 10 x 10 μm^2 deflection mode image (Figure 5.2 A) resembles that for the electrode cycled in $LiPF_6$/EC-DMC without added water (Figure 5.1 C top). Multiple, 50 to 200 nm deposits are randomly formed on the surface, indicating highly localized dissolution of aluminum and passivation of the surface. However, a higher magnification, height mode image (Figure 5.2 B) indicates a significant increase in the surface roughness. Such uniform surface roughening can be explained by reaction of HF, formed from the hydrolysis of the $LiPF_6$, with the aluminum oxide film on the surface, and formation of a new, oxyfluoride layer. A similar reaction has been proposed previously by Kanamura *et al.*[6]

Roughening of the aluminum surface in the presence of fluoride is also commonly observed in aqueous solutions. For example, Hurlen and coworkers observed that the presence of F^- stimulates the anodic dissolution (hence, roughening) of passivated aluminum, without completely destroying the passivation.[68] The authors concluded that this process occurs mostly by a transport-limited reaction of fluoride with aluminum ions dissolving at the metal surface. A similar conclusion was reached by Richardson *et al.*, who investigated the passivation of aluminum in aqueous fluoride solutions with

impedance measurements.[69] Their results were consistent with rapid removal of the surface oxide film and its replacement by a complex oxyfluoride film.

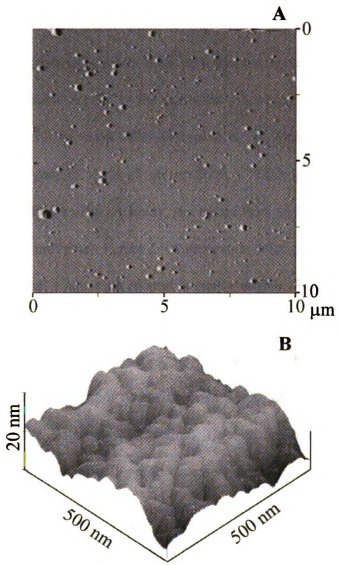

Figure 5.2. AFM images of an electropolished aluminum surface after 3 potentiodynamic scans in 1M $LiPF_6$/EC-DMC with 500 ppm of added H_2O (5 mV/s; 2000-5000 mV vs. Li/Li^+). (A) Deflection mode image. (B) Height mode image.

5.2.3. *Ex situ* atomic force microscopy - $LiClO_4$/EC-DMC/H_2O

The electrochemical and microscopic observations of aluminum corrosion in $LiClO_4$/EC-DMC and $LiClO_4$/PC, contaminated with water (Chapter 4), showed that the impurity is detrimental to the passivation of the metal. Significant pitting of the aluminum surface was observed. SEM, EDS, and Raman spectroscopy results have shown that oxidation products deposit in the corrosion pits when the water level is kept below 500 ppm. Figure 5.3 presents AFM images of a pit formed on the aluminum surface after 2 potentiodynamic scans (5 mV/s; 2000 – 5000 mV vs. Li/Li^+) in 1M $LiClO_4$/EC-DMC with 500 ppm H_2O. Clearly, the formations on the surface are mounds (pits filled with corrosion products). Figure 5.3A presents a deflection mode image of the mound. The square-shaped, 1 μm high mound is easily visible. Figure 5.3B presents a height mode image of the same mound. Lateral progress of the corrosion can be clearly observed as two distinct rectangular shapes, one inside the other. It seems that the $LiClO_4$/EC-DMC/H_2O mixture is not corrosive toward the entire oxide film, as intact regions are present at the edges of the mound. This observation indicates that the corrosion process starts locally, probably at the pores or defects in the oxide film. It then proceeds at the interface between aluminum and aluminum oxide layer. As aluminum is being dissolved, formation of $Al(ClO_4)_3$ probably occurs, as indicated by EDS and Raman data (Chapter 4). Since the $Al(ClO_4)_3$ is soluble in both PC and EC-DMC, its precipitation indicates that local supersaturation conditions are met. Breakage of the oxide film occurs, as the solid corrosion products deposit and lift the oxide film up from the surface.

Such a mechanism would require relatively fast migration of the ClO_4^- through the oxide film. Since corrosion does not occur in dry $LiClO_4$ solutions, as the surface passivates during the first scan, then one of the roles of water in the corrosion process might be increasing the ClO_4^- partitioning rate through the oxide film. This may occur due to the changes in the solvation sphere of the ClO_4^- in the presence of water. In anhydrous solvent, ClO_4^- is solvated by ethylene carbonate and dimethyl carbonate (or propylene carbonate) molecules. ClO_4^- - EC/DMC (PC) complexes have a structure in which non-polar groups are sticking out, thus partitioning of ClO_4^- into a highly hydrophilic aluminum oxide film is hindered. It is supposed that the addition of water to the solvent makes the solvation sphere more polar, thus allowing it to penetrate oxide film more easily.

EDS and Raman measurements indicated that in solutions of higher water concentration (> 500 ppm), ClO_4^- was not present, or present at much lower levels, inside the pits, than in solutions with lower water content. This might indicate formation of the pits without corrosion products deposited inside. AFM images presented in Figure 5.4 are the examples of a pit formed on the electropolished surface after 2 potentiodynamic scans (5 mV/s; 2000 – 5000 mV vs. Li/Li^+) in 1M $LiClO_4$/EC-DMC with 1000 ppm of added H_2O. A large pit, roughly 2.5 μm deep and 5 μm across, is clearly visible. This pit is not filled with the corrosion products, as was observed for electrolyte with lower water content. There is also a significant amount of the loose solid material present on the surface around the corrosion pit. The "empty" pit may indicate that at the higher water levels, solubility of $Al(ClO_4)_3$ increases, and thus, it does not accumulate inside the pit. To investigate this possibility further, *in-situ* ECAFM measurements were performed.

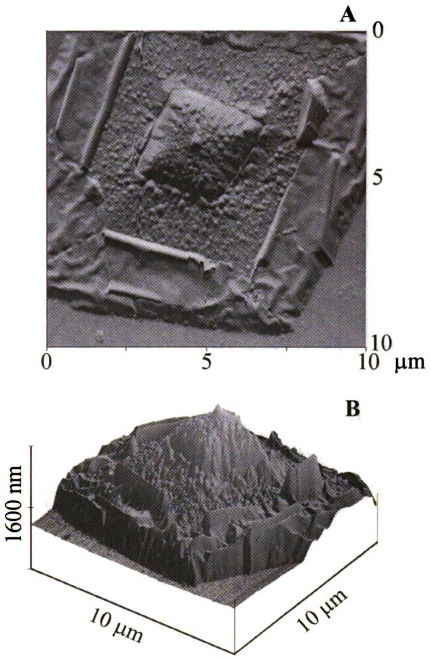

Figure 5.3. AFM images of a mound formed on the electropolished aluminum surface after 2 potentiodynamic scans (5 mV/s; 2000 – 5000 mV vs. Li/Li^+) in 1M $LiClO_4$/EC-DMC with 500 ppm of added H_2O. (A) Deflection and (B) height mode images of the same mound.

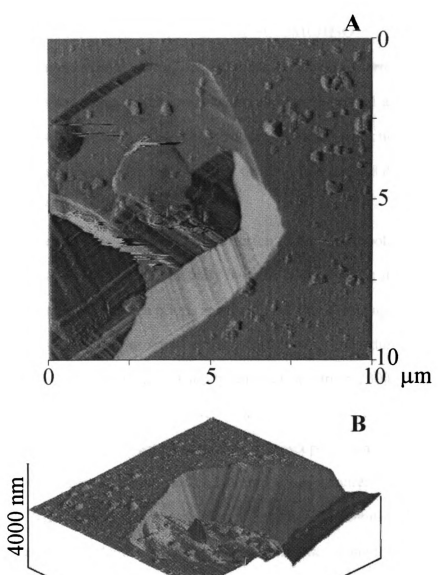

Figure 5.4. AFM images of a pit formed on the surface of electropolished aluminum after 2 potentiodynamic scans (5 mV/s; 2000 – 5000 mV vs. Li/Li^+) in 1M $LiClO_4$/EC-DMC with 1000 ppm of added H_2O. (A) Deflection and (B) height mode images of the same pit.

5.2.4. *In situ* atomic force microscopy - $LiClO_4$/EC-DMC/H_2O

ECAFM is known to be a very useful technique for studying corrosion of metals *in-situ*.[55,56] It allows for direct correlation between the charge passed and the changes in electrode surface structure brought about by the electrochemical reactions. The objective of these measurements was to learn more about the pit formation and development in the $LiClO_4$/EC-DMC/H_2O.

Previously presented data showed that corrosion of the electropolished aluminum is highly localized and that pits form randomly over the surface. Since it is not possible to predict where the pits will form, a priori, and due to the fact that images are restricted to 15 x 15 μm (AFM scanner limitations) or less, the following procedure was used. First, the electrode was subjected to 2 potentiodynamic cycles from 3300 to 4500 mV vs. Li/Li^+ at 3 mV/s in 1M $LiClO_4$/EC-DMC with 1000 ppm of added H_2O, so that pit formation could be observed with an optical microscope. Then, the AFM tip was positioned manually over the pitted area and an image was acquired to confirm presence of a pit/mound. The electrode was then subjected to additional potentiodynamic scanning (3^{rd} and 4^{th} scan) and the AFM images were recorded *in situ*, during the polarization.

Figures 5.5 through 5.8 present the data for 1M $LiClO_4$/EC-DMC with 1000 ppm of added H_2O. Figure 5.5 presents the cyclic voltammetric i-E curves recorded at 3 mV/s for the two scans during which AFM images were collected. A response indicative of pitting corrosion is clearly visible for both scans with E_{pit} equal to 4100 and 4200 mV vs. Li/Li^+ for the 3^{rd} and 4^{th} scan, respectively, and E_{pass} = 3450 mV vs. Li/Li^+ for both scans. The current at 4500 mV for both scans was 155 and 175 μA, respectively. Both, the current at this potential and the anodic charge increase with cycle number, consistent with an increasing electrode area involved in the corrosion process.

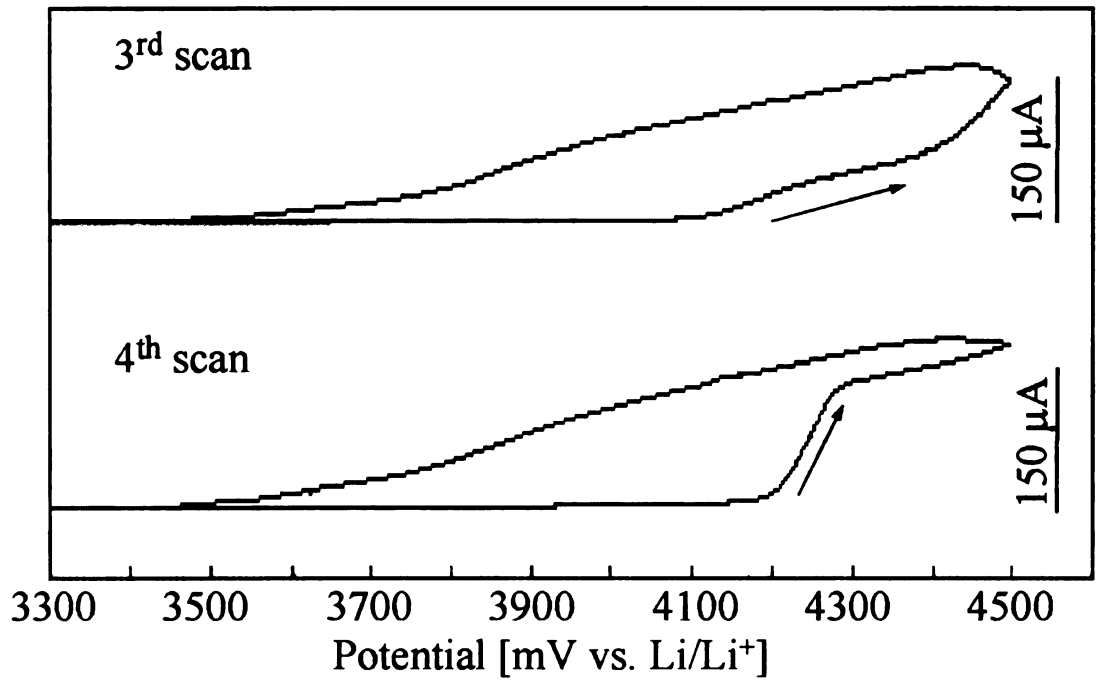

Figure 5.5. Cyclic voltammetric i-E curves for electropolished aluminum recorded at 3 mV/s in 1M $LiClO_4$/EC-DMC with 1000 ppm of added H_2O. The measurements were made in the AFM fluid cell.

Figure 5.6A presents a sequence of the 9 x 9 μm^2 AFM images (deflection mode) of the corrosion mound recorded at the beginning (top), the mid point (middle), and the end (bottom) of the 3rd potentiodynamic scan. A circular formation, ~ 100 nm high and ~ 3.5 µm in diameter is visible on the surface at the beginning. There are also two smaller circular pits present to the upper left of the circular mound (indicated by an arrow). This kind of small pit is often observed on the electropolished surface, and originates from the electropolishing process itself.[32] Since, there was no evidence that these pits take an active part in the corrosion in 1M $LiClO_4$/EC-DMC/H_2O, they provided a convenient reference point on the aluminum surface.

Figure 5.6B presents a sequence of the cross sectional profiles obtained from the height mode images of the developing mound recorded at different potentials. Each profile was taken through the middle of the circular mound (see Figure 5.6A top).

Analysis of the profiles shows that the growth of the corrosion pit and redeposited products are directly related to the applied potential, and thus the anodic charge passed. There is little change in the height or diameter of the deposits between 3300 and 4200 mV during the positive scan. At 4300 mV, the pit width and both the horizontal and vertical size of the deposit begin to increase until the repassivation potential (3450 mV) is reached during the reverse scan. There also appears to be a temporary collapse of the growing mound at 4200 mV during the reverse scan, after which the mound continues growing until repassivation potential is reached.

Figure 5.7A presents a sequence of the 11 x 11 μm^2 deflection mode ECAFM images of the same region of the surface during the 4^{th} potentiodynamic scan. Figure 5.7B presents a sequence of image cross sections taken at different applied potentials through the middle of the corroding area. Interestingly, the corrosion mound developed during the 3^{rd} potentiodynamic scan, fully collapses at the beginning of the 4^{th} scan. It remains in the collapsed state until the E_{pit} (4500 mV) is reached, at which potential it starts growing again. The mound then continues growing until a potential of 4200 mV is reached during the reversed scan. At this potential, the mound suddenly breaks open and detaches from the surface, leaving behind a ~1 μm deep pit and large number of loosely-bound, solid corrosion products, that give rise to the streaks in the AFM image (last image, Figure 5.7A).

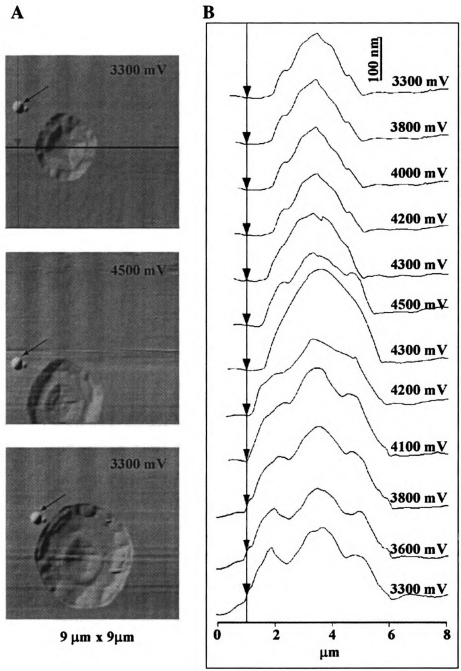

Figure 5.6. *In situ* ECAFM measurements of an electropolished aluminum surface in 1M $LiClO_4$/EC-DMC with 1000 ppm of added H_2O. (A) Deflection mode images of a mound and (B) height mode profiles for a cross section through the middle of the corrosion mound, as shown on the top image. The electrode potentials are indicated on the AFM images and the cross sectional profiles, and they correspond to the i-E curve presented in Figure 5.5 (3^{rd} scan).

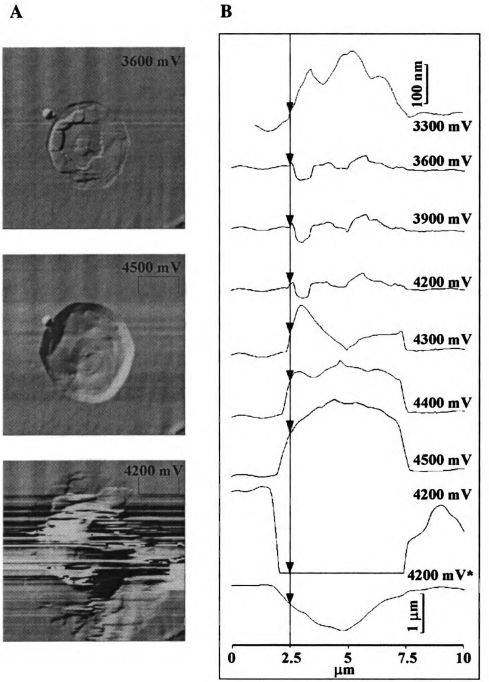

Figure 5.7. *In situ* ECAFM measurements in 1M $LiClO_4$/EC-DMC with 1000 ppm of added H_2O. (A) Deflection mode images of the mound and (B) cross sectional profiles through the middle of the mound. The electrode potentials are indicated on the AFM images and the cross sectional profiles, and they correspond to the i-E curve presented in Figure 5.5 (4^{th} scan).

The potential dependent horizontal and vertical growth of the corrosion pit and deposited products, during both potentiodynamic scans, is depicted in the Figure 5.8. The data for the 3rd scan were obtained from the cross section profiles presented in Figure 5.6B. The data for the 4th scan were obtained from the profiles presented in 5.7B and two profiles, not shown in Figure 5.7B, recorded at 3800 and 3300 mV during the reverse potential sweep of the 4th scan. It appears that after reaching E_{pit}, the deposited products grow vertically and this growth is later followed by horizontal expansion. This result can be explained by the following mechanism in which, at E_{pit}, corrosion starts at an exposed aluminum surface, as this surface is more active than an oxide-coated one. Corrosion undercuts the oxide film, and the growth of the solid corrosion product deposit lifts the oxide film. This process is observed as a horizontal growth of the deposit.

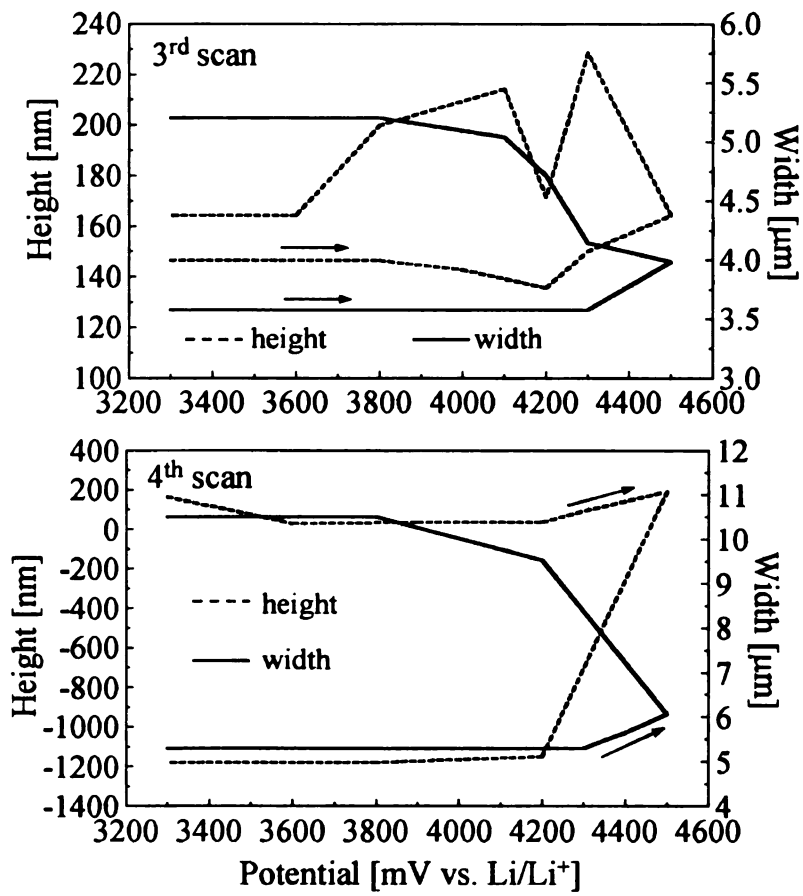

Figure 5.8. Horizontal and vertical development of the corrosion product deposit.

The sudden collapse of the deposit and its detachment from the surface, leaving an exposed pit, cannot be explained by increased solubility of the corrosion products in the presence of water. If deposit solubility was the cause, it should be relatively constant during the course of the entire potentiodynamic cycle, not a sudden transition as was observed. A reasonable possibility is the evolution of gaseous products, primarly O_2, formed from the oxidative decomposition of water according to reaction:

$$2H_2O \rightarrow O_2 + 4\,H^+ + 4\,e^- \ (4.27\ V\ vs.\ Li/Li^+) \qquad [1]$$

The evolution of gaseous oxidation products can also explain another observation made from the analysis of Figure 5.8. It seems that the horizontal growth is much faster after the sudden collapse of the mound. This can be explained by the fact that once gas escapes from the corroding area it forms a vacuum that is quickly filled with the fresh electrolyte solution. As a result of an increase in the electrochemically active area, the corrosion proceeds at a higher rate.

Considering all the information, the following mechanism can be envisioned for the corrosion process in $LiClO_4$/EC-DMC with added water impurty. In the first step, very localized corrosion starts at defects in the oxide film. At high anodic potentials (>4000 mV), decomposition of water, as well as dissolution of aluminum occurs. The corrosion products deposit in the newly formed pit, forming a mound on the surface. At low water levels (< 500 ppm), the evolution of oxygen is not significant and the corrosion site remains filled with and partially passivated by the corrosion products. At high water

impurity levels, evolution of oxygen occurs to a greater extent, and this leads to the formation of the gas bubbles. These bubbles coalesce into a larger bubble that eventually releases from the surface, raising the product layer. This process may lead to formation of empty pits on the surface. This process destroys the passivation layer provided by the deposited corrosion products leading to a larger area of aluminum exposed to the solution and an increased rate of corrosion. Kelly *et al.* observed that passivity of iron in $LiClO_4$/PC mixtures depends strongly on the amount of water present in the electrolyte/ solvent mixture.[31] The authors reported that at water levels less than 500 ppm, passivation through formation of salt film consisting of $Fe(ClO_4)_2$, occurs. At higher water levels, the iron surface lacks passivity and significant corrosion occurs at potentials greater than 4.1 V vs. Li/Li^+. They attributed the lack of passivation to increased solubility of $Fe(ClO_4)_2$ and local acidification of the electrolyte/solvent mixture as a result of water oxidation. Data presented in this work show that a similar mechanism of corrosion may be occuring on aluminum surfaces. ECAFM results show, however, that higher water levels may also lead to increased corrosion through mechanical disruption of the deposited salt film ($Al(ClO_4)_3$) by evolution of gaseous oxidation products.

5.3. Conclusions

AFM imaging shows clearly that passivation of aluminum in $LiPF_6$/EC-DMC and $LiClO_4$/EC-DMC is accompanied by formation of a layer of solid deposits layer. In $LiPF_6$, this layer forms both during anodic polarization and at open circuit conditions. Addition of water to $LiPF_6$/EC-DMC leads to surface roughening due to attack of the

fluoride on the oxide film. This process does not destroy passivity due to formation of an oxyfluoride layer. The addition of water to $LiClO_4$/EC-DMC leads to significant localized corrosion of aluminum surface. Pits, filled with solid corrosion products (mounds), form in the electrolyte at added water levels below 500 ppm. At higher water levels, "empty" pits are observed. Their formation may be assigned to disruption of the deposits by gaseous products evolving during oxidation.

CHAPTER 6

6. Aluminum Corrosion in $LiPF_6$/EC-DMC and $LiClO_4$/EC-DMC – Investigations Using the Electrochemical Quartz Crystal Microbalance (EQCM)

6.1. Introduction

Electrochemical quartz crystal microgravimetry (EQCM) is an analytical technique that combines electrochemistry with an ultra-sensitive mass measurement provided by a quartz crystal microbalance (QCM). The technique allows a direct correlation to be made between the charge passed through an electrode and the mass change induced on the surface as a result of the charge passed. It allows for the investigation of the mechanisms of electrochemical reactions that induce a mass change on the electrode. The EQCM has provided important information about electrochemical phenomena such as underpotential deposition, electropolymerization, double layer stucture, electrolyte adsorption, electrochemically-driven self-assembly, and corrosion.[70-72 and references therein]

The EQCM measurement involves two simultaneously measured variables, mass and charge. Measurement of charge can be accomplished in straightforward way by employing a potentiostat or galvanostat, whereas the mass changes are determined indirectly from the measurement of the oscillation frequency change of a quartz crystal

resonator (QCR). The QCR consists of a piezoelectric quartz crystal, usually in the form of disc that is sandwiched between two metal electrodes. During the operation, a high frequency AC electric field is applied between the electrodes, and across the thickness of the crystal. This causes the QCR to oscillate in the mechanically resonant shear mode. The frequency of the oscillation is very sensitive to interfacial mass changes at the electrode surface. The relationship between the change in QCR mass (Δm) and the change in oscillation frequency (Δf) was first recognized and described by Sauerbrey,[73] and is contained in the following equation:

$$\Delta f = \frac{-2nf_0^2}{A\sqrt{\mu_Q \rho_Q}} \Delta m = -K\Delta m \qquad [6.1]$$

where f_0 is the fundamental frequency of the quartz resonator [Hz], μ_Q is the shear modulus of AT-cut crystal ($2.947 \cdot 10^{11}$ dyn/cm^2), ρ_Q is the density of quartz (2.648 g/cm^3), A is the piezoelectrically active area [cm^2] and n is the overtone number; K - is the sensitivity factor that includes all the values that are constant for a given experimental setup.

The negative sign in the Sauerbrey equation indicates that a mass decrease is accompanied by an oscillation frequency increase, whereas a mass increase leads to a decrease in the oscillation frequency. This equation also shows the origin of the extraordinary sensitivity of mass measurements performed with QCM. For example, operating at a resonant frequency of 10 MHz provides a theoretical sensitivity of 0.22 Hz·cm^2·ng^{-1}. Since the frequency can be measured very accurately to ± 1 Hz, a 10 MHz EQCM can detect a mass change of 4.4 ng·cm^{-2}. Such sensitivity corresponds to detecting less than 2% of a monolayer of Pb atoms deposited on gold.[74]

Further interpretation of EQCM data is accomplished in following manner. Since the electrochemical charge represents the total number of electrons transferred in a given electrochemical process (e.g., deposition), it corresponds to a mass change on the electrode surface. This mass change can be easily calculated from the Faraday Law according to the equation:

$$\Delta m = \frac{W}{z} \cdot \frac{\Delta Q}{F} \qquad [6.2]$$

where: W is the apparent molecular weight [g/mol]; z is the number of electrons; Q is the charge passed [C]; F is the Faraday constant (96486 C/mole).

By substituting equation [6.2] into equation [6.1] and rearranging, the following equation is obtained:

$$\frac{W}{z} = -\frac{F}{K} \cdot \frac{\Delta f}{\Delta Q} \qquad [6.3]$$

It is evident that all the parameters on the right side are either a constant (F and K) or are determined during the experiment (Δf and ΔQ). Thus, this relationship allows for the determination of the molecular weight per electron (W/z), which is characteristic for the electrochemical process that leads to the observed mass change.

Several limitations of the Sauerbrey equation have to be recognized, however, for data analysis to be meaningful. A major assumption is that the mass added or lost at the oscillator surface does not experience any shear deformations during oscillation. This is a good approximation for thin, rigid films. It may however lead to many errors when investigating formation of the thick, soft materials (e.g., polymers).[70,71] It is also important to recognize the fact that, as implied by Sauerbrey equation, the QCR is sensitive to mass changes per unit area of oscillation. Thus the QCR is most useful when

probing processes that occur uniformly across its surface – processes that can be represented as a change in mass per unit area. Recognizing this limitation is very important, as many electrochemical corrosion processes lead to very localized dissolution of the surface, thus limiting evaluation of the results to qualitative, rather than quantitative conclusions. Other factors that may influence the operation of the QCR are the electrode surface roughness and the total mass (frequency) change experienced by the QCR. Rough surfaces may lead to entrapment of solvent molecules, which are than recognized by the QCM as a mass increase. This is not usually a serious problem as long as the polished crystals are used and significant surface roughening does not occur during measurement.[71] Also, if the total frequency change does not exceed a few % of the fundamental frequency of the crystal, the dependence between interfacial mass change and oscillation frequency change remains linear.[71]

The corrosion/passivation of aluminum in lithium-ion battery electrolytes was recently studied with the EQCM by Yang *et al.*[7] The authors investigated various presently used or possible lithium-ion battery electrolytes, including $LiPF_6$, $LiBF_4$, $LiClO_4$, $LiCF_3SO_3$, $LiC(CF_3SO_2)_3$, and $LiN(CF_3SO_2)_2$. They found that aluminum corrodes significantly in PC containing $LiCF_3SO_3$, $LiC(CF_3SO_2)_3$, and $LiN(CF_3SO_2)_2$. The authors observed mass loss from the electrode after anodic polarization in these three electrolytes. More detailed EQCM studies of aluminum corrosion in $LiN(CF_3SO_2)_2$/PC revealed that the corrosion process entails formation of an adsorbed aluminum compound or non-adherent film that subsequently desorbs. It was also found that potentiodynamic polarization of aluminum in $LiPF_6$/PC and $LiBF_4$/PC leads to formation of a protective film after the first potentiodynamic scan. An increase in the electrode mass was observed

in such cases. In $LiClO_4$/PC formation of the oxidation product layer was also observed during the first potentiodynamic scan. This layer, however, did not prevent surface oxidation during subsequent scans.

In this chapter, the corrosion/oxidation of aluminum in $LiPF_6$/EC-DMC and $LiClO_4$/EC-DMC was investigated with the EQCM. The experimental setup is described in Chapter 2. The measurements were conducted using commercial, 10 MHz, polished QCRs, with aluminum electrodes evaporated on the surface. Theoretical mass sensitivity of the crystals was 4.4 ng/Hzcm^2 and linearity of the Sauerbrey equation was assumed. The aluminum electrode thickness was measured with SEM to be ~ 200 nm. Although the exact procedure by which aluminum electrodes were evaporated on the crystal surface is not known, it is anticipated that an oxide layer formed on the surface with a thickness of 1 – 4 nm, which is typical for air-formed aluminum oxide films.[32] Prior to the measurements, the aluminum QCRs were rinsed with DMC and dried in a flow of Ar. These electrodes are referred to as untreated. For some measurements, the native aluminum oxide was damaged by uniform mechanical polishing with 0.1 μm size diamond powder, in hexane, under an inert Ar atmosphere, rinsed with hexane, and dried in a flow of Ar. Complete removal of the native oxide layer could not be ensured as the polishing was limited, due to thinness of the aluminum electrodes. These electrodes are referred to as mechanically polished.

6.2. Results and discussion

Results presented in the previous chapters indicate that aluminum passivates in dry $LiClO_4$/EC-DMC and $LiPF_6$/EC-DMC. AFM images indicated the formation of a solid passivation layer on the surface. XPS data revealed that in $LiPF_6$/EC-DMC the passivation layer is rich in fluoride, and in $LiClO_4$/EC-DMC rich in perchlorate. The formation of a solid passivation layer should be evidenced by increased electrode mass after polarization. Also, by comparison of the charge passed during polarization with the change in mass, the apparent mass per electron (W/z) characteristic of the oxidation process can be determined (see Equation 6.3). Table 6.1 summarizes the various possible oxidation products along with the W/z values characteristic for their formation.

Chemical composition	W/z (g/equiv)
Al_2O_3	8
AlOF	11.7
Al_2OF_4	15.3
$Al(OH)_3$	17
$Al(OH)_2F$	17.7
$Al(OH)F_2$	18.3
AlF_3	19
$Al(ClO_4)_3$	99.5
$Al(PF_6)_3$	145

Table 6.1. Chemical compositions and W/z values for possible passivation film species.

6.2.1. OCP measurements

Figure 6.1 presents results of open circuit potential (OCP) measurements in 1M $LiPF_6$/EC-DMC for a mechanically polished electrode. The mass change of the electrode was also monitored. Both the potential and mass of the electrode increase during the 1-h period consistent with increased passivation of the surface by reaction deposits (e.g., AlF_3). The rate of increase is the highest at the beginning and then leads toward a more constant value.

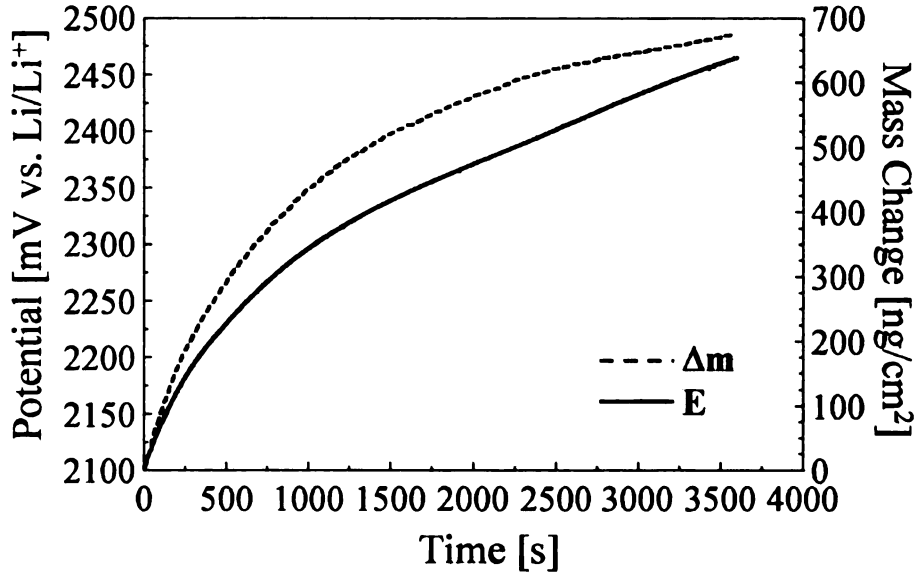

Figure 6.1. Time dependent open circuit potential and mass change measurements for mechanically polished aluminum during exposure to 1M $LiPF_6$/EC-DMC.

Potential and mass change curves similarly shaped to these were also observed in 1M $LiClO_4$. Table 6.2 summarizes the results of OCP measurements in 1M $LiPF_6$/EC-DMC and 1M $LiClO_4$/EC-DMC for mechanically polished and untreated aluminum electrodes. It is evident that the passivation layer forms in either electrolyte and on both types of surfaces. Interestingly, the OCP values observed on the untreated aluminum surface were more positive (noble) than the ones reported in Chapter 3 for the electropolished surface.

This is probably due to a different, less defective aluminum oxide film present on evaporated aluminum.

Electrolyte	OCP [mV vs. $LiLi^+$]$^{a)}$	Δm [ng/cm^2]$^{b)}$
	Mechanically Polished	
$LiClO_4$	2200 ± 80	400 ± 100
$LiPF_6$	2350 ± 50	500 ± 100
	Untreated	
$LiClO_4$	2600 ± 50	400 ± 150
$LiPF_6$	2800 ± 100	700 ± 150

Table 6.2. Summary of OCP-EQCM data for mechanically polished and oxide coated aluminum electrodes. a) – at 1-h mark, b) – during the 1-h period.

6.2.2. EQCM measurements in $LiPF_6$/EC-DMC and $LiClO_4$/EC-DMC – mechanically polished surface

Formation of a passivation layer on aluminum electrodes was also investigated with cyclic voltammetry combined with QCM. The voltammogram and associated change in mass (Δm) for a mechanically polished aluminum electrode in 1M $LiPF_6$/EC-DMC, after a 1-h soak at OCP, are presented in Figure 6.2. During the first scan, there is an anodic charge of 3 mC/cm^2 passed between 2700 and 5000 mV. Little charge is passed during the subsequent scan indicating that passivation of the aluminum surface occurs. The anodic charge recorded during potentiodynamic cycling is accompanied by increase in the electrode mass. The mass gain was equal approximately 320 and 60 ng/cm^2 for the 1st and 2nd potentiodynamic cycles, respectively. These results indicate the formation of

a solid passivation layer on the surface. The mass gain is best matched to that caused by a charge transfer with a mass increase per electron (W/z) of 11. The normalized charge change (ΔQ_n, which is $W\Delta Q/(zF)$) with W/z = 11 is presented in Figure 6.2B. The result suggests the formation of AlOF (W/z = 11.7). It is also possible that mixed oxidation products with an average mass-to-charge ratio of 11 are formed during anodic polarization (Table 6.1). This result is in agreement with results of the XPS analysis presented in Chapter 3. The XPS data indicated formation of a fluoride-rich passivation layer (e.g., AlF_3, AlOF).

Recently, Yang *et al.* performed an EQCM investigation of aluminum passivation in 1M $LiPF_6$/PC.[7] The authors observed a similar oxidation charge and passivation of the electrode during the first potentiodynamic scan. They also observed an increase in the electrode mass, which indicated the formation of a solid passivation layer on the surface. The apparent mass-to-charge ratio reported in their studies was equal 26. This number would appear to indicate that a product with a higher W/z was formed. The authors did not assign any specific product to the observed W/z value. The analysis of their results, however, suggests a possible explanation for the observed difference in W/z. ΔQ_n values presented by the authors did not track Δm well, especially for the second potentiodynamic cycle. There was significant, constant mass increase observed in their studies even at the potentials where no current was observed in voltammetric data. This indicates that the electrochemical oxidation observed in their studies was accompanied by another process that, independently from polarization, leads to a mass increase. The authors did not comment on this issue at all. Rough correction of their data to eliminate this constant mass increase yielded a W/z value of approximately 18 g/equiv. This result

is within the range of formation of mixed aluminum fluoride/oxyfluoride layers (see Table 6.1), as proposed in this and other studies.[2,4]

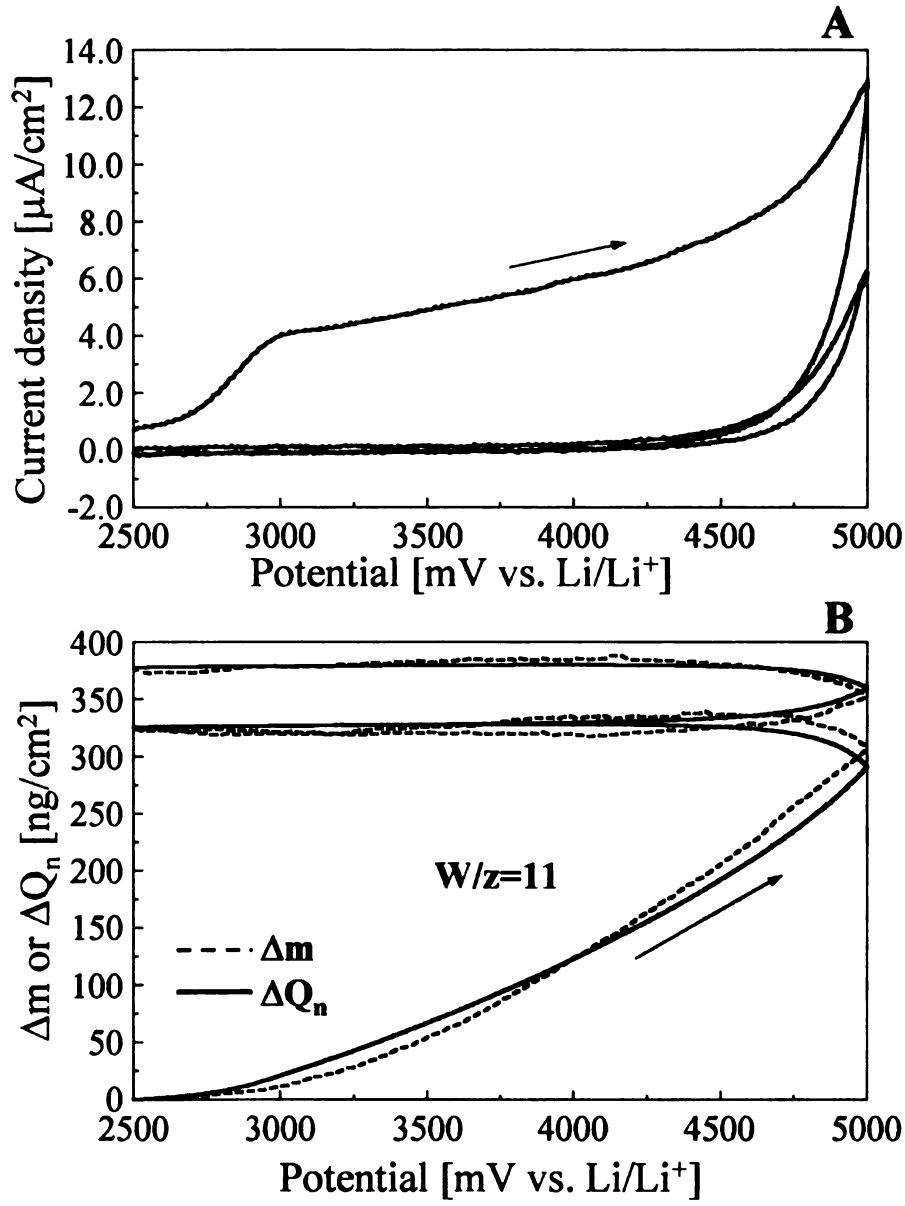

Figure 6.2. (A) Cyclic voltammogram, and (B) mass change (Δm) and normalized charge change (ΔQ_n with W/z = 11) versus potential profiles for mechanically polished aluminum in 1M $LiPF_6$/EC-DMC during the first two potentiodynamic cycles. Scan rate = 5mV/s.

Cyclic voltammetric i-E curves and corresponding mass change profiles for mechanically polished aluminum in 1M $LiClO_4$/EC-DMC, after 1h at OCP, are presented in Figure 6.3. Similarly to what was observed in $LiPF_6$/EC-DMC, passivation occurs during the first potentiodynamic scan, as little anodic charge is passed during the subsequent cycle. The oxidation charge is also accompanied by a mass increase on the surface. The mass gain is best matched to that caused by a charge transfer with W/z of ~60. The normalized charge change (ΔQ_n) with W/z = 60 is presented in Figure 6.2B. Interestingly, calculated ΔQ_n does not track the measured Δm over the whole potential range, in contrast to what was observed for $LiPF_6$/EC-DMC. At the beginning of the initial scan, the mass increase is lower than the calculated ΔQ_n. This indicates that two or more different processes take place at different potentials. To investigate this more, the apparent mass per electron ($W/z = F \cdot \Delta m / \Delta Q$) was plotted against potential and is presented in Figure 6.3C. At the beginning of the first positive sweep, W/z stays below 17 up to 4000 mV, indicating the formation of mixed aluminum oxide/hydroxide product. Such a product may form from the reaction between aluminum and trace water present in the electrolyte/solvent mixture. W/z gradually increases up to 24 by 4800 mV. This indicates an increasing proportion of some heavier oxidation product in the overall reaction. At potentials close to the positive limit (5000 mV), W/z rises quickly and reaches values over 60, indicating the formation of an even heavier product.

XPS data reported in Chapter 3 indicated $Al(ClO_4)_3$ as a possible oxidation product. The formation of pure $Al(ClO_4)_3$ on the surface would be evidenced by a W/z of 99.5. The observed W/z was much lower, however. There are two possible explanations for this observation. First, a mixture of aluminum oxide/hydroxide and aluminum perchlorate

forms on the surface, thus the observed W/z is an average value for a mixed oxidation product. On the other hand, it is possible that the $Al(ClO_4)_3$ that forms is not strongly attached to the surface, and thus, it does not give rise to a signal characteristic of its formation. Both possibilities seem feasible. The first one is supported by formation of a lighter ($Al_2O_3/Al(OH)_3$) oxidation product that is visible at the beginning of the first positive scan. The second one is evidenced by the slight mass decrease observed at positive limits during the second scan. Mass loss indicates that at highly anodic potentials partial detachment of the passivating layer occurs. It is possible that due to an increased oxidation rate at positive potentials, dissolution of aluminum and formation of $Al(ClO_4)_3$ interferes with the already formed passivating layer and leads to observed mass loss.

Yang *et al.* briefly investigated corrosion/passivation of mechanically polished aluminum in 1M $LiClO_4$/PC.[7] They found that potentiodynamic polarization leads to the deposition of a heavy product, which is characterized by a W/z of 220. This deposit, however, was not effective at passivating the surface as substantial currents were observed during the second potentiodynamic scan. For example, the oxidation charge observed during the second cycle was only ~ 25% lower than the charge recorded for the first cycle. Interesting, however, is the fact that the i-E curves recorded by the authors showed characteristics of pitting corrosion. The authors did not address this observation and they also did not assign the W/z value to any oxidation product, or mixture of products.

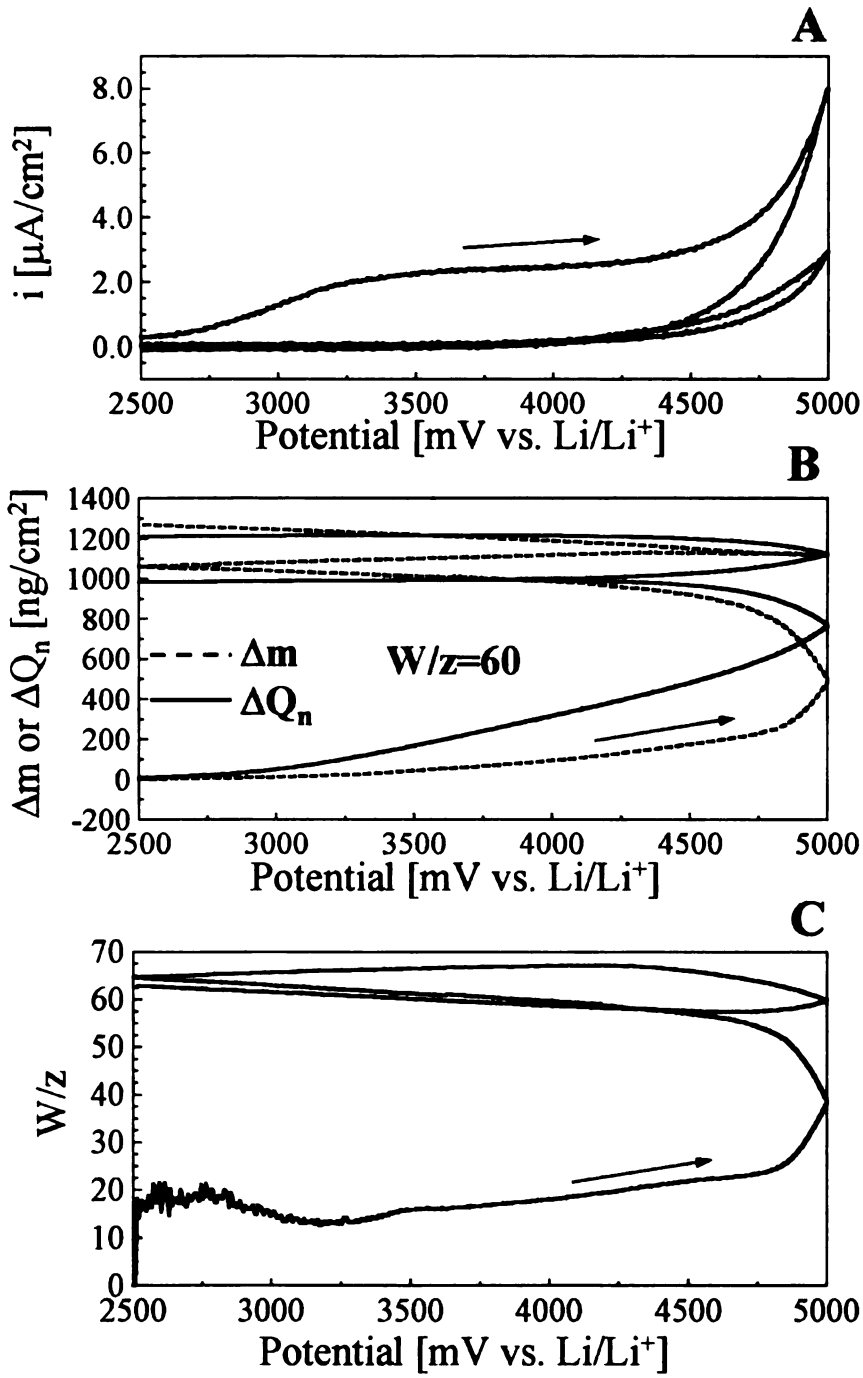

Figure 6.3. (A) Cyclic voltammogram, (B) mass change (Δm) and normalized charge change (ΔQ_n with W/z = 60) diagram, and (C) W/z change with potential diagram for mechanically polished aluminum in 1M $LiClO_4$/EC-DMC during the first two potentiodynamic cycles. Scan rate = 5mV/s.

6.2.3. EQCM measurements in $LiPF_6$/EC-DMC and $LiClO_4$/EC-DMC – untreated surface

Passivation of untreated aluminum surfaces in $LiClO_4$/EC-DMC and $LiPF_6$/EC-DMC was also investigated. Figures 6.4 and 6.5 present EQCM data recorded during potentiodynamic cycling at 5 mV/s in $LiPF_6$/EC-DMC and $LiClO_4$/EC-DMC, respectively. These figures present also the calculated normalized charge change (ΔQ_n) with corresponding W/z ratios. Clearly, passivation of the surface occurs in both electrolytes. It is important to point out that, compared to mechanically polished surfaces, the onset potential for the oxidation current is shifted positively (to ~ 3800 mV) in both electrolytes. This observation agrees with the much higher OCP values recorded for untreated surfaces (Table 6.2).

Figure 6.4B presents a normalized charge change (ΔQ_n) calculated with W/z = 11 for untreated surface in $LiPF_6$/EC-DMC. This value is the same, as that observed for mechanically polished surfaces, indicating that the oxidation processes are of the same nature and involve formation of aluminum oxyfluoride layer.

The normalized charge change for $LiClO_4$/EC-DMC is presented in Figure 6.5B. The best fit of electrochemical charge data to measured electrode mass gain was obtained for W/z = 22. This value is much lower than the average value obtained on mechanically polished surface and indicates a much lower proportion of $Al(ClO_4)_3$ in the passivation layer. The passivation layer is mostly composed of mixed aluminum oxide and aluminum hydroxide.

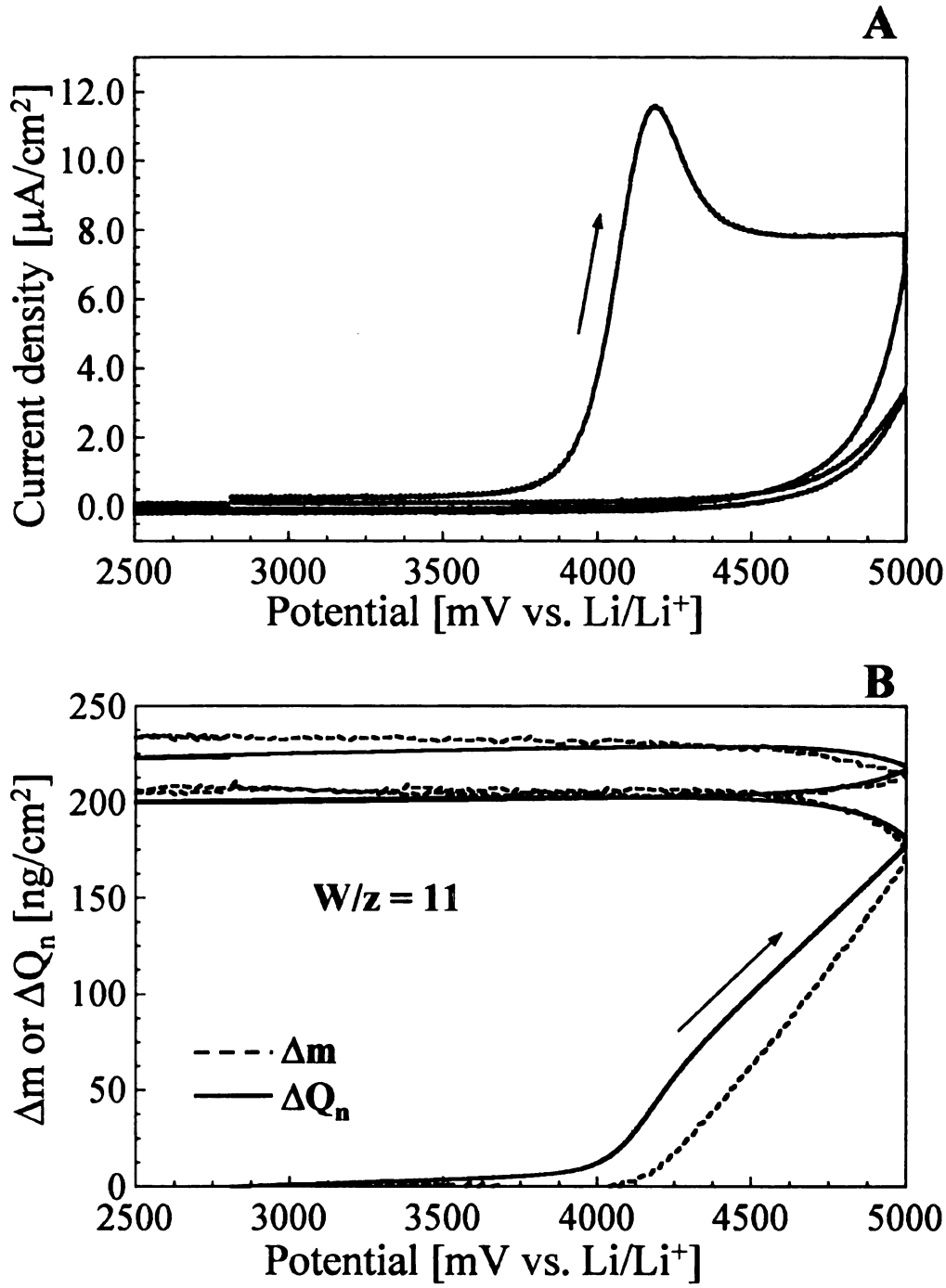

Figure 6.4. (A) Cyclic voltammogram, and (B) mass change (Δm) and normalized charge change (ΔQ_n with W/z = 11) profiles for untreated aluminum in 1M $LiPF_6$/EC-DMC during the first two potentiodynamic cycles. Scan rate = 5mV/s.

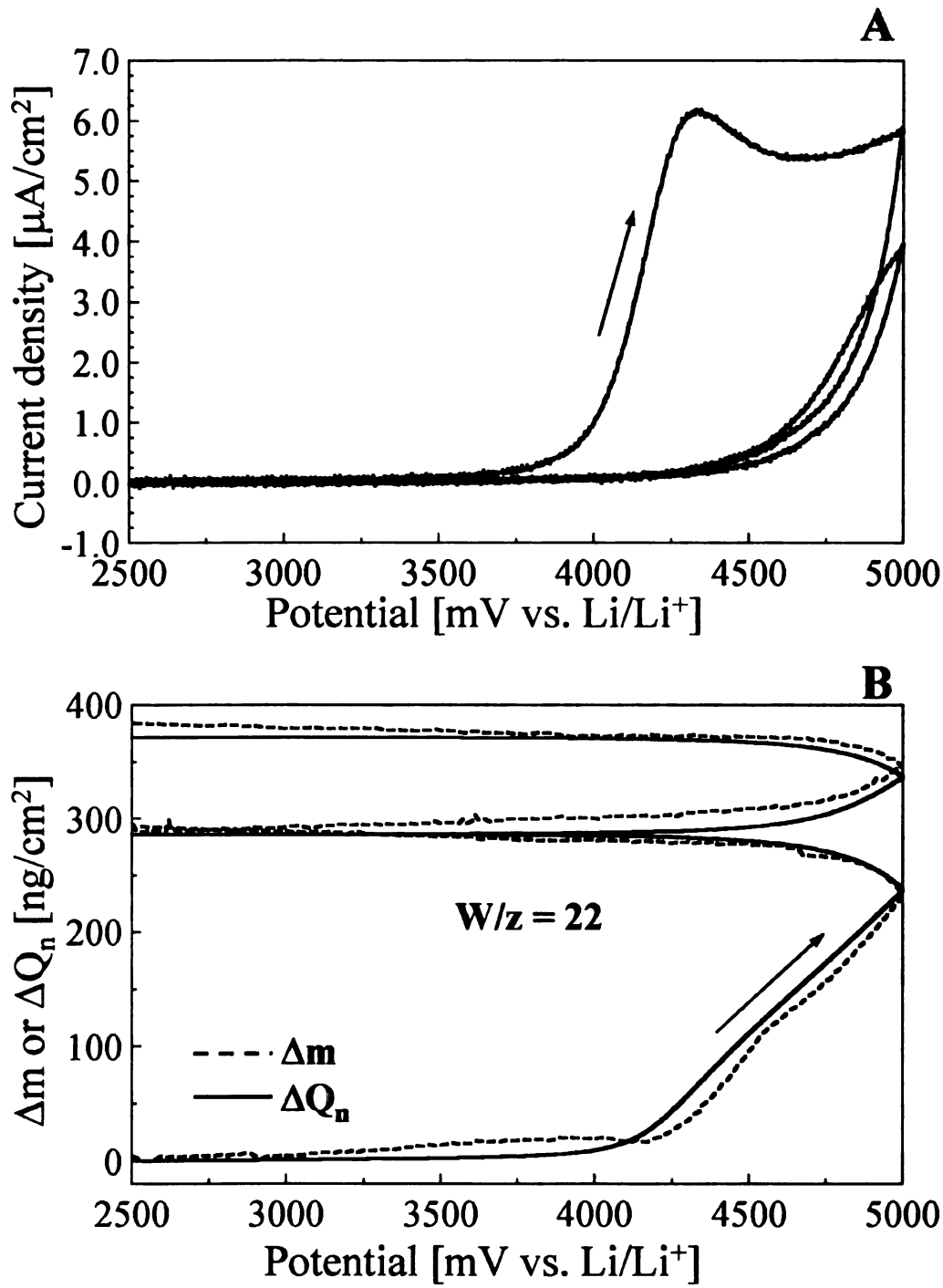

Figure 6.5. (A) Cyclic voltammogram, and (B) mass change (Δm) and normalized charge change (ΔQ_n with W/z = 22) profiles for untreated aluminum in 1M $LiClO_4$/EC-DMC during the first two potentiodynamic cycles. Scan rate = 5mV/s.

6.2.4. EQCM measurements in 1M $LiClO_4$/EC-DMC and 1M $LiPF_6$/EC-DMC – influence of water contamination

The potentiodynamic i-E curves and associated mass change (Δm) profiles for untreated aluminum in 1M $LiPF_6$/EC-DMC with 500 ppm of added water are presented in Figure 6.6. A large oxidation peak current of 18 $\mu A/cm^2$ is observed at ~ 4200 mV. The oxidation charge during the first cycle was similar to one observed in dry electrolyte (~2 mC/cm^2). The surface becomes passivated during the first potentiodynamic cycle as only a very small current was flowing during the second cycle. Passivation was accompanied by deposition of solid oxidation product on the surface as indicated by the mass increase (Figure 6.6B). Clearly, the addition of water does not cause significant corrosion or mass loss of aluminum in $LiPF_6$/EC-DMC. The normalized charge change (ΔQ_n) is best fitted to the Δm with a W/z = 15. This indicates the formation of slightly heavier oxidation product compared to dry electrolyte (W/z = 11). It may be explained by formation of a passivation layer with a higher content of fluoride (e.g., Al_2OF_4) due to the oxidation in the presence of increased amounts of F^- formed from the hydrolysis of $LiPF_6$, as was proposed in Chapter 4. Formation of $Al(OH)_3$ (W/z =17), according to reaction [4.2], may also explain higher W/z values observed in the presence of water.

Completely different behavior was observed in $LiClO_4$/EC-DMC with added water. Figure 6.7 presents voltammetric i-E curves and associated mass change profiles for untreated aluminum in 1M $LiClO_4$/EC-DMC with 500 ppm of added water. It is evident that the surface passivation does not occur during the first cycle. The onset potential for the oxidation current is ca. 3200 mV. The mass change also begins at this potential.

The oxidation charge recorded during the second cycle (8.1 mC/cm^2) is more than twice that for the first cycle (3.5 mC/cm^2). There is also clear evidence for pitting corrosion as the i-E curve forms characteristic crossover, with the current during the reverse scan being higher than during the forward scan. E_{pit} and E_{pass} are equal, respectively, 3200 and 3150 mV for the first cycle and 3150 and 3100 mV for the second cycle. The values for both E_{pit} and E_{pass} are much lower than the values reported previously in Chapter 4. This may be due to the different forms of aluminum used in both studies. Crystalline aluminum metal is apparently much more corrosion resistant than a film of small aluminum aggregates evaporated on a quartz surface.

The QCM data show that during the initial stage of potentiodynamic polarization, up to ~4500 mV, an increase in the electrode mass occurs. This increase is characterized by W/z = 17, consistent with the formation of $Al(OH)_3$. This is in agreement with the EDS and Raman spectroscopic results reported in Chapter 4. However, at potentials more positive than 4200 mV a mass loss is observed. The mass decreases until the repassivation potential of ~ 3200 mV is reached during reverse sweep. Similar behavior is seen during the second scan with a much larger mass loss. If one assumes that the oxidation charge is associated exclusively with dissolution of aluminum, the mass loss corresponding to the 11.6 mC/cm^2 charge would be 1080 ng/cm^2 (W/z = -9). This value is roughly comparable to the total mass loss of ~800 ng/cm^2 observed after the second scan.

Dissolution and loss of aluminum is in contradiction to the results presented in Chapters 4 and 5, which revealed the deposition of an $Al(ClO_4)_3$-rich layer during anodic polarization with 500 ppm of added water. Also, the current and charge observed in the

i-E potentiodynamic curves continuously increases with scan number at potentials more positive than E_{pit}. The i-E curves reported in Chapter 4 showed a clear current maximum and diffusion limited current decrease. These observations indicate different corrosion mechanisms and may result from the type of aluminum used – bulk aluminum vs. a thin-film evaporated on the quartz. Optical microscopy and AFM were used to image the surface after potentiodynamic polarization to further investigate the nature of aluminum corrosion.

Figure 6.8 presents photomicrographs (top) and AFM images (bottom) of the untreated aluminum surface after 2 potentiodynamic cycles in 1M $LiClO_4$/EC-DMC with 500 ppm of added water. Round pits, from 20 to 150 μm in diameter, are visible on the electrode surface. The deflection mode AFM image (C) shows that the pit is essentially empty of corrosion products with only small deposit visible in the middle of the pit. The height mode AFM image taken at the pit edge shows a height of ~200 nm, which is the thickness of the aluminum film on the quartz crystal. This indicates complete dissolution of the aluminum inside a pit. This observation agrees with the EQCM data showing aluminum dissolution. It also indicates a reason for the corrosion current increase at all potentials positive of E_{pit}. As corrosion proceeds only laterally in the thin film, the corrosion products do not block the access to the corroding surface, thus no current peak and diffusion-limited current decrease are observed. It is important to recognize that the QCM data can be treated only qualitatively and not quantitatively, because linearity of Sauerbrey equation cannot be assumed at highly localized corrosion where dissolution of aluminum occurs.[70]

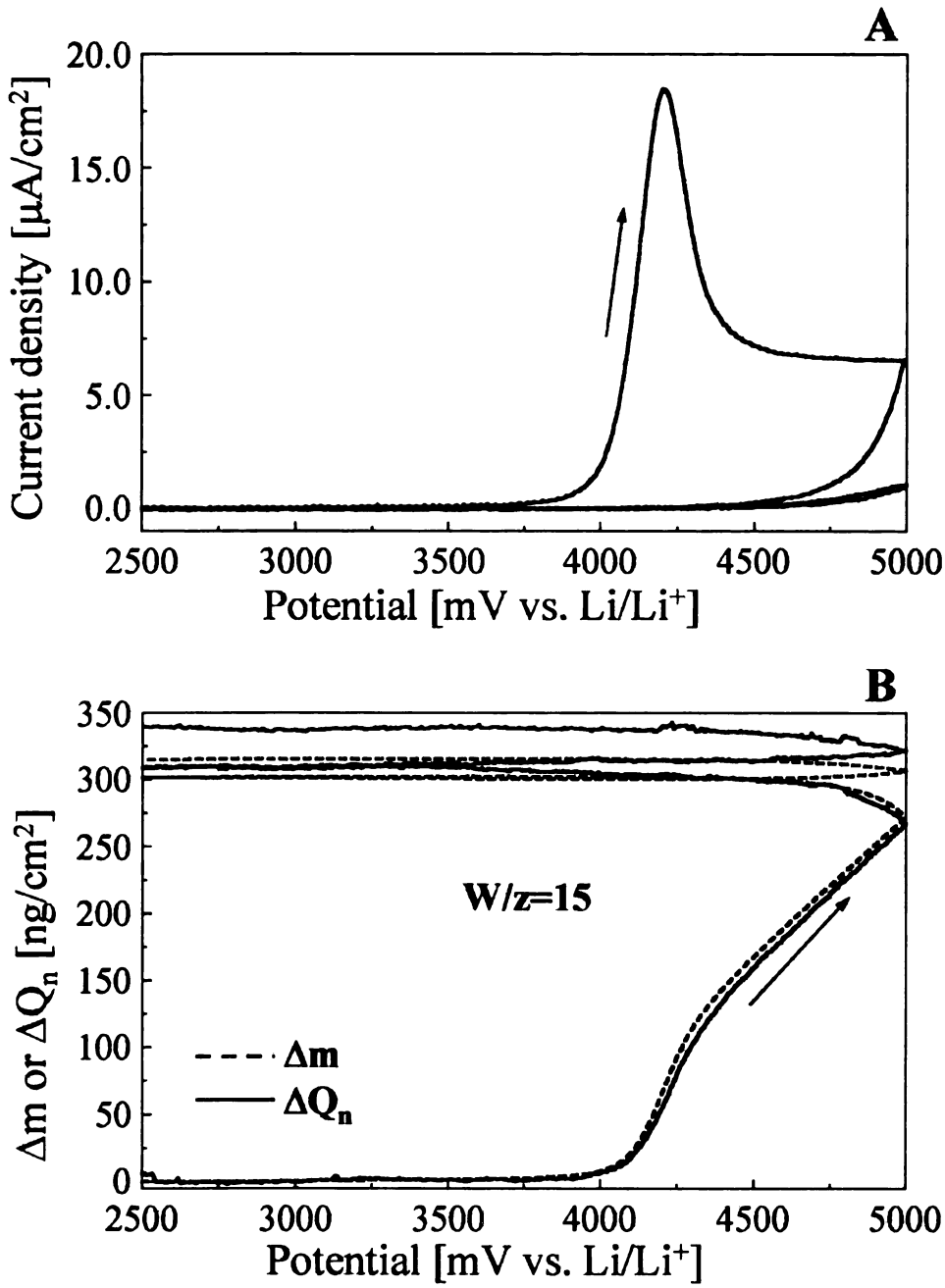

Figure 6.6. (A) Cyclic voltammogram, and (B) mass change (Δm) and normalized charge change (ΔQ_n with W/z = 15) profiles for untreated aluminum in 1M $LiPF_6$/EC-DMC with 500 ppm of added water during the first two potentiodynamic cycles. Scan rate = 5mV/s.

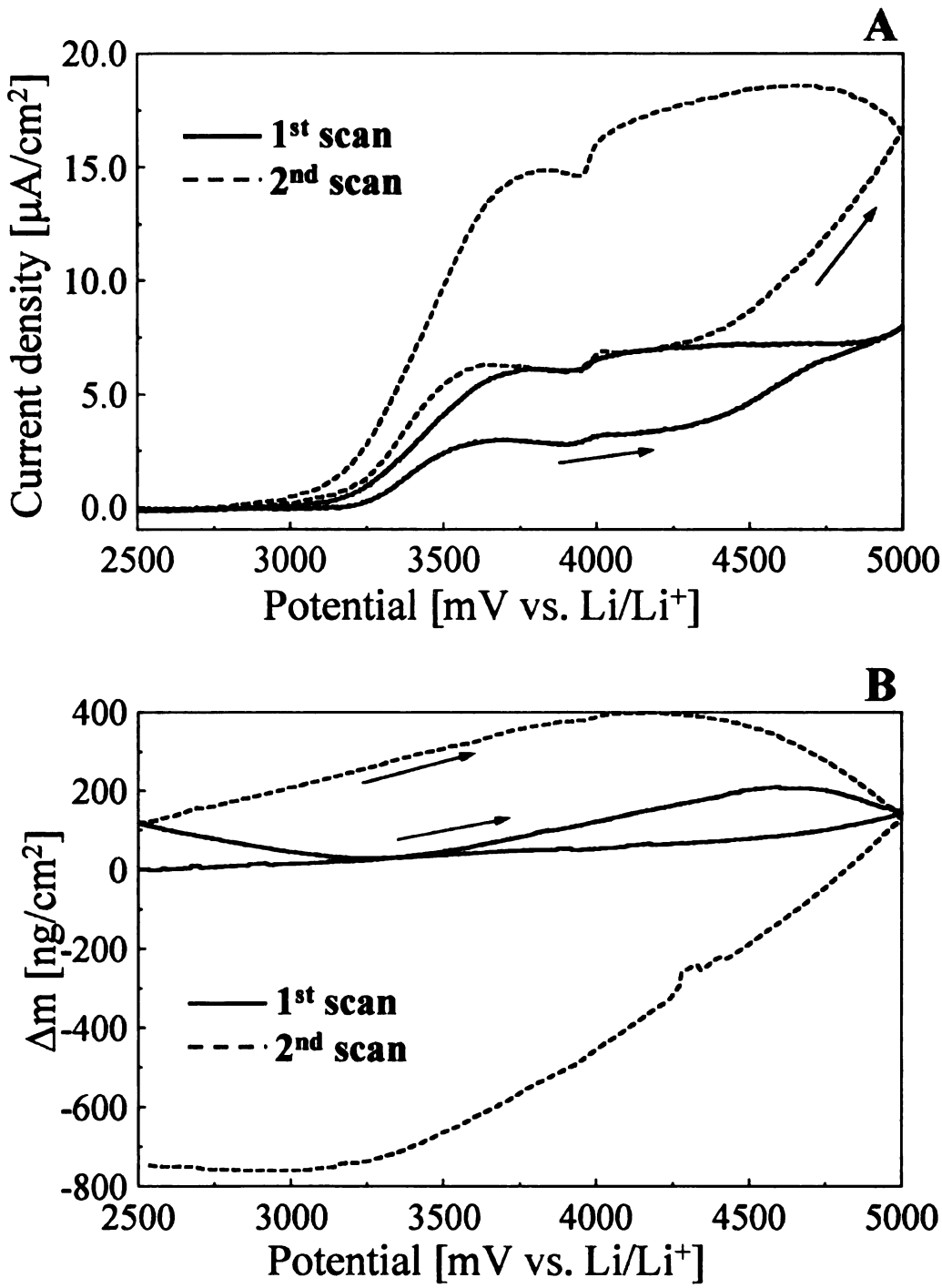

Figure 6.7. (A) Cyclic voltammogram, and (B) mass change (Δm) profile for untreated aluminum in 1M $LiClO_4$/EC-DMC with 500 ppm of added water during the first two potentiodynamic cycles. Scan rate = 5mV/s.

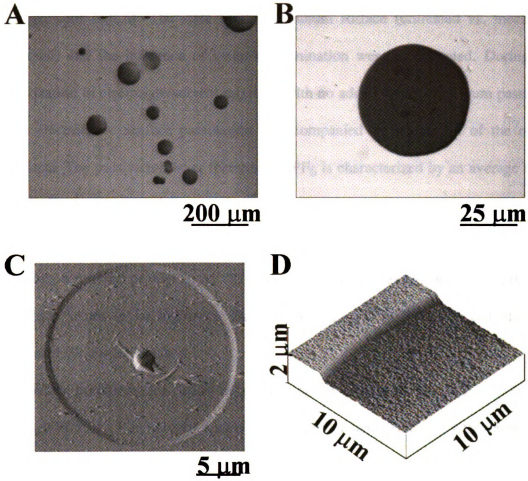

Figure 6.8. (A), (B) Photomicrographs of the circular pits formed on the untreated aluminum surface after 2 potentiodynamic scans in 1M $LiClO_4$/EC-DMC with 500 ppm of added water. Scan rate = 5mV/s. (C) AFM deflection mode image of one of the pits. (D) AFM height mode image of the edge of the pit. The height of the edge is equal to 200 nm.

6.3. Conclusions

Corrosion/passivation of aluminum in $LiClO_4$/EC-DMC and $LiPF_6$/EC-DMC was studied with EQCM. The state of the aluminum surface (untreated vs. mechanically polished) and the influence of water contamination were investigated. During anodic polarization in electrolyte/solvent mixtures with no added water, aluminum passivates in both electrolytes. Surface passivation is accompanied by deposition of the oxidation products. The passivation layer formed in $LiPF_6$ is characterized by an average apparent molecular weight per electron (W/z) of 11 equiv/g, consistent with the formation of aluminum oxyfluoride (AlOF). The passivation layer formed in $LiClO_4$/EC-DMC is probably a mixture of Al_2O_3, $Al(OH)_3$, and $Al(ClO_4)_3$. The proportion of $Al(ClO_4)_3$ in the layer seems to be higher on the mechanically polished (W/z = 60) than on the untreated (W/z = 22) surface.

Water contamination leads to passivation of aluminum in $LiPF_6$/EC-DMC. An average W/z of 15, consistent with a fluoride and/or hydroxide rich passivation layer is observed. In $LiClO_4$/EC-DMC, the presence of water leads to catastrophic pitting corrosion and loss of aluminum from the thin film.

CHAPTER 7

7. Summary

Corrosion susceptibility of aluminum in $LiPF_6$/EC-DMC, $LiPF_6$/PC, $LiClO_4$/EC-DMC, and $LiClO_4$/PC in the absence and presence of added water impurity was investigated in the present studies. The electrochemical measurements (CV, CA, and OCP) were combined with microscopic imaging (OM, SEM, and AFM) and surface analysis techniques (XPS, EDS and EQCM) to understand processes that govern the stability of aluminum in selected non-aqueous electrolytes. It was found that:

1. None of the four investigated electrolyte/solvent systems is corrosive toward aluminum in the absence of added water (below 50 ppm), at least up to 5 V vs. Li/Li^+. A solid passivation layer forms on the aluminum surface at such conditions. AlF_3, AlOF, Al_2O_3, and LiF were found as the major components of a passivation layer formed in $LiPF_6$-based solutions, whereas the layer formed in $LiClO_4$ consisted mostly of $Al(ClO_4)_3$, Al_2O_3, and $Al(OH)_3$.

2. Anodic polarization in $LiClO_4$/EC-DMC and $LiClO_4$/PC, in the presence of added water, lads to pitting and progressive corrosion. Passivity of aluminum is disturbed at added water levels as low as 50 ppm. Water levels higher than 500 ppm significantly

increase the rate of corrosion. This is most probably due to increased dissolution of $Al(ClO_4)_3$ and the evolution of gaseous oxidation products, which disturb the layer of solid corrosion products and enhance transport of solvent and electrolyte toward the metal surface.

3. Anodic polarization in $LiPF_6$/EC-DMC and $LiPF_6$/PC in the presence of added water does not cause pitting and corrosion. The surface remains effectively passivated by the highly insoluble aluminum oxyfluoride/hydroxyfluoride layer.

4. An oxide layer, present on the electropolished aluminum, offers additional corrosion protection in the electrolyte/solvent mixtures without added water impurity. It does not, however, protect aluminum from pitting that occurs in $LiClO_4$/EC-DMC and $LiClO_4$/PC in the presence of added water impurity. At water levels lower than 500 ppm, pits that form on the surface are filled with the deposited corrosion products (mostly $Al(ClO_4)_3$ and $Al(OH)_3$). Higher water levels lead to increased corrosion rates and formation of empty pits. This is due to evolution of gaseous oxidation products from the pit interior.

5. Considering the mechanism of aluminum passivation it was found that at open circuit conditions aluminum passivates through salt film formation in $LiPF_6$ and solvent adsorption in $LiClO_4$. During anodic polarization, aluminum passivates by salt film formation in both electrolytes. In $LiClO_4$, it is a precipitate of $Al(ClO_4)_3$, whereas in $LiPF_6$, a salt film forms from the reaction between aluminum and F^-

formed from the hydrolysis of PF_6^-. The passivation layer formed in $LiClO_4$ is less stable than in $LiPF_6$. This is due to slow dissolution of the $Al(ClO_4)_3$ layer in organic solvent. Water interferes with both solvent adsorption and salt film formation.

6. Finally, the electrolyte type ($LiClO_4$ vs. $LiPF_6$) not the solvent (PC vs. EC-DMC) has the most significant effect on the corrosion susceptibility of aluminum.

REFERENCES

1. R. W. Revie, *Uhlig's Corrosion Handbook*, Wiley-Interscience, New York, (2000).

2. K. Kanamura, T. Okagawa, and Z.-I. Takehara, *J. Power Sources*, **57,** 119 (1995).

3. K. Kanamura, S. Toriyama, S. Shiraishi, and Z.-I. Takehara, *J. Electrochem. Soc.*, **142,** 1383 (1995).

4. J. W. Braithwaite, A. Gonzales, G. Nagasubramanian, S. J. Lucero, D. E. Peebles, J. A. Ohlhausen, and W. R. Cieslak, *J. Electrochem. Soc.*, **146,** 448 (1999).

5. L. J. Krause, W. Lamanna, J. Summerfield, M. Engle, G. Korba, R. Loch, and R. Atanasoski, *J. Power Sources*, **68,** 320 (1997).

6. K. Kanamura, T. Umegaki, S. Shiraishi, M. Ohashi, and Z.-I. Takehara, *J. Electrochem. Soc.*, **149,** A185 (2002).

7. H. Yang, K. Kwon, T. M. Devine, and J. W. Evans, *J. Electrochem. Soc.*, **147,** 4399 (2000).

8. C. W. Walker, Jr., J. D. Cox, and M. Salomon, *J. Electrochem. Soc.*, **143,** L80 (1996).

9. W. K. Behl and E. J. Plichta, *J. Power Sources*, **72,** 132 (1998).

10. J. L. Goldman and A. B. McEwen, *Electrochem. Solid-State Lett.*, **2,** 501 (1999).

11. M. Z. A. Munshi, R. Gopaliengar, and B. B. Owens, *Solid State Ionics*, **27,** 259 (1988).

12. H. S. Choe, B. G. Carroll, D. M. Pasquariello, and K. M. Abraham, *Chem. Mater.*, **9,** 369 (1997).

13. Y. Chen, T. M. Devine, J. W. Evans, O. R. Monteiro, and I. G. Brown, *J. Electrochem. Soc.*, **146,** 1310 (1999).

14. Y. Matsuda, Y. Ouchi, and H. Tamura, *J. Appl. Electrochem.*, **4,** 53 (1974).

15. L. Bai and B. E. Conway, *J. Electrochem. Soc.*, **137,** 3737 (1990).

16. S. Licht, G. Levitin, C. Yarnitzky, and R. Tel-Vered, *Electrochem. Solid-State Lett.*, **2,** 262 (1999).

17. M. Ue, F. Mizutani, S. Takeuchi, and N. Sato, *J. Electrochem. Soc.*, **144,** 3743 (1997).

18. M. Ue, K. Shima, and S. Mori, *Electrochim. Acta*, **39,** 2751 (1994).

19. M. Morita and Y. Matsuda, *J. Power Sources*, **60,** 179 (1996).

20. L. A. Pawlick and R. G. Kelly, *J. Corros. Sci. Eng. [Electronic Publication: http://www.cp.umist.ac.uk/JCSE/Vol1/PAPER4/Paper4.htm]*, **1,** (1995).

21. R. Umebayashi, N. Akao, N. Hara, and K. Sugimoto, *J. Electrochem. Soc.*, **149,** B75 (2002).

22. S. Megahed and B. Scrosati, *Interface*, **4,** 34 (1995).

23. I. Buchmann, *Batteries in a Portable World*, Cadex Electronics Inc., Richmond, Canada, (2001).

24. P. Arora, R. E. White, and M. Doyle, *J. Electrochem. Soc.*, **145,** 3647 (1998).

25. J. R. Owen, *Chem. Soc. Rev.*, **26,** 259 (1997).

26. M. Zhao, S. Kariuki, H. D. Dewald, F. R. Lemke, R. J. Staniewicz, E. J. Plichta, and R. A. Marsh, *J. Electrochem. Soc.*, **147,** 2874 (2000).

27. K. Kanamura, S. Toriyama, S. Shiraishi, and Z.-I. Takehara, *J. Electrochem. Soc.*, **143,** 2548 (1996).

28. G. S. Frankel, *J. Electrochem. Soc.*, **145,** 2186 (1998).

29. R. G. Kelly and P. J. Moran, *Corros. Sci.*, **30,** 495 (1990).

30. J. F. Scanlon, J. Kruger, and P. J. Moran, *J. Electrochem. Soc.*, **140,** 1268 (1993).

31. R. G. Kelly, P. J. Moran, J. Kruger, C. Zollman, and E. Gileadi, *J. Electrochem. Soc.*, **136,** 3262 (1989).

32. S. Wernick, *The Surface Treatment and Finishing of Aluminium and Its Alloys*, Finishing Publications Ltd., Middlesex, England, (1990).

33. R. C. Weast, ed., *CRC Handbook of Chemistry and Physics*, CRC Press, Inc., Boca Raton, FL, (1980).

34. P. A. Malachesky, in *Encyclopedia of Electrochemistry of the Elements*, Vol. VI (A. J. Bard, ed.), Marcel Dekker, Inc., New York, 1976.

35. R. T. Atanasoski, *J. Serb. Chem. Soc.*, **57,** 935 (1992).

36. G. Eggert and J. Heitbaum, *Electrochim. Acta*, **31,** 1443 (1986).

37. E. Cattaneo and J. Ruch, *J. Power Sources*, **44,** 341 (1993).

38. D. A. Shifler, P. J. Moran, and J. Kruger, *Corros. Sci.*, **32,** 475 (1991).

39. D. A. Shifler, P. J. Moran, and J. Kruger, *J. Electrochem. Soc.*, **139,** 54 (1992).

40. P. Novak, P. A. Christensen, T. Iwasita, and W. Vielstich, *J. Electroanal. Chem. Interfacial Electrochem.*, **263,** 37 (1989).

41. D. Battisti, G. A. Nazri, B. Klassen, and R. Aroca, *J. Phys. Chem.*, **97,** 5826 (1993).

42. K. A. Rodgers, *Clay Miner.*, **28,** 85 (1993).

43. W. H. Leong and D. W. James, *Aust. J. Chem.*, **22,** 499 (1969).

44. R. G. Kelly, P. J. Moran, E. Gileadi, and J. Kruger, *Electrochim. Acta*, **34,** 823 (1989).

45. P. Zelenay, M. Winnicka-Maurin, and J. Sobkowski, *J. Electroanal. Chem. Interfacial Electrochem.*, **278,** 361 (1990).

46. J. N. Butler, D. R. Cogley, and E. Grunwald, *J. Phys. Chem.*, **75,** 1477 (1971).

47. G. Binning, H. Rohrer, C. Gerber, and E. Weibel, *Phys. Rev. Lett.*, **49,** 57 (1982).

48. G. Binnig, C. F. Quate, and C. Gerber, *Phys. Rev. Lett.*, **56,** 930 (1986).

49. B. Drake, C. B. Prater, A. L. Weisenhorn, S. A. Gould, T. R. Albrecht, C. F. Quate, D. S. Cannell, H. G. Hansma, and P. K. Hansma, *Science*, **243,** 1586 (1989).

50. S. Manne, P. K. Hansma, J. Massie, V. B. Elings, and A. A. Gewirth, *Science*, **251,** 133 (1991).

51. N. Ikemiya, S. Miyaoka, and S. Hara, *Surf. Sci.*, **327,** 261 (1995).

52. B. J. Cruickshank, D. D. Sneddon, and A. A. Gewirth, *Surf. Sci.*, **281,** L308 (1993).

53. P. Mrozek, Y.-E. Sung, M. Han, M. Gamboa-Aldeco, A. Wieckowski, C.-H. Chen, and A. A. Gewirth, *Electrochim. Acta*, **40,** 17 (1995).

54. C. A. Alves and M. D. Porter, *Langmuir*, **9,** 3507 (1993).

55. K. Kowal, J. DeLuccia, J. Y. Josefowicz, C. Laird, and G. C. Farrington, *Mater. Res. Soc. Symp. Proc.*, **409,** 201 (1996).

56. R. M. Rynders, C. H. Paik, R. Ke, and R. C. Alkire, *J. Electrochem. Soc.*, **141,** 1439 (1994).

57. G. Bertrand, E. Rocca, C. Savall, C. Rapin, J. C. Labrune, and P. Steinmetz, *J. Electroanal. Chem.*, **489,** 38 (2000).

58. U. Kamachi Mudali and Y. Katada, *Electrochim. Acta*, **46,** 3735 (2001).

59. J. Li and D. J. Meier, *J. Electroanal. Chem.*, **454,** 53 (1998).

60. N. Ikemiya, T. Kubo, and S. Hara, *Surf. Sci.*, **323,** 81 (1995).

61. J. Zak and M. Kolodziej-Sadlok, *Electrochim. Acta*, **45,** 2803 (2000).

62. K. Kowal, L. Xie, R. Huq, and G. C. Farrington, *J. Electrochem. Soc.*, **141,** 116 (1994).

63. J. Y. Josefowicz, L. Xie, and G. C. Farrington, *J. Phys. Chem.*, **97,** 11995 (1993).

64. F. Bellucci, G. Capobianco, A. Deganello, A. Glisenti, T. Monetta, and G. Moretti, *Mat. Sci. Forum*, **289-292,** 1311 (1998).

65. Y. S. Cohen, Y. Cohen, and D. Aurbach, *J. Phys. Chem. B*, **104,** 12282 (2000).

66. D. Aurbach, B. Markovsky, M. D. Levi, E. Levi, A. Schechter, M. Moshkovich, and Y. Cohen, *J. Power Sources*, **81-82,** 95 (1999).

67. D. Aurbach, A. Zaban, Y. Ein-Eli, I. Weissman, O. Chusid, B. Markovsky, M. Levi, E. Levi, A. Schechter, and E. Granot, *J. Power Sources*, **68,** 91 (1997).

68. T. Hurlen and K. H. Johansen, *Acta Chem. Scand., Ser. A*, **A39,** 545 (1985).

69. J. A. Richardson and G. C. Wood, *J. Electrochem. Soc.*, **120,** 193 (1973).

70. M. R. Deakin and D. A. Buttry, *Anal. Chem.*, **61,** 1147A (1989).

71. M. D. Ward, in *Physical Electrochemistry* (I. Rubinstein, ed.), p. 293, Marcel Dekker, New York, 1995.

72. M. D. Ward and D. A. Buttry, *Science*, **249,** 1000 (1990).

73. G. Sauerbrey, *Z. Physik*, **155,** 206 (1959).

74. M. R. Deakin and O. Melroy, *J. Electroanal. Chem. Interfacial Electrochem.*, **239,** 321 (1988).